LBNL-41643

ERNEST ORLANDO LAWRENCE
BERKELEY NATIONAL LABORATORY

Ultrafast Studies of Organometallic Photochemistry: The Mechanism of Carbon-Hydrogen Bond Activation in Solution

Steven Eric Bromberg

Chemical Sciences Division

May 1998

Ph.D. Thesis

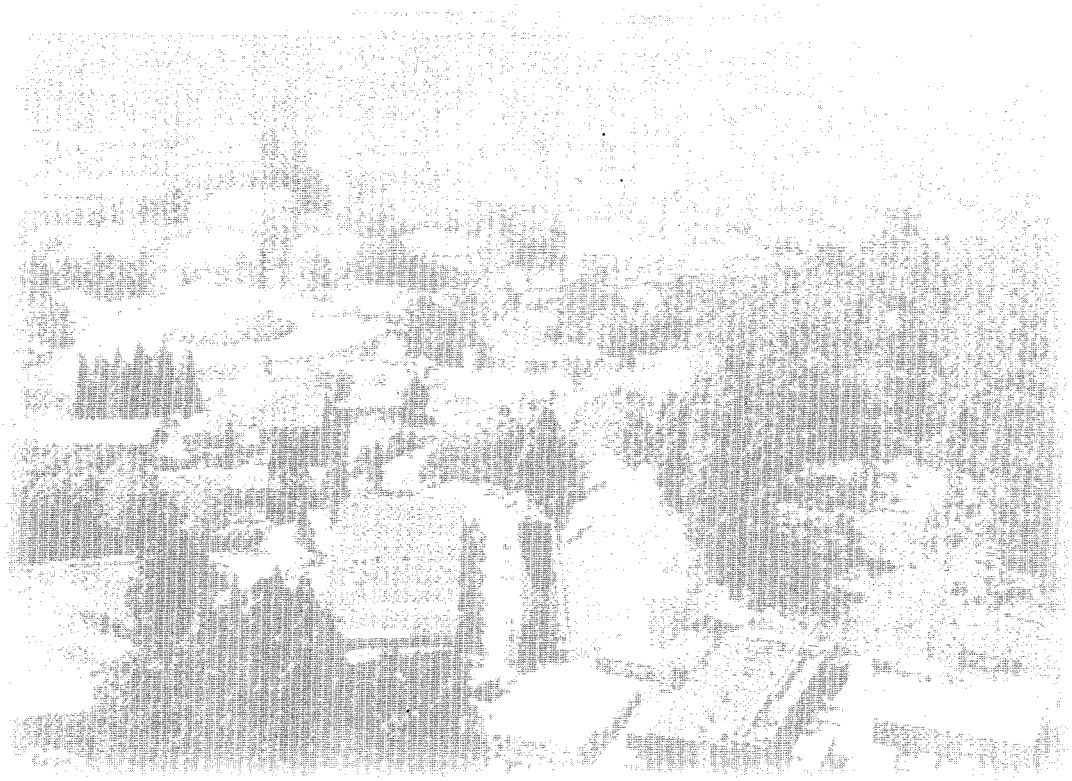

DISCLAIMER

Portions of this document may be illegible in electronic image products. Images are produced from the best available original document.

LBNL - 41643

Ultrafast Studies of Organometallic Photochemistry: The Mechanism of Carbon-Hydrogen Bond Activation in Solution

by

Steven Eric Bromberg
Ph.D. Thesis

Department of Chemistry
University of California, Berkeley

and

Chemical Sciences Division
Lawrence Berkeley National Laboratory
University of California
Berkeley, California 94720

May 1998

This work was supported by the Director, Office of Energy Research, Office of Basic Energy Sciences, Chemical Sciences Division, of the U.S. Department of Energy under Contract No. DE-AC03-76SF00098.

Ultrafast Studies of Organometallic Photochemistry:

The Mechanism of Carbon-Hydrogen Bond Activation in Solution

by

Steven Eric Bromberg

Abstract

Ultrafast Spectroscopic Studies of Organometallic Photochemistry:

The Mechanism of Carbon-Hydrogen Bond Activation in Solution

by

Steven Eric Bromberg

Doctor of Philosophy in Chemistry

University of California, Berkeley

Professor Charles B. Harris, Chair

When certain organometallic compounds are photoexcited in room temperature alkane solution, they are able to break or "activate" the C—H bonds of the solvent. Understanding this potentially practical reaction requires a detailed knowledge of the entire reaction mechanism. Because of the dynamic nature of chemical reactions, time-resolved spectroscopy is commonly employed to follow the important events that take place as reactants are converted to products. For the organometallic reactions examined here, the electronic/structural characteristics of the chemical systems along with the time scales for the key steps in the reaction make ultrafast UV/Vis and IR spectroscopy along with

nanosecond Step-Scan FTIR spectroscopy the ideal techniques to use for this study.

The combination of temporal and structural information available from ultrafast infrared spectroscopy makes this technique a valuable tool for studying the structure of short-lived reaction intermediates. Therefore, an initial attempt was made to adapt a current UV/Vis system to operate in the IR by developing a high-power mid-infrared light source. A CW carbon-monoxide gas laser was modified to operate in Q-switched mode using an acousto-optic modulator. While Q-switched output was observed, a combination of poor stability and insufficient overall power made this approach less desirable in light of more recent solid state laser advances.

An initial study of the photophysics of (non-activating) model metal carbonyls centering on the photodissociation of $M(CO)_6$ (M = Cr, W, Mo) was carried out in alkane solutions using ultrafast IR spectroscopy. Geminate recombination was found to make a significant contribution to the observed non-unit photosubstitution quantum yield in each of these systems. A decay of less than 300 fs was observed in the IR absorption of the pentacarbonyls which was assigned to reformation of the parent species after only one or two collisions with the surrounding solvent cage. Details of the solvent dependence of the product formation and bleach recovery dynamics are also discussed.

Next, picosecond UV/vis studies of the C—H bond activation reaction of $Cp^*M(CO)_2$ (M = Rh, Ir), conducted in room temperature alkane solution, are described in an effort to investigate the origin of the low quantum yield for bond cleavage (~1%). The results of these experiments lead to an explanation of the origin of the low yield: most molecules are promoted to a non-dissociative excited state after excitation, which decays in

30-40 ps to the ground state without losing a CO ligand. Since these species never go on to photochemically lose a CO ligand they are consequently unable to generate the reactive intermediates and cleave the C—H bonds.

To monitor the chemistry that takes place in the reaction *after* CO is lost, a system with higher quantum yield is required. The reaction of $Tp^*Rh(CO)_2$ (Tp^* = HB-Pz_3^*, Pz^* = 3,5-dimethylpyrazolyl) in alkanes has a quantum yield of ~30%, making time resolved spectroscopic measurements possible. From ultrafast IR experiments, two subsequently formed intermediates were observed. The first intermediate vibrationally cools in 23 ps before reacting in another 200 ps to form a second, longer lived species. Using Step-Scan FTIR spectroscopy, the timescale for the decay of this intermediate and the formation of the final bond activated product was found to be on the order of 200 ns. The nature of these intermediates are discussed and the first comprehensive reaction mechanism for a photochemical C—H activating organometallic complex is presented.

To my mom and dad

Table of Contents

List of Figures

Acknowledgements

"The most wasted of all days is the one without laughter" e e cummings

***

During my time here at Berkeley, I have come to appreciate this quote more and more (and by this definition, I don't think I wasted too many days). Of course, there were times when the laughter stopped - but it always came back. That's the important part and it's due in no small part to the people I've met along the way...

When I came to graduate school I was fascinated by both laser technology and transition metal chemistry. I would like to thank my adviser Charles Harris for allowing me the independence and freedom to pursue a project that would ultimately let me combine these two areas of study. I have also appreciated the understanding and compassion he showed in the difficult personal situation I faced when I had to go home for a semester while my father was sick with cancer.

The dedication that Vijaya Narasimhan has shown to the members of the Harris group is inspiring. She is always willing to go out of her way for us and has helped me navigate and occasionally even bypass (now that's something!) the vast bureaucracy that is Berkeley.

I would like to acknowledge the National Science Foundation for my funding and the Department of Energy for specialized equipment used in the experiments presented in this dissertation.

Jason King was the senior grad student in the liquids side of the group when I joined and with neverending patience, taught Matt, Carsten, and me - the three new first-

years - about ultrafast spectroscopy. I learned even more important lessons from watching the way Jason interacted with others and how he established his priorities.

The work in this thesis would not have been possible without one of the hardest working people I know, Dr. Tim Lian. I want to thank Tim for helping me to stay focussed so I could get things done.

One of the great things about the Harris Group is the two unique directions of research that go on at the same time. This means that you can always get some outside opinions on your work - until the story gets told one too many times... Even more important is that it brings together people with different interests that may not otherwise have the opportunity to interact. In light of this I would like to thank the members of the surface side for all their help: Dr. Robert Lingle, Jason McNeill, Nien-Hui Ge, Chung Wong, Kelly Gaffney, Simon Liu, and Andre Miller.

The liquid side has accomplished a great deal in the past few years as a direct result of our teamwork. I want to thank Matt Asplund and Haw Yang for their substantial contribution to this work and for advancing the project to the next stage. The younger students Ken Kotz, Matt Wilkens, and Preston Snee all brought their share of enthusiasm to the liquids side which was much appreciated.

I want to especially thank Matt Asplund for getting 95% of my jokes (the other 5% weren't that good anyway) and for matching mine with an equal number of his own such that between the two of us we probably could have written several years worth of talkshow monologues.

The people that I mentioned above are the ones that put the "group" in Harris

Group.

My project also gave me the opportunity to work with Professor Robert Bergman, who always took the time to talk with us about our latest developments. I want to thank him for sharing his enthusiasm for science with me. Bruce Macnamara and Jake Yeston, both members of Professor Bergman's group, always came through with samples even when they had all their own work to do.

As an undergraduate at Brandeis, I did not fully appreciate the time I spent working directly with Professor I. Y. Chan both in and out of the lab. He taught me many important lessons and I can still hear his words: "An experiment isn't supposed to work - you have to make it work." I can't remember how many times I've now said that... I want to thank Chan not only for teaching me science but for sharing his thoughts and wisdom at the same time.

I met Dusty Baber when I began working in Chan's lab. Even though I was only an undergrad, he treated me like a full member of the group. His hard work and friendly attitude helped confirm my decision to go on to graduate school and once again showed me the importance of sticking with a project - and of course the benefits of having your own set of tools for lab!

I thank all the people that have answered my many questions or graciously let me borrow equipment over the past 6 years. In particular, I want to thank Andreas Kadavanich and Mike Tauber who were around from the beginning. You can always count on those guys.

I want to thank Shannon McBride for her friendship and support. She is one of the

reasons that my last year in graduate school has been the best.

Lastly, I would like to thank my family for their constant support. My mom and dad were always behind me even though the move to Berkeley was so far away from home. My parents always stressed the value of education and this was one of the reasons I went to graduate school. I can't thank them enough for all they have given me.

Introduction

Progress in science has always been highlighted by pivotal discoveries that immediately push forward the boundaries of what is known and what is possible. However, the vast majority of scientific progress is incremental. Beginning with some questions, experiments are designed to provide information that may be used to answer these questions. Throughout this process, new questions inevitably arise but due to practical constraints such as funding, time, or manpower, most new lines of questioning are not pursued. Another reason that important questions can remain unanswered is that while the technology and expertise necessary to solve the problem may exist, they may be unfamiliar or inaccessible. This situation is somewhat special because in this case scientific issues are not the only limiting factors. By involving other scientists with fresh viewpoints, the project can be pushed forward and can lead to significant advances. Even though interdisciplinary teamwork is not always an option, there are other times when initiative, funding, time, manpower, and outside assistance are all in place leading to a collaboration. The work presented in this thesis describes the results of just such a collaboration.

***

In 1967, R. G. W. Norrish and G. Porter shared the Nobel prize "for their studies of extremely fast chemical reactions, effected by disturbing the equilibrium by means of very short pulses of energy". This work, which began in the 1940s, extended the boundaries of what could be monitored during a chemical reaction, and thus became a pivotal period in the development of chemistry. By allowing access to the visible spectra of

species generated *during* a reaction, Norrish and Porter began an entirely new field of chemical research. As a result of their work, the analysis of reactants and products could be complemented by analysis of the reaction intermediates, allowing them for the first time to directly follow reaction mechanisms.

Their technique began with an intense light flash called the "photolysis flash" produced in an argon tube which lasted 0.1 milliseconds and had an energy as high as 1000 Joules giving peak powers of 10 watts. An electronic delay circuit controlled another flash called the "spectroscopic flash" which was sent through the reaction tube and into a spectrograph. Spectra were then collected as a function of the time between the photolysis flash and the spectroscopic flash [1].

In the fifty years since the initial prizewinning work was carried out, the development of the laser and its subsequent application to chemistry have all but redefined what was meant by "extremely fast chemical reactions" and "very short pulses of energy". Using current technology, compact solid-state lasers routinely generate picosecond and femtosecond photolysis and spectroscopic "flashes" with peak powers of 10^9 watts [2]. These "ultrafast pulses" can be used to resolve the most fundamental and fleeting of chemical events that occur nearly 10 orders of magnitude faster than those observed by Norrish and Porter. Examples of such ultrafast processes include bond breakage and formation, vibrational relaxation, intermolecular rearrangement, and isomerization, all of which have been monitored in real time. By characterizing these processes in relatively simple chemical systems, it is possible to start to understand the behavior of other more complex systems that also go through these fundamental steps. Over the past decade,

many studies have focussed on establishing a framework for understanding the initial physical processes that take place during chemical reactions. We can now make use of this knowledge base to help distinguish between the many different physical and chemical processes that are observed while reactants are converted to products. In this way, the mechanisms of important reactions can be determined beginning with the initial ultrafast dynamics and continuing through the reaction kinetics all the way to the formation of the final products.

Organometallic chemistry is one field which has much to gain from the study of reaction mechanisms. Development has been rapid over the last several decades with the discovery of a wealth of new and useful reactivity and synthetic methods. The driving force behind much of the new research is the search for novel and efficient catalysts. Such rapid growth is particularly notable in the area of photochemistry because of the selectivity possible with light-induced reactions. Since many efficient photoreactions do not have thermal counterparts even when carried out under the harsh conditions of high temperatures and pressures, photochemistry is a valuable synthetic route for preparative chemists.

A specific challenge facing synthetic chemists is that of developing a method for using alkanes as starting materials for industrial organic synthesis. The difficulty arises from the fact that while alkanes are among the most abundant hydrocarbons present in petroleum feedstocks they are also some of the most unreactive species in organic chemistry. Their relatively inert nature is due to their strong C—H bond energies which are typically 90-100 kcal/mol. As a result, there has been considerable effort aimed at perfecting a catalytic process to break or 'activate' the C—H bonds and convert the alkanes

to other more reactive species such as alcohols and/or ketones. A large step toward this goal came when the first evidence of intermolecular photochemical C—H bond activation of alkanes by $Cp^*Ir(PMe_3)H_2$ was reported in 1982 [3]. When dissolved in alkane solution and irradiated with UV light, this molecule reacts with the alkane solvent, cleaving a C—H bond to produce products with Metal—Carbon and Metal—Hydrogen single bonds. This reaction represents the first step in functionalizing saturated hydrocarbons in a homogeneous catalytic process. Since then, many different complexes have been found to undergo this reaction and the chemistry has been extensively explored and utilized despite the fact that all of the individual mechanistic steps were not well understood. Indeed, a comprehensive, rational investigation into this industrially desirable C—H activation reaction cannot be complete without a detailed knowledge of the nature of the reactive intermediates involved in the reaction.

Here, the collaborative nature of my research becomes clear. Observation of these fleeting species requires the use of specialized ultrafast spectroscopic techniques, a field in which the Harris group has considerable expertise. At the same time, the ideal chemical systems are not usually commercially available and require considerable synthetic skills to produce in useable quantities, a task perfectly suited for members of the Bergman group. By combining a knowledge of the physical processes needed to understand chemical dynamics with a knowledge of the chemistry and reactivity of some complex reactions, my dissertation describes the significant progress we have made in organometallic chemical research.

Chapter 1 introduces the experimental techniques used in this study. In these

experiments, an ultraviolet pulse of light is used "instantaneously" excite the organometallic species. The energy deposited in the molecule may then initiate a chemical reaction by breaking a bond and/or be dissipated to the solvent. During these processes, the electronic (UV/Vis) or vibrational (IR) transitions in the newly created species are recorded as a function of time after the initial excitation.

In contrast to the UV/Vis technique, ultrafast infrared spectroscopy was not an established technique in our lab at the outset of my graduate study. Consequently, the goal of my initial work was to extend our group's effort to acquire spectroscopic capabilities in the infrared region. We attempted to adapt current visible systems for the IR using a separate CW infrared source and the technique of gated upconversion. This technique uses sum frequency generation of the IR source and a separate ultrafast visible pulse to detect ultrafast modulations in the CW beam. While it had the benefit of allowing the use of conventional CW IR sources such as a CO laser, the technique was not without its drawbacks. The biggest problems lied in the poor signal to noise of detection due to low IR intensity. This problem was accentuated by a low repetition rate. In an effort to develop a high power IR light source, I modified a CW CO laser to operate in pulsed Q-switched mode. By Q-switching the laser, we hoped that the increase in power over the duration of the pulse (effectively CW on ultrafast timescales) would be sufficient for use with gated upconversion at 10 Hz. While Q-switching was achieved, issues of stability and reliability ultimately ended this endeavor in favor of newer solid state laser techniques. We then shifted our efforts to building an infrared system based on a Ti:Sapphire oscillator and dye amplification.

Chapter 2 describes the first experiments done using our femtosecond IR spectrometer. As an initial study, we investigated the ultrafast dynamics of $M(CO)_6$ (M=Cr, W, Mo) dissociation in different alkane solutions. After UV photolysis at 295 nm, both the bleach of the parent molecules and the absorption of the pentacarbonyl intermediate were probed with 240 fs time resolution. The bleach recovery dynamics were found to be wavelength dependent, indicating that hot parent molecules are formed and that the bleach recovery time is determined by the vibrational cooling time. The measured percentage of bleach recovery in n-heptane is less than the expected value calculated from the photosubstitution quantum yield measurements, suggesting that the initial recovery of the bleach is faster than our time resolution. The kinetics of the A_1 vibrational mode region of the pentacarbonyl species have been measured to probe the formation and decay of the nascent product. The absorption of the product is formed with an instrument response limited risetime indicating that the generation of the product is much faster than 240 fs. The longer time kinetics in this region reflect the vibrational cooling of the product. A fast decay with time constant of less than 300 fs is present in all the wavelengths probed and its spectrum appears to resemble the early time spectrum of the hot pentacarbonyl species. This fast decay, observed in all three different metal carbonyls, is attributed to the fast geminate recombination of the pentacarbonyl with photodissociated CO ligand after only one to two collisions with the solvent cage.

Using picosecond transient absorption spectroscopy we began our investigation into C—H bond activation chemistry by examining the dynamics of $Cp^*Ir(CO)_2$ ($Cp^* = C_5Me_5$) in cyclohexane and $Cp^*Rh(CO)_2$ in n-pentane solution at room temperature

following 295 nm UV excitation. These experiments are detailed in Chapter 3. A transient absorption with an instrument limited risetime was observed for Ir from 440 to 740 nm and for Rh from 500 to 650 nm. Each transient can be fit to a biexponential decay consisting of a fast component of 2-3 ps and a slower component of 30-40 ps. These transients are attributed to excited state absorptions. Taking into account independent femtosecond IR studies of the ground state recovery, our data suggest that most excited state molecules relax through non-dissociative excited states, decaying to the ground state without the loss of CO. These results offer an explanation for the low C—H bond activation quantum yields observed on preparative irradiation of $Cp^*Ir(CO)_2$ and $Cp^*Rh(CO)_2$.

In order to study the actual chemistry involved in the C-H bond activation reaction, the dynamics of $Tp^*Rh(CO)_2$ (Tp^*=HB-Pz_3^*, Pz^*=3,5-dimethylpyrazolyl) was studied in room temperature cyclohexane and n-pentane solution after UV photolysis at 295 nm. The results of this work are detailed in Chapter 4. With a 30% quantum yield this molecule allowed us to generate a high enough concentration of intermediates to observe using ultrafast IR spectroscopy. We found that 50% of the bleach of the parent molecule CO stretching bands at 1981 and 2054 cm^{-1} recovers with a 70 ps time constant. A new vibrationally hot species with an absorption centered at 1972 cm^{-1} is formed immediately after photolysis which cools with a 23 ps time constant. This species is assigned to a solvated monocarbonyl intermediate. The vibrationally deactivated form of this intermediate decays with a 200 ps time constant to form a new species at 1990 cm^{-1} which was harder to assign. Separate experiments on the related $Bp^*Rh(CO)_2$ (Bp^* = H_2B—Pz_2^*, Pz^* = 3,5-dimethylpyrazolyl) complex revealed that this peak results from a

solvent complex in which one of the pyrazolyl arms dechelates from the Rh center. Observation of the C—H bond activated alkyl hydride necessitated the use of a technique like step-scan FTIR to monitor longer timescales. Using this technique, we showed that the final C—H activated product is formed in 230 ns. Taken together, these experiments represent the first direct observation of the intermediates involved and the overall timescale of the C—H oxidative addition in room temperature alkane solution.

References

1. R. G. W. Norrish, G. Porter, *Nature* **164**, 658 (1949).

2. W. Weaver, T. Gustafson, *Spectrochimica Acta Reviews* **15**, 527-579 (1993); J. D. Simon, *Review of Scientific Instruments* **60**, 3597-3624 (1989).

3. A. H. Janowicz, R. G. Bergman, *J. Am. Chem. Soc.* **104**, 352 (1982)

Chapter 1: Experimental

Nothing tends so much to the advancement of knowledge as the application of a new instrument. -Sir Humphrey Davy

***

1.1 Picosecond UV/Vis Spectrometer

1.1.1 Motivation: Ultrafast UV/Vis spectroscopy

Chemical reactions are fundamentally dynamic in nature. The rate at which molecular structures and energies change during a reaction is characteristic of the particular chemical process taking place. As a result, much can be learned about reaction mechanisms by measuring these parameters as they evolve. Because the eventual outcome depends so strongly on the physical processes taking place immediately after the reaction is initiated, a significant research effort has concentrated on characterizing these short time dynamics. As is common in the physical sciences, the development and availability of the necessary experimental instruments were crucial to the advancement of the field. In this case, the modelocked dye laser [1-3] was one of the first tools commonly used to study ultrafast dynamics. With the optimal cavity conditions determined by the laser dye, these oscillators operated in the visible portion of the spectrum. Based on these lasers, the first ultrafast spectrometers were designed to monitor changes in visible light absorption. This portion of the spectrum corresponds to molecular electronic transitions and recording ultrafast

changes in this region has yielded significant information about bond breakage and formation, vibrational energy transfer, and solvent caging.

1.1.2 Picosecond UV/Vis Spectrometer

The Ultrafast UV/Vis experiments described in this dissertation were carried out using a laser system based on an amplified synchronously pumped dye laser. This laser system was originally completed in 1983 and has therefore been previously described numerous times [4-6]. The layout of the system is shown in Figure 1.1. A modelocked argon ion laser operating at 76 MHz and producing 514 nm, ~100 ps pulses (3-5 nJ of energy per pulse) is used to pump the dye laser. In this configuration (R6-G dye), the output of the dye laser consists of 1-2 ps pulses centered around 590 nm. The pulses are extremely low in energy with only 200-400 pJ per pulse and must therefore be amplified. This is achieved in a three-stage amplifier line pumped by a frequency doubled, Q-switched Nd:YAG laser running at 10 Hz. Portions of the full ~250 mJ output of the Nd:YAG are sent to each of three amplifier cells with 4% going to the first cell, 6% to the second, and the remaining 90% going to the third. This amplification scheme produces a 10 Hz train of 1 ps, 1 mJ pulses centered around 590 nm.

Spectroscopic experiments are carried out using a pump-probe scheme in which one pulse excites the sample and induces a chemical/physical change in the test molecule. After a specified time delay, a second pulse interrogates the sample to monitor absorption changes as a function of time. Time delays are accomplished using a translation stage to adjust the distance the pump pulse travels with respect to the probe pulse. Taking into account the speed of light and the length of the stage, the longest time delay that can be

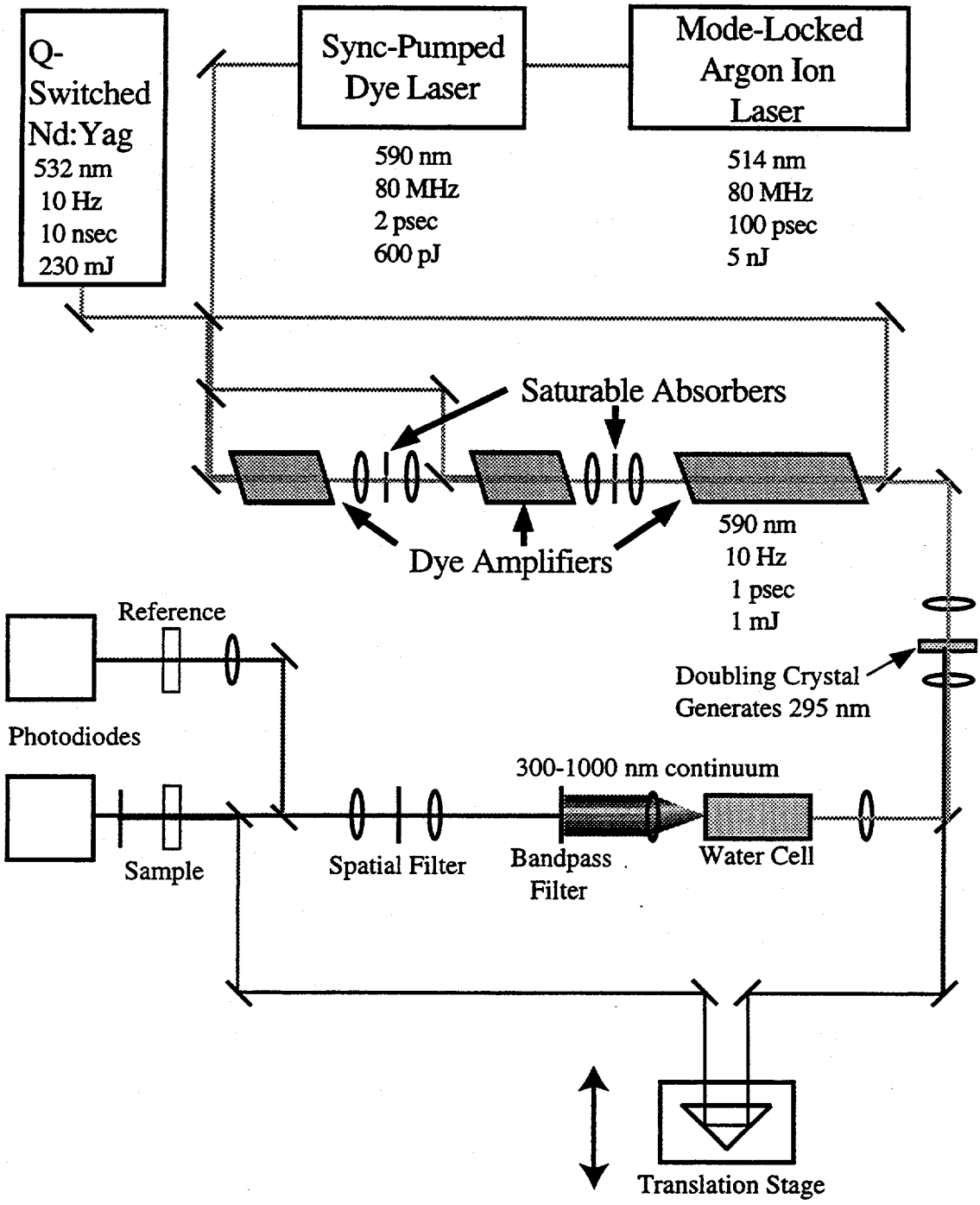

Figure 1.1 - Picosecond UV/Vis Spectrometer

achieved with a single round trip of the pulse down the entire 1 meter stage is approximately 6 nanoseconds. The minimum step size of the stage (10 μm) sets the minimum time step for the system at 66 fs. For UV excitation experiments, the pump pulse is generated by frequency doubling the amplified 590 nm output with a 1 mm KDP crystal which converts approximately 10% of the pulse into 295 nm. The remaining visible light is then separated from the UV pump pulse by a dichroic beam splitter and focussed into a water cell to generate an ultrafast continuum. Bandpass filters with 10 nm FWHM are placed after the continuum to select the desired probe wavelength. In order to maximize sensitivity, the probe beam is split into signal and reference channels. This configuration compensates for laser fluctuations in each pulse by measuring only the ratio of the signal to reference which is independent of the absolute laser power. The sample is placed in the signal beam path and the UV pump and Vis probe beams are overlapped inside the sample cuvette. The signal and reference beams are each focussed onto silicon photodiode detectors. Any UV light not absorbed by the sample is filtered out to allow only the probe beam to reach the detector. The output from the photodiodes is processed by gating, integrating, and then digitizing the pulses. Next the digitized pulses are transferred to a computer where the signal to reference ratio is calculated for each shot. Once the ratio is recorded, the computer moves the translation stage to the next stage delay setting before more shots are recorded. Averaging multiple pulses at a given delay position decreases the noise such that signals as small as 1 mOD can be measured.

1.2 Ultrafast IR Upconversion: Q-Switching the CO Laser

1.2.1 Motivation: Ultrafast Infrared Spectroscopy

The relative ease with which visible ultrashort light pulses were produced drove the initial wave of UV/Vis pump-probe experiments. Most of these experiments were carried out using small molecules with simple visible spectra, easing the task of assigning the transients. However, as more information was collected and organized on these molecules, the systems chosen for study became larger and more complex. As the molecular complexity is increased, the assignment of transients responsible for the overlapping electronic spectra becomes increasingly ambiguous. Consequently it is difficult to obtain accurate information about the structure of complex chemical intermediates from visible spectroscopy.

Infrared spectroscopy, on the other hand, does not suffer from the same drawbacks as visible spectroscopy. In the infrared region, spectra are composed of distinct, well-resolved peaks which are extremely sensitive to changes in molecular structure [7]. The major problem that has hindered the use of ultrafast infrared pump probe spectroscopy has been the lack of a suitable ultrafast IR light source. To solve this problem, researchers have developed several creative methods that obviate the need for an ultrashort pulse IR oscillator.

There are four main techniques which have been used to perform ultrafast IR spectroscopy. They can be grouped according to whether or not the IR sources are pulsed or CW:

Group I: Ultrafast IR Pulses	Group II: CW IR Sources
1. Optical parametric generation [8, 9]	1. Semiconductor Switching [10, 11]
2. Difference frequency generation [12, 13]	2. CW Gated upconversion [14]

Techniques in Group I make use of nonlinear optical processes to generate IR pulses from visible or near infrared (NIR) lasers. Time resolution is determined by the initial visible or NIR pulses. On the other hand, techniques in Group II begin with CW infrared sources and need external methods to measure dynamics. Here, time resolution is achieved using separate visible pulses to either (1) "chop" the IR beam to produce ultrashort IR pulses or (2) mix the IR signal with a visible pulse in a nonlinear crystal.

An initial test of semiconductor switching experiments in our laboratory using a CW carbon monoxide laser as the IR source yielded some data with signal to noise limited by low IR signal intensity [6]. After considering the low signal to noise ratio along with equipment requirements for other techniques, the decision was made to try gated upconversion (GU) as the next attempt to move in the direction of ultrafast IR spectroscopy. Like semiconductor switching, GU also has the distinct benefit of independent time and frequency resolution compared to other techniques in which these parameters are directly coupled through the uncertainty principle. The CO laser was chosen as the infrared source because of its 400 cm^{-1} tunability range in the vibrational infrared centered around 1800 cm^{-1}, and its relatively high power compared to other IR sources. Unfortunately, the results of preliminary upconversion experiments with a 10 Hz picosecond spectrometer revealed that the CW CO laser was not powerful enough for the

system to live up to expectations. These experiments showed that an inherent weakness in our implementation of the upconversion scheme was that the IR power was still too low to average away the noise at our slow 10 Hz rep rate. Specifically, the low IR power could not generate enough upconverted photons to allow the use of insensitive but linear photodiode detectors, instead requiring the use of sensitive but noisy photomultiplier tubes. At higher repetition rates (kilohertz) the noise from the PMTs could be decreased substantially in a reasonable amount of time by signal averaging but at 10 Hz, the time needed for averaging to the same extent was prohibitively long. After analyzing the problem for possible solutions which did not require an entirely new laser system, it was concluded that the only way to increase the upconverted signal without damaging the $LiIO_3$ upconversion crystal was to increase the power of the IR source.

1.2.2 The CO Laser

Before discussing the plan to increase the CO laser power, an explanation of some of the concepts behind this type of laser is in order. The laser medium consists of a mixture of gases including He, N_2, CO, and Air. High CO vibrational states are generated through two different pathways by a DC electric discharge running through the laser medium. After the discharge creates a plasma, the electrons in the plasma can either directly excite the CO (eq. 1.1), or they may excite the He (eq. 1.2) or N_2 (eq 1.3) which then transfer their energy to the CO through collisions (eqs. 1.4, 1.5).

$$CO + e^- \longrightarrow CO^* + e^- \quad (1.1)$$

$$He + e^- \longrightarrow He^* + e^- \quad (1.2)$$

$$N_2 + e^- \longrightarrow N_2^* + e^- \quad (1.3)$$

$$CO + He^* \longrightarrow CO^* + He \quad (1.4)$$

$$CO + N_2^* \longrightarrow CO^* + N_2 \quad (1.5)$$

$$CO^* \longrightarrow CO + h\nu \quad (1.6)$$

Infrared light is then emitted from vibrational-rotational transitions in the vibrationally excited ground electronic state of CO (eq. 1.6).

The design and operation of the Harris group CW CO laser has been previously described [6]. Briefly, it consists of a quartz laser tube with inlets on each end for inflow and exhaust of the gas mixture which is evacuated from the tube by a mechanical pump. The windows are made of CaF_2 and are permanently sealed on the ends of the tube at Brewster's angle. The active medium was 150 cm long inside a ~200 cm long cavity (depending on the cavity design) with a gold coated mirror on one end and a diffraction grating on the other (Figure 1.2). The grating was tuned such that the zeroth order diffraction was coupled out of the cavity and the first order diffraction was aligned with the end mirror. Electrodes at each end were fused to endcaps in the laser tube and supported a discharge of approximately 12 kV and 5-10 mA under lasing conditions. To control the spatial mode of the laser, irises were placed next to the Brewster windows on each side of the cavity and were generally closed down to 1 cm to produce a TEM_{00} mode. With liquid nitrogen cooling, laser output is tunable from 1600 cm^{-1} to 2000 cm^{-1}. The flowing configuration produced approximately 5 watts when all CO lines were lasing.

1.2.3 The Q-Switching Technique

The most hopeful method for increasing the power enough for upconversion to be effective with the existing laser system is Q-switching. Q-switching generates intense laser

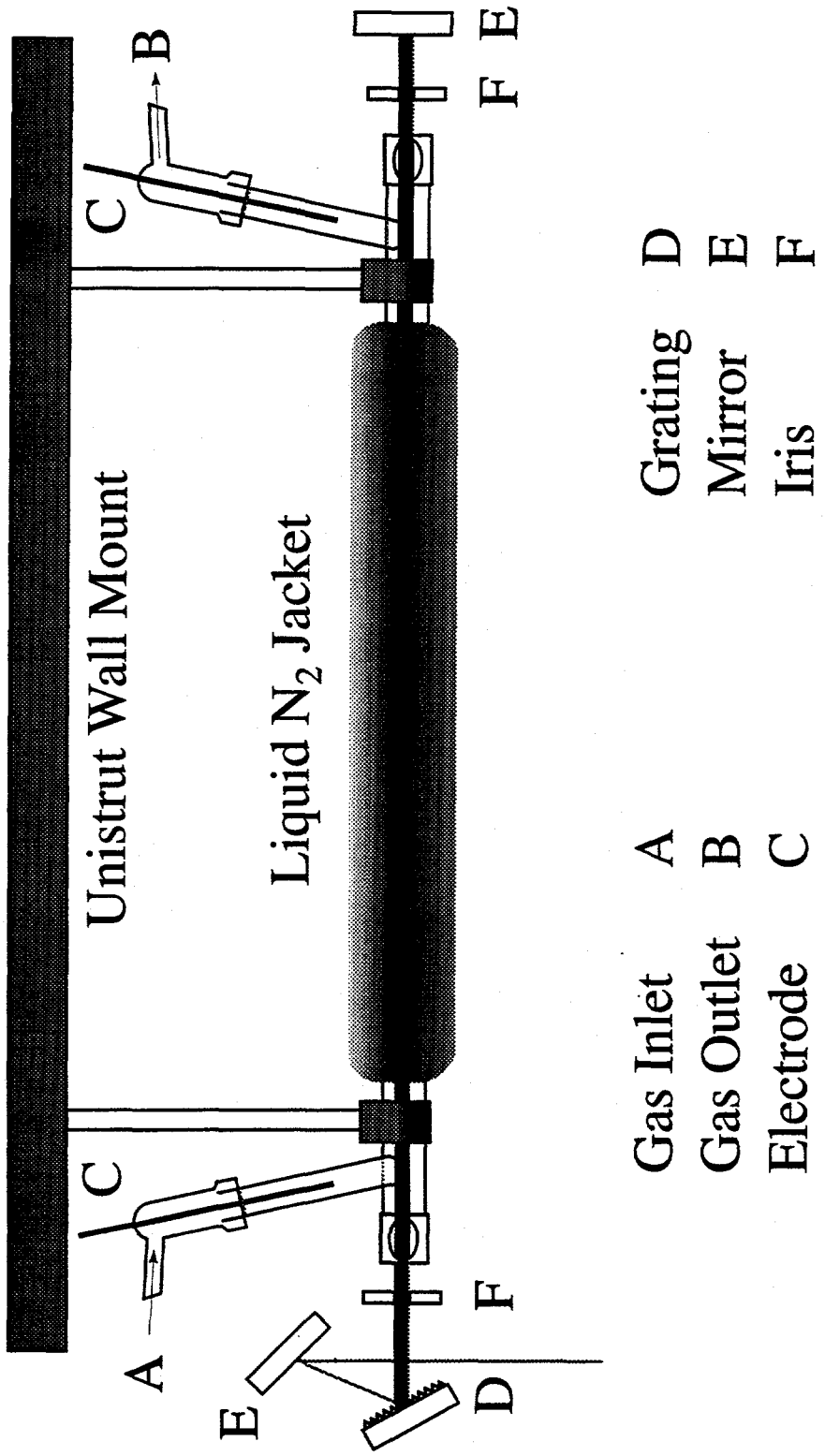

Figure 1.2 - The Layout of the CW Carbon Monoxide Laser

output in a short burst. In this technique, the laser cavity is initially blocked (lowering the quality factor, or Q, of the cavity), allowing the gain inside the lasing medium to build up to a much larger than usual population inversion [15]. Once this enhanced inversion is produced, feedback inside the cavity is restored and the cavity is allowed to lase. The rapid buildup of stimulated emission results in a short pulse with peak power that can be orders of magnitude larger than the CW power. This idea can be easily understood with the following description of a typical two-level system that shows gain at a frequency ν corresponding to separation between energy levels [16]. If the upper level is populated at a rate R by an electric discharge and has a relaxation time of τ, then the decay rate for an excited state population n is n/τ. Without a means of feedback at the frequency ν, the maximum population of the upper level is given by equation 1.7.

$$n_{max} = \tau R. \tag{1.7}$$

If the system is suddenly allowed to resonate at frequency ν, the buildup of coherent radiation inside the resonator will drastically reduce the population of the upper level. In this case, the power removed from the cavity from this burst of radiation or Q-switched pulse is given by equation 1.8 where P_Q is the Q-switched power and T is the width of the pulse.

$$P_Q = n_{max} h\nu / T = R h \nu \tau / T \tag{1.8}$$

The energy of the pulse is then given by

$$W_Q = P_Q T = n_{max} h\nu \ . \tag{1.9}$$

The Q-switched pulse may be as short as nanoseconds depending on the system gain since it may make only a few roundtrips through the resonator before returning to the CW power

level. For the most ideal case, this power level will be the rate of populating the upper level times the energy separation (eq. 1.9)

$$P_{CW} = Rh\nu = (n_{max}/\tau)h\nu \tag{1.10}$$

This approximate treatment leads to the following relations

$$P_Q/P_{CW} \sim \tau/T \tag{1.11}$$

$$W_Q \sim P_{CW}\tau \tag{1.12}$$

which show that for a laser system with a lifetime on the order of microseconds and sufficiently high gain such that T is on the order of nanoseconds, P_Q/P_{CW} may be as large as 10^3. While this treatment is approximate and ignores the influence of the laser level on the power output, it does indicate the potential benefits that Q-switching could have on increasing the power of our CO laser.

Since the invention of Q-switching in the early 1960's, several distinct methods for producing Q-switched pulses have been demonstrated. These include rotating mirrors, electrooptic and acoustooptic shutters, saturable absorbers, and thin film absorbers [15]. While each of these have found a place in various lasers, the only technique that had been previously applied to the CO laser was the rotating mirror [17-20]. Rotating the end mirror of the laser is one of the most direct ways of modulating the gain inside the cavity. The mirror is placed on a spinning motor shaft such that oscillation is only allowed to take place in the instant that the cavity is aligned. Although it is an inexpensive and simple approach to Q-switching, this method has several drawbacks which made it unsuitable for inclusion into an upconversion scheme. In addition to vibration and mechanical noise which complicate alignment, the most significant drawback is the inability to synchronize

the Q-switching time with the rest of the laser setup. This is because each of the critical parameters of repetition rate, high cavity Q time, and low cavity Q time are directly coupled. Therefore, we required another technique which allowed independent control over these parameters. Both acoustooptic and electrooptic modulators permit these parameters to be separately adjusted. Electrooptical Pockels cells have the benefit of extremely fast switching time ($\leq$10 ns), a large hold-off ratio and precise timing. However, these gains come with the expenses and complications associated with the electrooptic crystal and the fast-rising high-voltage power source. On the other hand, acoustooptics are much simpler, requiring straightforward Rf drivers and piezoelectrics to modulate the gain. The simplicity of its operation compared to the Pockels cell made the disadvantages of relatively slower opening time and lower hold-off ratio worth the initial trade.

1.2.4 Application of Q-Switching to the CO Laser

The practical matter of modifying the CO laser for Q-switched operation revolved around the choice of a suitable modulator and the adjustment of the laser cavity to accommodate the additional element. An acoustooptic modulator (AOM) is composed of three main elements: a diffractive crystal, a piezoelectric acoustic transducer, and an Rf driver. The crystal must have a density dependent index of refraction and must be transparent in the lasing region. If an Rf signal is relayed to the piezoelectric, an acoustic wave is generated within the crystal, creating a Bragg diffraction grating which deflects a percentage of the light out of the intracavity beam. This reduces the Q of the cavity, thereby inhibiting lasing and allowing the population to build up. When the signal is

removed, the grating disappears. This restores the Q, leaving the crystal free to transmit the intracavity light and allowing laser oscillation. In designing the acoustooptic, it is important to minimize reflection of the acoustic wave to keep it from reducing the diffraction efficiency of the Q-switch. Generally, a damping material is used to absorb most of the energy of the sound wave while the residual energy is made to reflect back off axis by angling the crystal side opposite the transducer. Because of its transmission and index of refraction characteristics, the optical module for these experiments was composed of anti-reflection coated germanium crystal. It was purchased from the Brimrose Corporation, model number GEM 4-1. A standard TTL pulse generator was used to control the model FFA-40-B2-F15 Rf driver. A diagram of the Q-switch and control electronics is shown in Figure 1.3.

For a slow opening AOM, the build-up time of the pulse can depend on the time needed to open the Q-switch. A faster switch will create a shorter pulse, leading to a higher peak power. The switching speed itself depends on the sound velocity within the block of transparent material and on the diameter of the laser beam because the switching time is effectively the time required for the sound wave to traverse the beam path. Hence, the smaller the intracavity laser beam, the faster the speed of the Q-switch. During CW operation, the beam diameter of the CO laser was set to 1 cm. With a Q-switch rise time of .18 μs/mm, the time needed to open the switch at this diameter is almost 2 μs. This is an order of magnitude longer than the ~100 ns pulsewidths we expect based on previous work. To optimize the performance of the Q-Switch, the laser cavity had to be altered to ensure that the beam diameter was approximately 1-2 mm. A pair of lenses was inserted

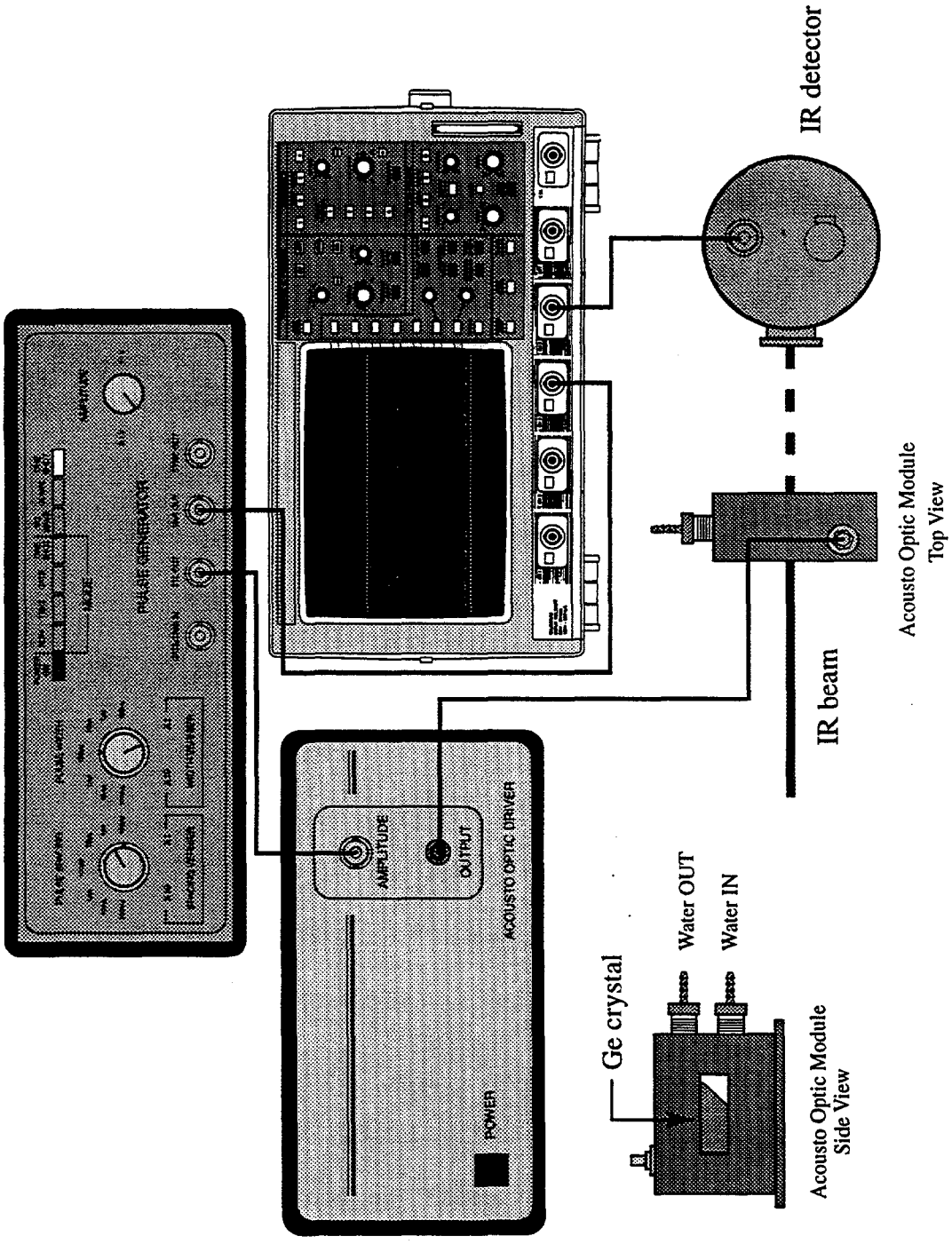

Figure 1.3 - Q-Switch Electronics Layout

into the cavity (see Figure1.4) to telescope the beam in order to decrease the size of the intracavity beam without closing the irises and lowering power. The lens assembly consisted of a plano-concave and a plano-convex lens set approximately 17-18 cm apart depending on the overall cavity length (to compensate for collimation). This served to decrease the beam diameter by a factor of 5 and maintain the necessary collimation and laser power.

In addition to having a fast opening time, the Q-switch must also extinguish the laser cavity as much as possible to allow the population to build up to its maximum. Since the 50% diffraction efficiency of the AOM is relatively low, the ability of the Q-switch to block the cavity had to be checked. One way to determine the switching ability is to measure the time needed for oscillation to build up in the cavity. The buildup time T_b is given by equation 1.13: [15]

$$T_b = \frac{1}{r-1}\left(\frac{T}{\delta_c}\right)\ln\left(\frac{n_{ss}}{n_i}\right) \tag{1.13}$$

where r is the normalized inversion ratio, T is the round-trip time inside the laser cavity, δ_c is the fractional power loss per round-trip, n_{ss} is the steady state photon number, and n_i is the initial photon number. The inversion ratio itself is defined as

$$r \equiv \frac{N_i}{N_{th}} \tag{1.14}$$

with N_i as the population inversion immediately after opening the switch and N_{th} as the threshold inversion just after switching. The ratio can be used to determine how well the Q-switch blocks the cavity because the value of the ratio depends on the extent of inversion built up while the cavity was "blocked". Since the build-up time is inversely proportional to the normalized inversion ratio, and the rest of the parameters are fixed for the CO laser, a

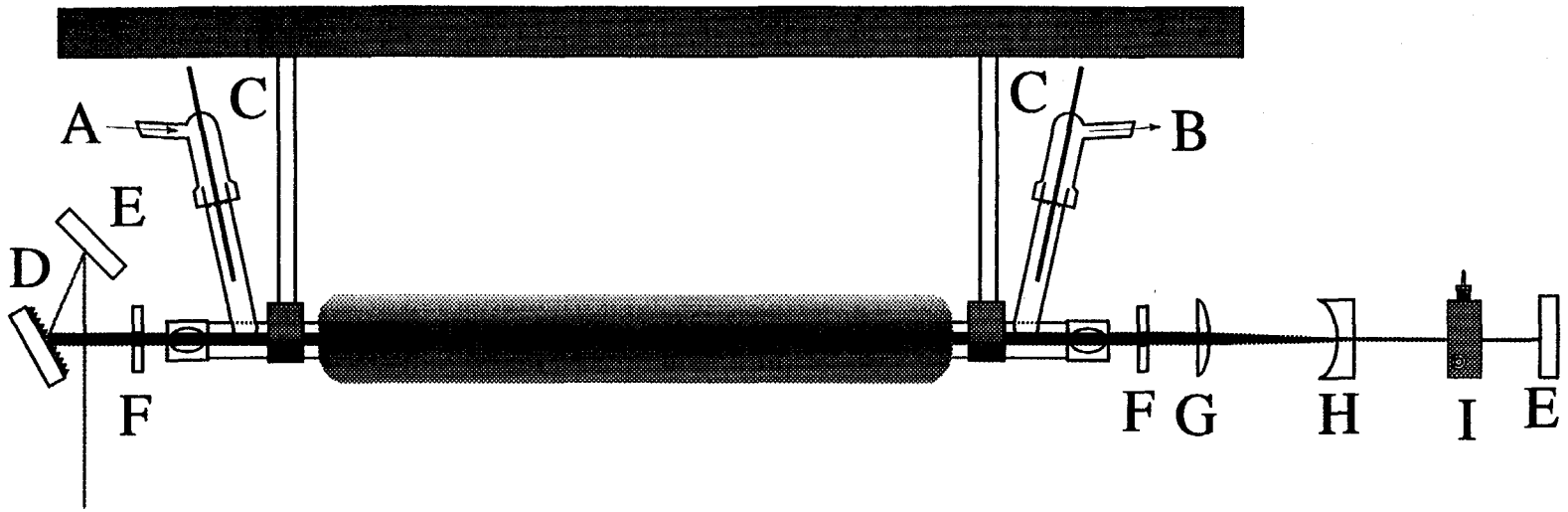

Gas Inlet	A	Iris	F
Gas Outlet	B	Convex Lens	G
Electrode	C	Concave Lens	H
Grating	D	Q-switch Module	I
Mirror	E		

Figure 1.4 - Carbon-Monoxide Laser Setup

measurement of the time can be used to determine the inversion ratio and find out how well the cavity is optimized for Q-switching.

The Q-switch was placed inside the laser cavity and the timing adjusted so that the switch was repeatedly opened for a chosen time and then closed for 500 μs (the recovery time is 350 μs [17] such that the laser should be fully recovered by the time the switch opens again). The average power was measured while the switch was modulated and then the open time was changed to a new value. Q-switch open times were varied over a series of intervals ranging from 520 μs to 10.7 ms. Recorded laser powers could be fit to an exponential curve corresponding to a build-up time of 690 μs (Figure 1.5). Using this value along with 13 ns for T, .01 for δ_c from our CO laser system, and the reasonable value of 10^{11} for $\frac{n_{st}}{n_i}$ [15], we find an inversion ratio r of only 1.05. This tells us that the laser is being pumped only 20% above threshold, indicating that the Q-switch is not fully extinguishing the cavity and that there is a significant amount of light leaking through during the diffracting interval.

One reason for this marginal cavity blocking is that the diffraction angle is quite small at only 11 degrees and lasing is still possible over a meaningful range of adjustment in the end mirror angle. Since the Q-switch is so close to the end mirror in this configuration, it is possible that the light that should be reflected out of the cavity is still within an acceptable lasing angle. To fix this problem, the cavity had to be lengthened to make sure that the diffracted light would strike the end mirror at an angle that would not allow it to lase. The laser was situated close to the edge of the optical table making it difficult to extend the cavity in the same configuration. Before moving the entire laser,

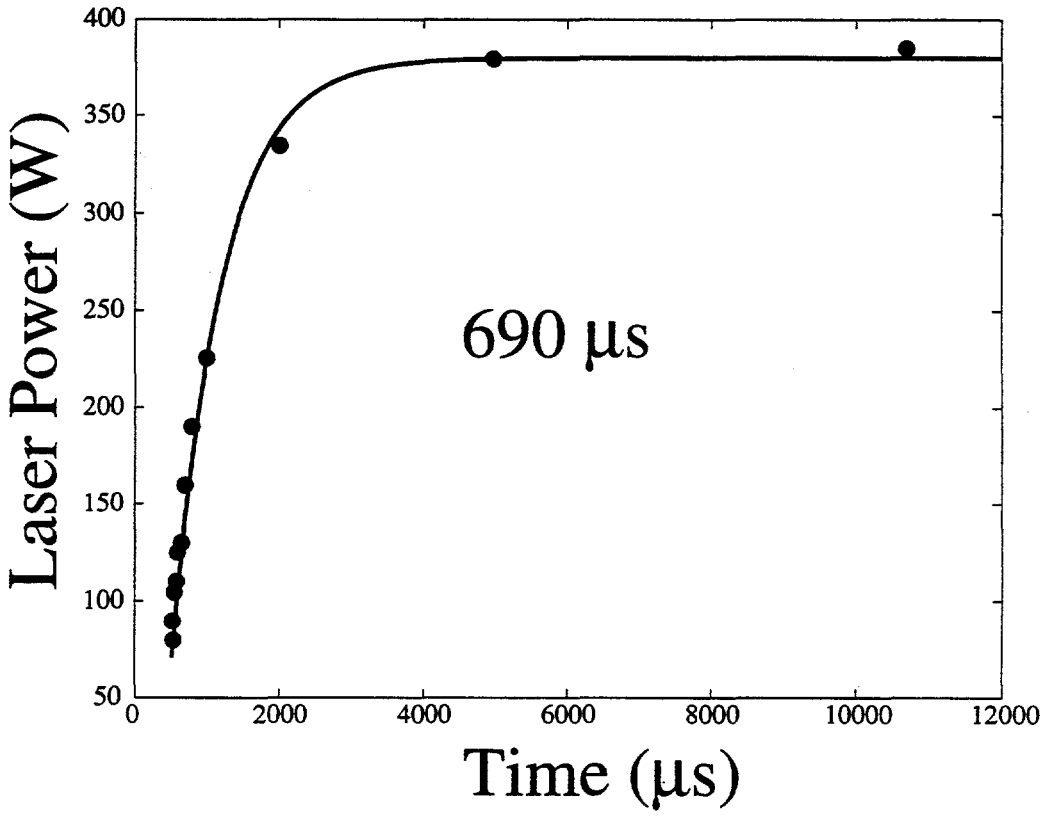

Figure 1.5 - CO Laser Power as a function of time with corresponding exponential fit.

several folded cavity designs were tried. Examples of these layouts are shown in Figure 1.6. These cavity designs had the benefit of allowing room for diagnostic tests of diffraction efficiency (50-60% depending on the cavity) and maximum collimation distance (cavity should be limited to ~220 cm from end of laser tube to end mirror). Unfortunately, the inability to maintain sufficient collimation over a convenient folded cavity length made these designs impractical.

After moving the laser, the linear cavity was rebuilt and optimized. In Q-switched operation, the most reliable results were achieved running at 20 KHz. Pulses of ~250 ns were recorded with an average power of 75 mW. A typical pulse is shown in Figure 1.7. This translates into a peak power of only 15 watts, substantially lower than originally expected. For these experiments, the Q-switch is kept open for 550 ns to allow the pulse to build up and then closed for another 50 μs to allow the laser to recover. While this time is significantly shorter than the 350 μs recovery time mentioned earlier, it is reasonable because of the low hold-off ratio of the acoustooptic. Since the laser is never completely extinguished, the maximum population inversion that can be achieved inside the cavity is a fraction of the optimal inversion possible for a completely blocked cavity. When the population inversion is depleted and the shutter is closed, the time needed to recover to the reduced inversion level is less than that for a completely extinguished (higher inversion ratio) cavity. This situation also explains the low Q-switched pulse peak power.

1.2.5 Conclusions

At this point, strategic decisions concerning our ultimate goal of ultrafast IR spectroscopy had to be made. While Q-switched pulses were realized, a combination of

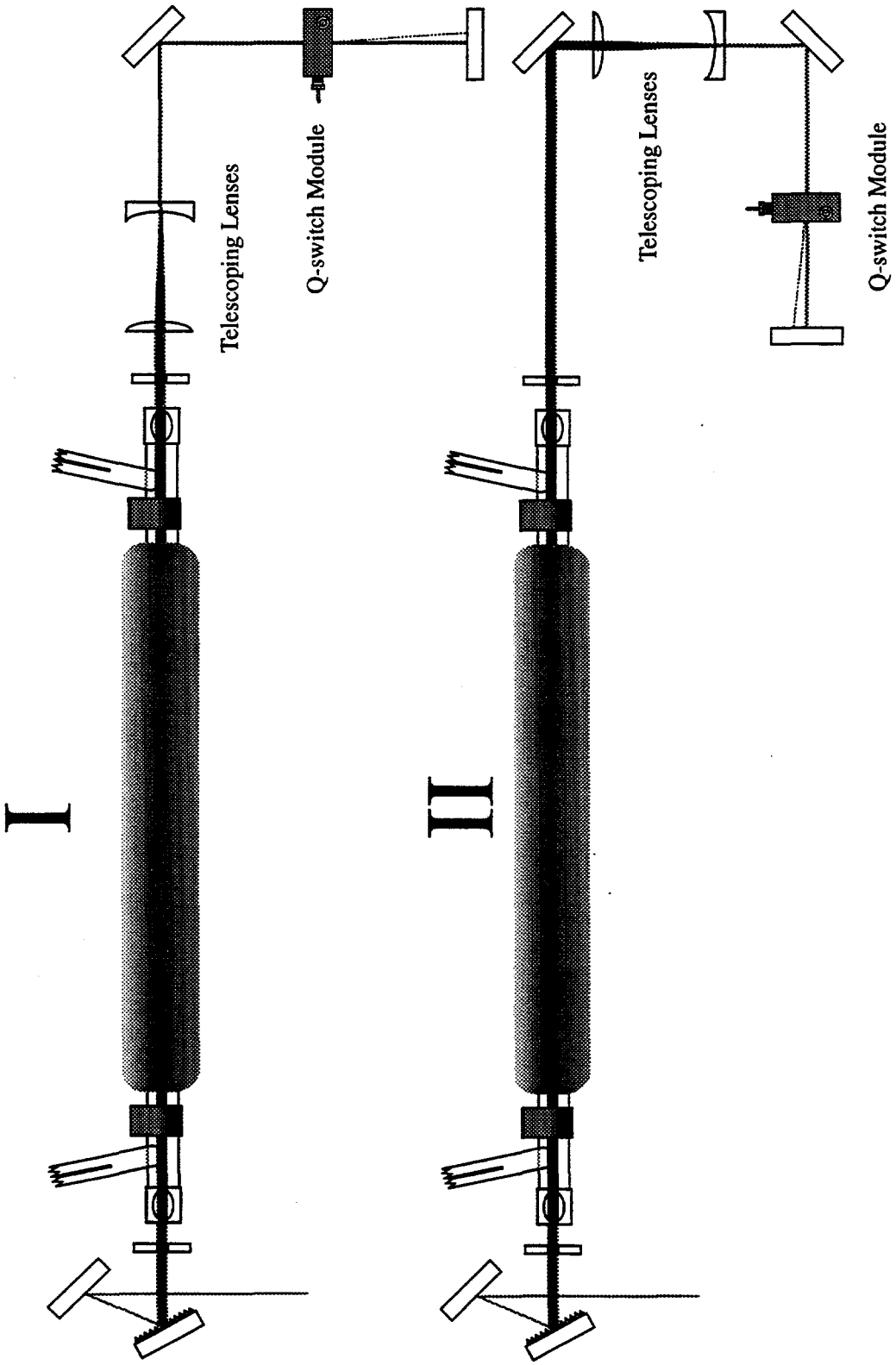

Figure 1.6 - Folded cavity designs

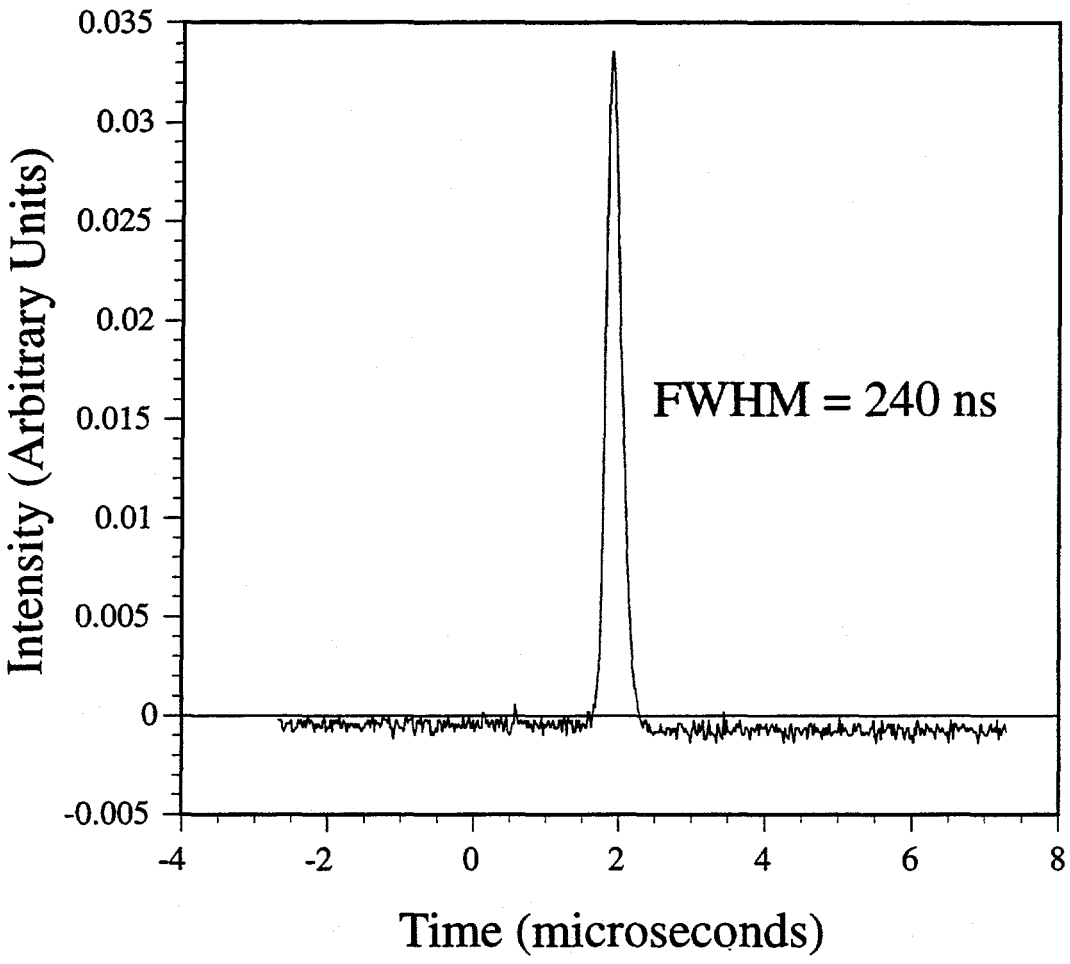

Figure 1.7 - Q-switched CO Laser Pulse

difficulties and emerging opportunities eventually led us to terminate the project before it was fully completed. Aside from the problem of low Q-switched power, which may partially be due to low CW power, there was also the issue of stability. With a great deal of effort, it was possible to align the CO laser to generate fairly uniform pulses. However, the slightest agitation (for example, water running through the Q-switch module, vibrations in the laser table, adjusting optics) was enough to disrupt the pulse train.

In retrospect, using a CO laser to do gated upconversion at a low repetition rate (even had Q-switching been ultimately successful),was probably not the best choice to move into the field of ultrafast IR spectroscopy. Ultrafast systems that used lower power commercial sealed-tube CO lasers were then in operation, compensating for the low signal to noise ratio by running at kilohertz rep rates and doing extensive signal averaging [14]. While fairly straightforward in its operation, the chemical nature of the laser also made it much less reliable than the emerging solid state ultrafast lasers that made difference frequency generation a much more attractive route.

1.3 Ultrafast IR Difference Frequency Generation

1.3.1 Motivation: Moving to Solid State Technology

Progress in ultrashort light pulse generation has historically been represented by advances in dye laser technology including the synchronously pumped dye laser [1-3] and the colliding pulse mode-locked (CPM) dye laser [21]. These lasers have been the standard tools for studying ultrafast dynamics over the past decade. One of the directions that ultrafast pulse research has taken in order to improve upon the dye-based systems is in the

area of new gain media. Specifically, solid-state media like the titanium doped sapphire laser have been supplanting dye based systems as the most popular ultrafast sources since modelocking was demonstrated in the Ti:sapphire system in the late 1980s [22-27]. Several characteristics make Ti:sapphire a better alternative ultrafast source. It has the broadest tuning range of any conventional laser with a bandwidth four times larger than organic dyes (660-1180 nm). The sapphire host is easy to handle, free from chemical degradation, and has a better thermal conductivity than dye solutions allowing it to handle substantially higher pump powers. In addition, the lack of a flowing dye solution increases the stability of the Ti:sapphire laser, which is crucial to sustaining modelocked operation. Because of the difficulties involved in the upconversion scheme, and all of the benefits of the new solid state technology, we decided to move our efforts to a Ti:sapphire based difference frequency generation system which is described in the next section.

1.3.2 Femtosecond IR Spectrometer

The ultrafast apparatus used in these studies is shown in Figure 1.8 and consists of a Ti:Sapphire oscillator [28] and dye amplifiers pumped by a 30 Hz Nd:YAG laser. The output of the Ti:Sapphire oscillator is amplified in a two-stage LDS 798 dye amplifier and compressed using a pair of prisms to produce 10 μJ pulses with 50 fs pulse width at 820 nm. This amplified light is then split into three beams. One beam is further amplified to obtain 20 μJ pulses at 820 nm with pulse widths of approximately 70 fs. The other two beams are used to generate two separate sources of white light continuum in sapphire windows. Desired wavelengths of the white light are selected by two band pass filters each having a 10 nm FWHM window and then amplified in two three-stage dye amplifiers to

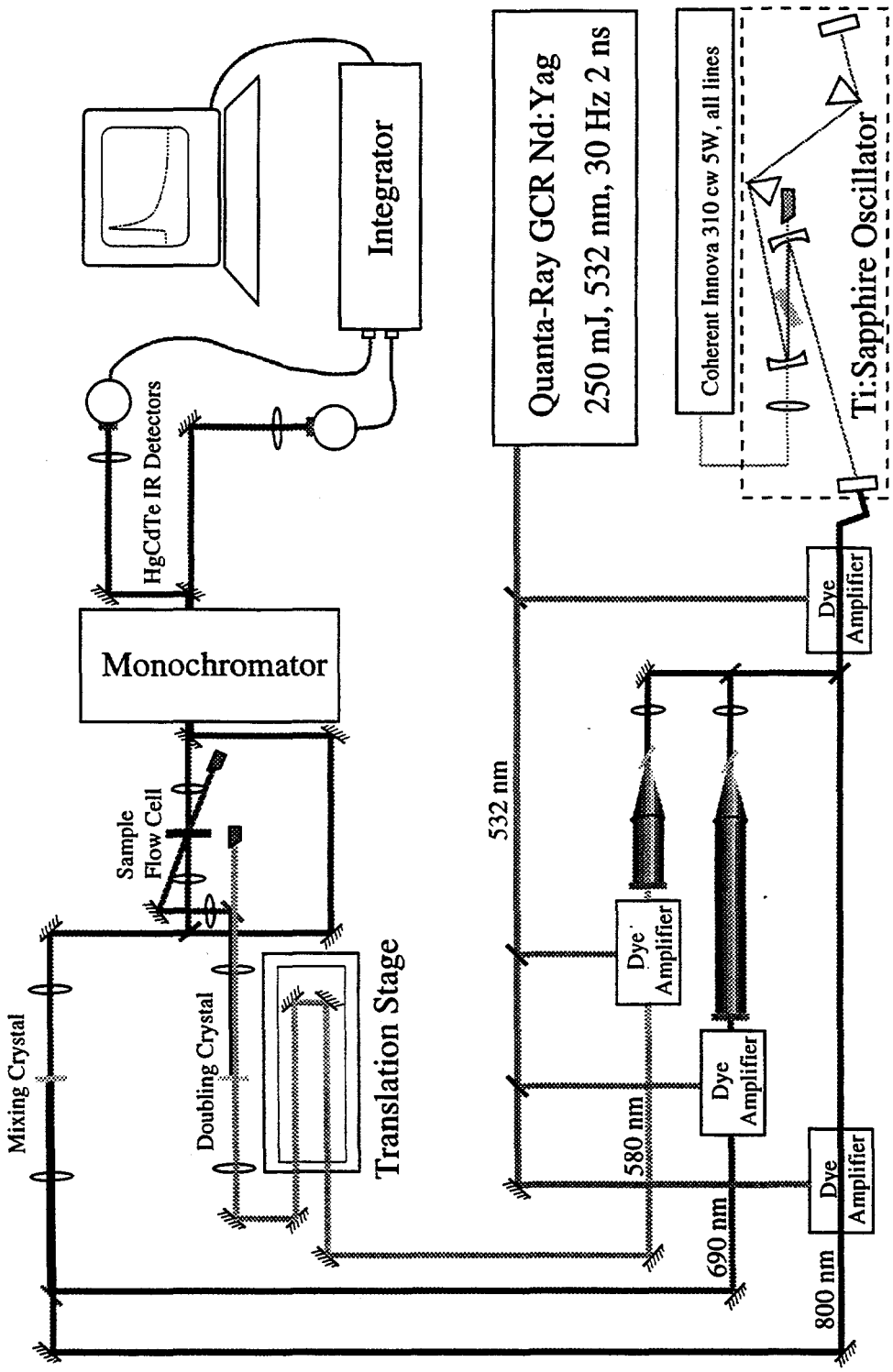

Figure 1.8 - Tunable Femtosecond Infrared Spectrometer

produce two independently tunable fs pulses from 560 nm to 1000 nm. For this experiment, LDS 698 is used in one amplifier chain to obtain 100 μJ, 700 nm pulses. Rhodamine 610 is used in another amplifier chain to produce 400 μJ, 590 nm light. The 590 nm light, which is compressed by a pair of prisms to shorten the pulse width to about 200 fs, is frequency doubled in a 300 μm thick BBO crystal to generate UV light at 295 nm. IR pulses in the 5 μm region are generated by mixing the amplified pulse at 700 nm with the 820 nm pulse in a 2 mm $LiIO_3$ crystal. The FWHM of the IR pulses is about 80 fs. The spectral band width is approximately 200 cm^{-1}, limited by the phase matching condition of the $LiIO_3$ crystal. By simply adjusting the phase matching angle, wavelengths from 1800 cm^{-1} to 2300 cm^{-1} can be generated without changing band pass filters. IR pulses in the 3 to 6 μm region can be generated by changing the band pass filters and the dye for the amplifier. The important feature of this system is that it produces two independently tunable fs pulses in addition to the 820 nm pulses, allowing us to generate independently tunable pump and probe pulses in UV, Visible and IR region.

The 590 nm beam is sent through a variable delay line before being frequency doubled. The resulting UV beam, focused to a spot size of 200 μm at the sample, is used to initiate the photoreaction. The subsequent changes in the IR absorption are probed by the IR beam. The probe IR beam is split into a signal and reference beam by a 50% Ge beam splitter. The signal beam, focused down to ~200 μm in diameter at the sample, is overlapped with the pump beam and recollimated afterwards. Both the signal (after the sample) and reference beam are then focused into a monochromater (CVI, Digikrom 240). The two beams travel parallel to each other, displaced vertically by 1 cm along the direction

of the monochromater slit. The slit size is variable from 10 μm to 2 mm. The IR beam size at the slit is about 300 μm and the slit is set to 400 μm during normal operation. The two beams are separated after the monochromater and focused onto a matched pair of liquid N_2 cooled HgCdTe detectors. The outputs from the two detectors are sent to two boxcar integrators and a digitizer. The high and low bounds from the signal and reference channels are set to be + 40% and - 40% of the average counts. The counts from the signal and the reference channels are normalized to remove shot to shot laser fluctuations. The fluctuation of the IR pulse intensity is normally in the 10% to 40% range. This normalization scheme gets rid of the noise caused by the probe laser fluctuations. As a result, the noise of the system is dominated by the dark counts of the detectors. The typical noise of the system after averaging 100 laser shots is about 0.1%. The time dependence of a signal at a particular wavelength is collected by setting the monochromater at a fixed wavelength and changing the delay of the UV pump beam. A spectrum is recorded by scanning the monochromater while the pump pulse is fixed at a given delay time. The spectral resolution is determined by the resolution of the monochromater. A 150 groove/mm grating is used in the monochromater and the slit width is set at 400 μm, leading to a wavelength resolution of about 4 cm^{-1}. The time resolution of the system is determined by the cross correlation of the pump and probe beams, which is about 240 fs for this experiment. The instrument response can be measured in a thin silicon wafer. A UV photon excites the electron into the conduction band giving rise to broad IR absorption (Figure 1.9). The rise time of the absorption signal, which is limited by the instrument response function, is well fitted by the integration of a gaussian function with a FWHM of

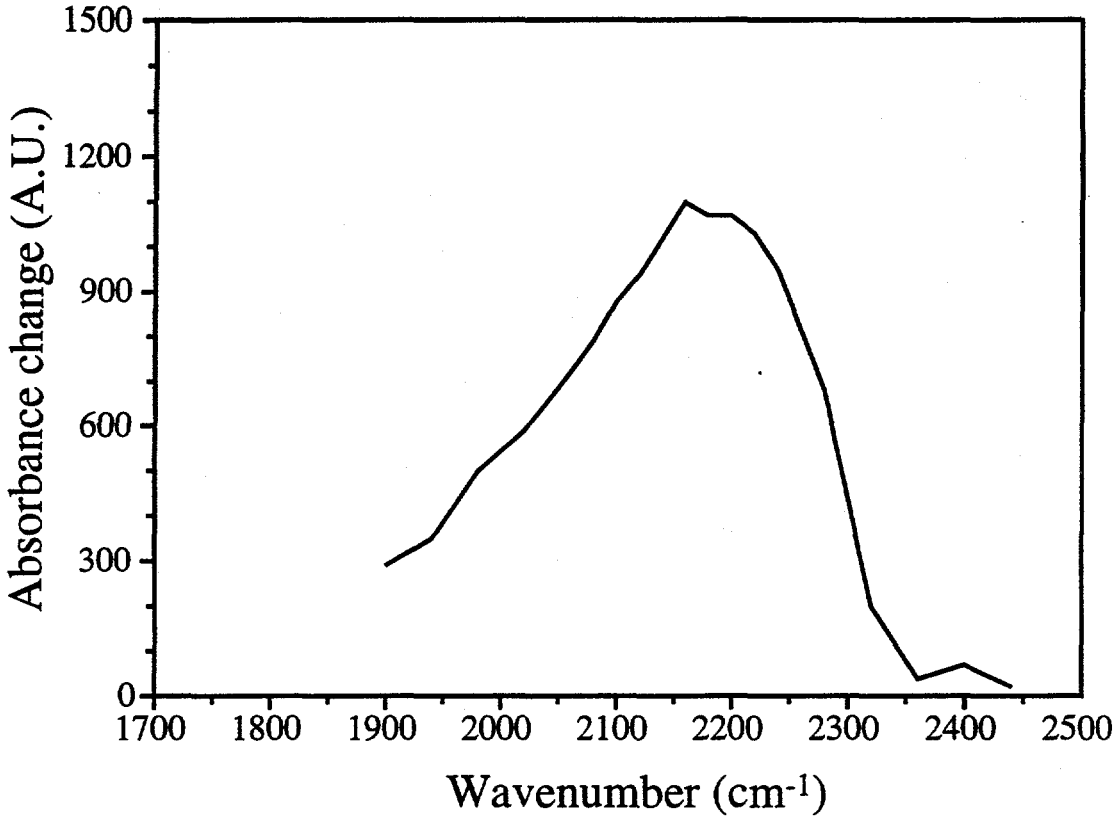

Figure 1.9 - Spectrum of IR pulse

240 fs (Figure 1.10). A more detailed description of the design and alignment of this system is in preparation [29].

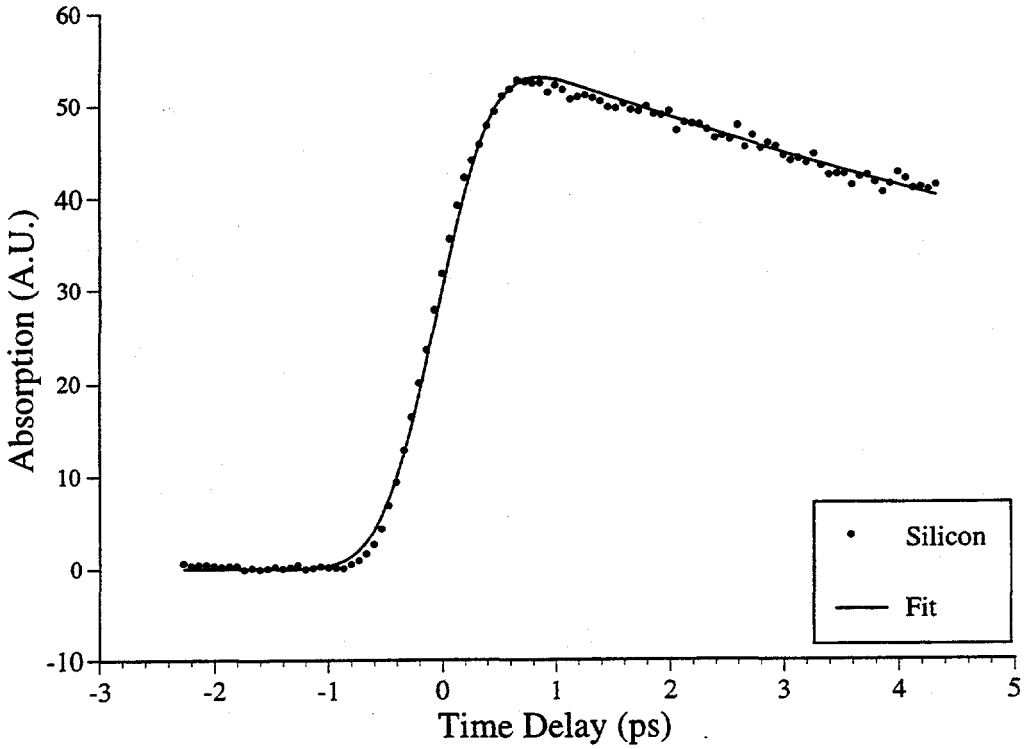

Figure 1.10 - Determining the T_0 and cross-correlation of the laser pulse.

1.4 Step-Scan FTIR Spectroscopy

1.4.1 Motivation: The Multiplex Advantage

One of the most intriguing aspects of monitoring chemistry as it takes place is the incredible range of timescales spanned during the reaction. For example, unimolecular events such as bond cleavage can take place in femtoseconds (10^{-15} s) and bond formation and energy dissipation need only picoseconds (10^{-12} s) to complete. The timescale for these individual events contrasts greatly with the timescale typically associated with the overall reaction which is often controlled by the rate of diffusion in the solvent ($<10^{-9}$ s). As a result, observation of all the different species produced throughout a chemical reaction requires the use of spectroscopic techniques designed for tracking chemical changes over these longer timescales. In principle, the same pump probe method used in the ultrafast experiments can be employed in the nanosecond regime. In practice, however, more efficient instruments take advantage of sufficient detector time response and multiplexing technology. Perhaps the best example of this concept is step-scan fourier transform infrared (FTIR) spectroscopy.

1.4.2 Step Scan FTIR Spectrometer

The spectrometer used in these experiments (Figure 1.11) has been reconfigured several times during the course of these and other ongoing experiments. Details of the modified Bruker IFS88 FTIR spectrometer including the electronics and optics are described elsewhere [30, 31]. The idea behind step-scan FTIR is quite ingenious. In a conventional interferometer, data is collected while the moving mirror continuously scans back and forth. This process generates a single static interferogram. However, in

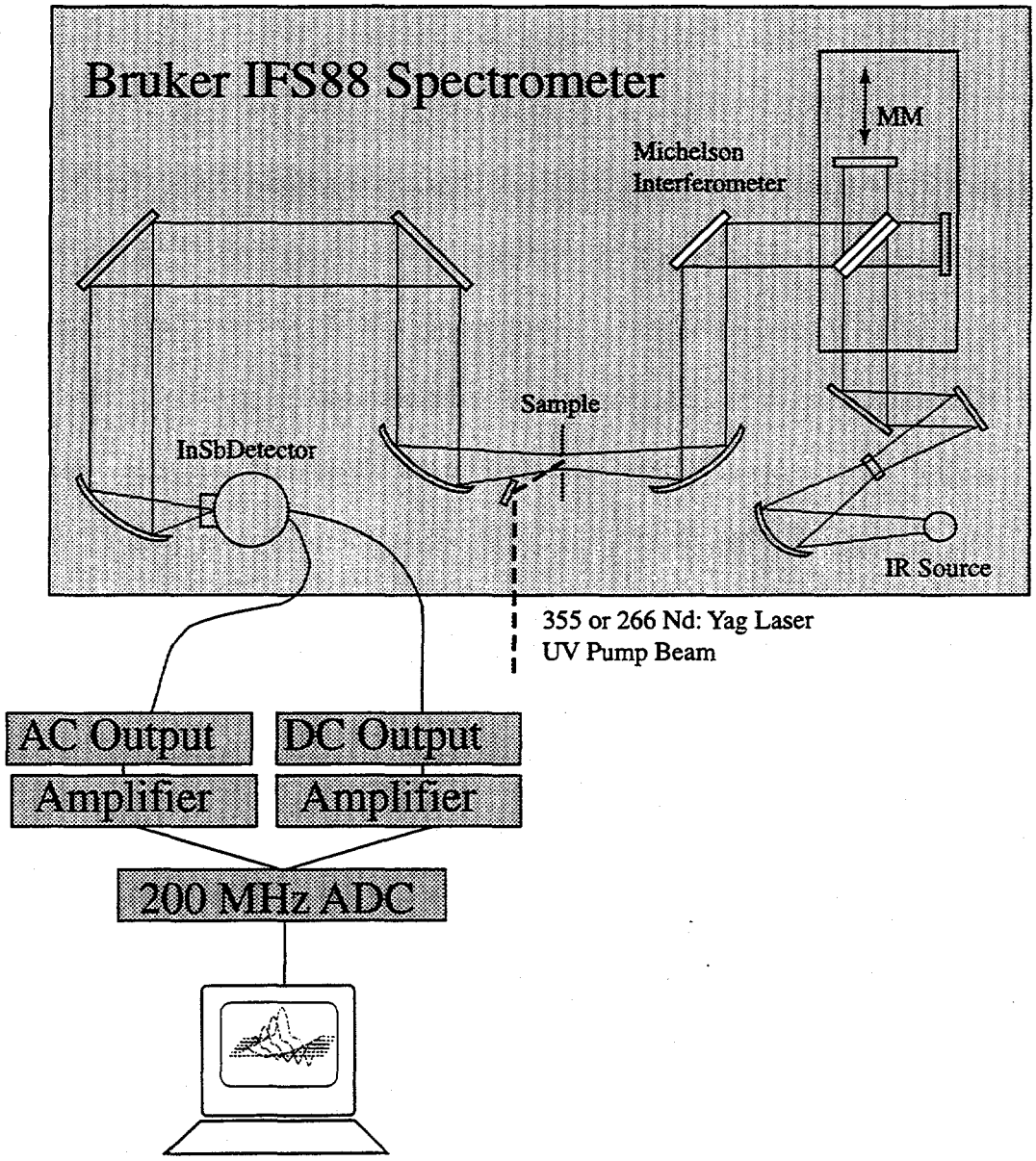

Figure 1.11 - Step-Scan FTIR System

step-scan mode, the mirror is moved through its path in small steps while laser pulse induced dynamics in the sample are recorded at each mirror position. After a number of flashes are averaged, the mirror is moved to its next position and the process is repeated over the entire range of the mirror. When the data collection process is completed, the computer assembles a set of time resolved interferograms which are Fourier transformed into time resolved difference spectra.

Transient absorption spectroscopy relies not only on the overall spectral change in intensity but also on the background spectral intensity. As a result, the single beam spectrum of the sample must also be recorded. To accomplish this, a special HgCdTe detector with simultaneous AC and DC outputs was used. First a DC coupled scan was taken without sample excitation. This data was saved and used to calculate the phase and single channel DC spectrum. Following measurement of the time resolved interferograms, the stored phase from the DC scan is used to rearrange the data to time resolved difference interferograms before they are Fourier transformed.

Because the sensitivity of the instrument is highly dependent on the stability of the stepping mirror position, great care was taken to minimize acoustic and mechanical noise in the laboratory while experiments were conducted. A floating optical table was used to isolate the spectrometer from building vibrations and all ventilation systems were disabled during data acquisition. The sample necessitated special handling as well. To avoid vibrations from the peristaltic sample pump, the airtight system was flowed from a main sample tank to another smaller reservoir held several feet above the laser table. The flow was maintained through the cell only by gravity while the pump kept the level of solution

constant in the reservoir constant. With all of the improvements to the system and our optimization of the experimental conditions, scans with 50 ns time resolution, 4 cm^{-1} frequency resolution took approximately 5 hrs. to achieve a signal to noise ratio of 10:1.

Chapter 2: Femtosecond Infrared Studies of the Dissociation and Dynamics of Transition Metal Carbonyls in Solution

We always thought that if we knew what "one" is we would also know what "two" is. For "one plus one makes two". Now we slowly realize that we still have a lot to learn about the "plus". -Sir Arthur Stanley Eddington

***

2.1 Introduction

Photolysis of transition metal carbonyls produces short-lived coordinatively unsaturated metal carbonyl intermediates, many of which are involved in important industrial or synthetic reactions [32-35]. Knowledge of the initial formation, relaxation and reactivity of these intermediates is therefore crucial to the understanding of the overall reaction mechanism. For this reason, the photochemistry of transition metal carbonyls has been extensively studied by ultrafast laser spectroscopy [14, 36-60]. In particular, with the advent of femtosecond infrared spectroscopy, a technique pioneered by Hochstrasser and coworkers [61], the detailed structure of short-lived reactive intermediates can be directly studied. The metal hexacarbonyls, $M(CO)_6$ (M=Cr, W, Mo), have long been used as model systems for the study of transition metal carbonyl photochemistry. Laser photolysis of gaseous $M(CO)_6$ under collisionless conditions proceeds through the loss of several carbonyl groups [62-65]. In a liquid solution [66] and low temperature matrix [67],

however, UV photolysis leads to efficient loss of a single CO ligand to form a pentacarbonyl intermediate. The lack of multiple CO ligand loss was attributed to the efficient energy relaxation of the highly energized metal carbonyl intermediates in the condensed phase environment [54-56]. Picosecond time resolved experiments indicate that the naked pentacarbonyl species, $Cr(CO)_5$ is solvated within 1-2 ps in methanol [46-50][51, 52] and cyclohexane [46-50]. The subsequent vibrational cooling of the solvated intermediate has been extensively studied by transient visible [36-40][46-50][51, 52] and IR [43-45] absorption spectroscopy and resonant Raman spectroscopy [68]. As a result of the photolysis, both the high frequency CO stretching mode and other low frequency modes are excited. While the isolated high frequency CO stretching modes relax on the 150 ps time scale [36-40][43, 44, 69][53], the low frequency modes in the molecule relax more rapidly, taking 10s of ps [36-40][43, 44, 69]. The time scale for the vibrational relaxation of these CO modes is similar to that of the parent molecules measured in IR pump and IR probe experiments [70-75].

While the solvation and vibrational relaxation of the pentacarbonyl species are well characterized, the early time dynamics such as dissociation and cage recombination are not as well understood. UV/Vis spectra of these molecules in alkanes show a strong singlet transition around 290 nm and a weaker triplet transition around 355 nm. It is not clear whether dissociation occurs from the singlet or triplet excited states. Wavelength dependent photosubstitution quantum yield measurements on $W(CO)_6$ in n-hexane solution have shown that the quantum yields are the same for excitation wavelengths ranging from 254 nm to 366 nm [76]. This suggests that dissociation proceeds from the lower lying

triplet state, and that there is an effective intersystem crossing from the singlet state to the triplet state. Femtosecond spectroscopic studies on these molecules [51, 52], however, suggest that dissociation may occur in the singlet state, as will be discussed in detail later. This model was also invoked in an earlier photoluminescence measurement in a low temperature gas matrix [77, 78]. The photosubstitution quantum yields in various solvents have been measured, ranging from 0.42 to 0.93 depending on the solvent [79, 80]. These yields should be interpreted as the yield for formation of solvated $W(CO)_5$ after the completion of any initial cage recombination. Two models have been proposed to account for the less than unit quantum yields [76][79, 80]. The first invokes a unit quantum yield for CO dissociation and a solvent dependent, rapid geminate recombination of CO. The second model suggests that the quantum yield for CO dissociation itself is not unity and that efficient radiative and nonradiative relaxation channels exist for the excited state molecules.

Although invoked to explain the non-unit quantum yield in the photodissociation of $M(CO)_6$ in solution [76][79, 80], geminate recombination of CO has never been directly observed in these hexacarbonyls nor has it been seen for other transition metal carbonyls. This process has, however, been observed in the solution phase photodissociation of simple diatomic molecules: I_2 [81] and I_2^- [82-86], polyatomic molecules: CH_2I_2 [87, 88], I_3^- [89-94], and metal carbonyl dimers [41, 42, 95][87]. Cage recombination is not limited to solution phase reactions. It has also been observed in photodissociation reactions in solids [96], high pressure gases [97, 98], and clusters [99-102][103, 104].

To elucidate the role of geminate recombination dynamics in these metal carbonyls,

ultrafast studies in the sub-picosecond regime are needed. The ultrafast dynamics of $M(CO)_6$ in alcohol and hexane solutions have been studied by femtosecond visible spectroscopy [51, 52]. A fast decay component with exponential time constant of 350 fs was observed in the 450 nm region after photolysis at 310 nm. The fast component was assigned to the absorption of an excited state while the 350 fs decay was interpreted as the time scale for the CO dissociation. This fast component was found to be similar for different central metal atoms, M=Cr, Mo and W, even though they have very different spin-orbit coupling. In light of this, it was suggested that the similarity in the early time dynamics meant that either photodissociation occurs in the singlet state or the intersystem conversion is much faster than the 100 fs time resolution of the experiment. This fast component was observed in the same spectral region of the visible absorption of the $M(CO)_5$ species. For this reason, the fast component was later suggested as possible evidence for fast geminate recombination of the $M(CO)_5$ fragment with CO [87]. From the optical spectra alone, it is difficult to determine whether the absorption is due to $M(CO)_5$ or the excited state of $M(CO)_6$. The IR spectra, however, are expected to be quite different for these two species. Both ground state $M(CO)_6$ and $M(CO)_5$ have a strong and distinct IR absorption making this reaction an ideal system for a femtosecond IR spectroscopic study [43, 44, 69]. To unambiguously assign the previously observed fast component and understand the ultrafast dynamics in the solution phase photodissociation of $M(CO)_6$, we have recently studied the bleach recovery dynamics of the parent CO stretching band and the product formation and decay dynamics for the three metal carbonyls in different alkanes using femtosecond infrared spectroscopy.

2.2 Experimental

$M(CO)_6$, obtained from Pressure Chemical, was dissolved in various alkane solutions. The sample was then pumped through a nozzle to produce a jet with a center thickness of 200 μm. For the experiments probing the bleach of parent molecules, the concentration of the sample, about 1mM, was adjusted so that the OD of the CO stretching mode of $M(CO)_6$ was ~1. For the experiments probing the $M(CO)_5$ absorption, the concentration of the sample, at ~3 mM, was adjusted so that the OD of the sample at 295 nm was ~1.0. The integrity of the samples was checked before and after experiments by FTIR spectra. IR kinetics and spectra were recorded using the femtosecond IR spectrometer described in Chapter 1.

2.3 Results

Figure 2.1 shows the bleach recovery dynamics of $M(CO)_6$ in heptane solution measured at the peak of the parent molecule T_{1u} CO stretching mode. The squares, triangles and circles are data points for M = Cr (1987 cm^{-1}), W (1983 cm^{-1}), and Mo (1989 cm^{-1}) respectively. The kinetics are fit by a constant bleach plus a single exponential rise function with a rise time of 110 ps, 70 ps and 70 ps as indicated by the thin lines. The percentage bleach recovery, the ratio of the amplitude of the exponential rise component to the total initial bleach is 15%, 15% and 6% for M = Cr, W and Mo respectively. For comparison, the signals from different samples are scaled to have the same initial bleach value. Bleach recovery dynamics in different solvents were also measured. The bleach recovery dynamics for $Cr(CO)_6$ in heptane and dodecane at 1987 cm^{-1} and 1988 cm^{-1} are

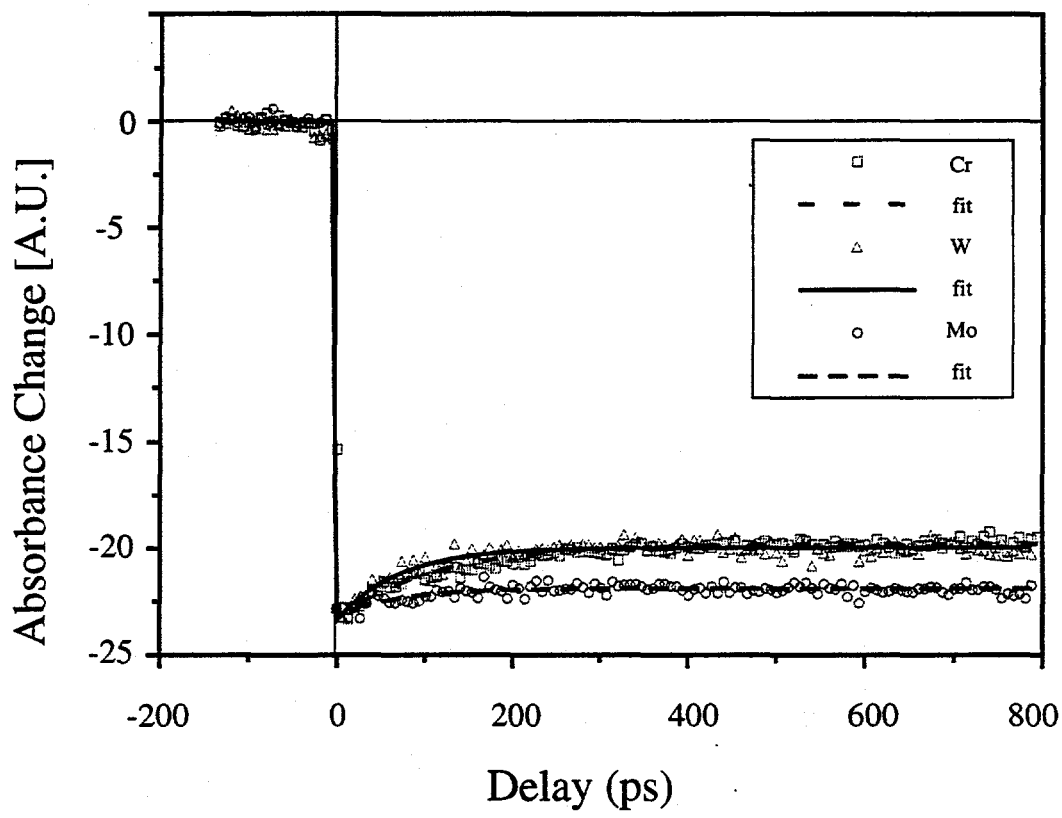

Figure 2.1 - Bleach recovery for $M(CO)_6$ in heptane measured at the peak of the T_{1u} CO stretching band at 1987, 1983, and 1989 cm^{-1} for M = Cr, W, and Mo.

shown in Figure 2.2. The measured percentage bleach recovery is 15% and 21% in heptane and dodecane. These kinetics are measured at the peak of the parent molecule CO stretching band. As will be discussed later, these values for bleach recovery should not be interpreted as the amount of parent molecules reformed, nor should the recovery time constant be taken simply as the time for reforming the parent molecules. The recovery dynamics for all three $M(CO)_6$ in different solvents are wavelength dependent near the parent molecule absorption band. Shown in Figure 2.3 are the kinetics for $W(CO)_6$ in heptane at 1983 cm^{-1} (circles), corresponding to the peak of the bleach, 1980 cm^{-1} (squares), and 1978 cm^{-1} (triangles). The data taken at 3 cm^{-1} on the high frequency side is indistinguishable from that taken at the peak and is left out for clarity. This wavelength dependent behavior is a signature of the vibrational cooling of hot parent molecules, which will be discussed in next section.

The spikes before t=0 seen in Figure 2.3 are due to perturbed free induction decay. This phenomenon, which is the result of vibrational coherent effects occurring on the same time scale as dephasing is known to obscure the study of early time dynamics using femtosecond IR spectroscopy. The details of the perturbed free induction decay in these complexes are described elsewhere [105].

Because the perturbed free induction signal is predominant around t=0 for probe wavelengths near the parent molecule bleach we need to probe at a wavelength region as far away from the parent CO stretching band as possible in order to study the fast dynamics of the $M(CO)_5$ species. The vibrationally hot $M(CO)_5$ species have broad absorptions, ranging from 1960 cm^{-1} to 1900 cm^{-1} [43, 44, 69]. Shown in Figure 2.4 are the long time

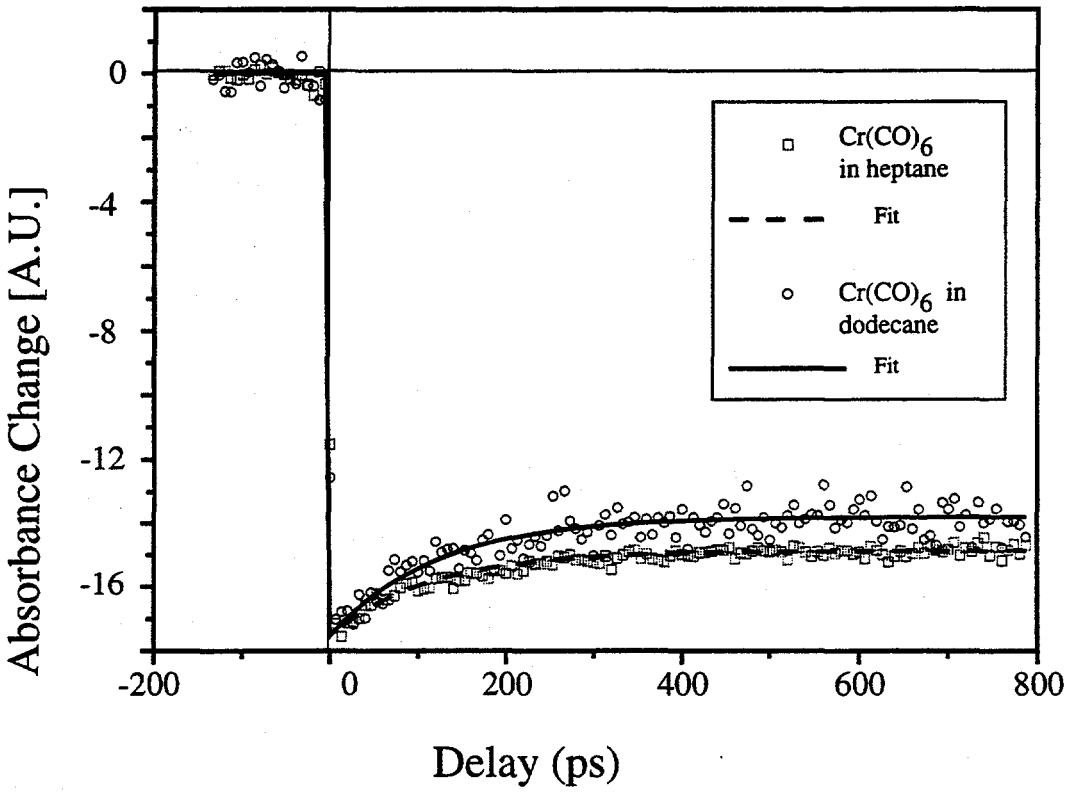

Figure 2.2 - Bleach recovery measured at the peak of the T_{1u} CO stretching band for $Cr(CO)_6$ in heptane and dodecane.

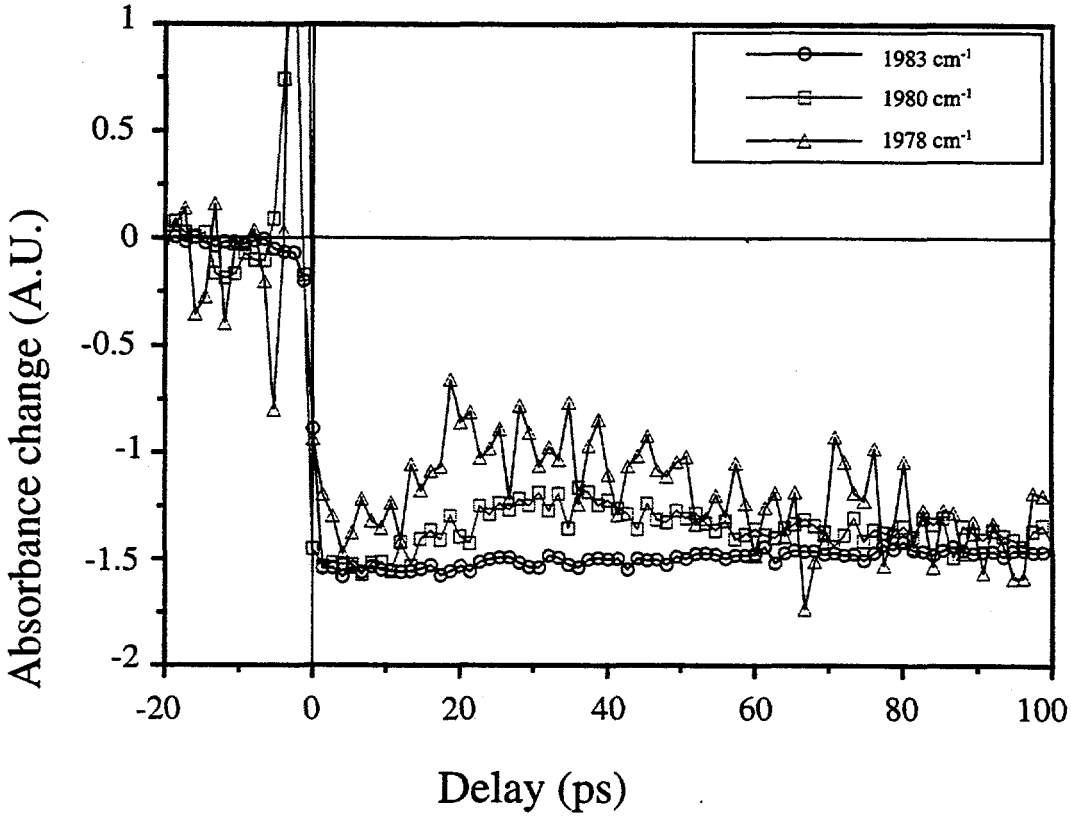

Figure 2.3 - Bleach recovery kinetics for $W(CO)_6$ in heptane at 1983, 1980, and 1978 cm^{-1}.

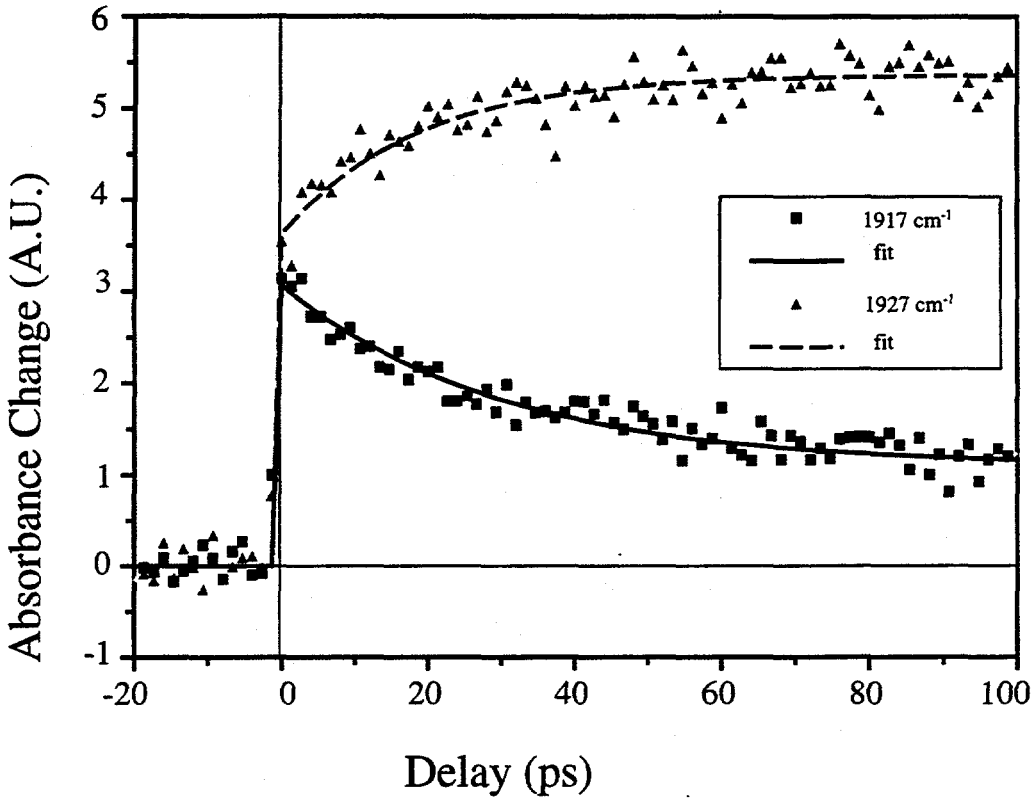

Figure 2.4 - Kinetics of the formation of $W(CO)_5$ in heptane probed at 1927 and 1917 cm^{-1}, represented by the triangles and squares respectively. The single exponential fits, the dotted and solid lines, give time constants of 22 and 26 ps, respectively.

kinetics of $W(CO)_6$ in heptane probing at 1927 cm^{-1}(the peak of the $W(CO)_5$ A_1 band), and 1917 cm^{-1}. The kinetics can be well fit by a 22 ps exponential rise function at 1927 cm^{-1} and a 26 ps exponential decay at 1917 cm^{-1}. These wavelength dependent kinetics follow the vibrational cooling dynamics of the solvated $W(CO)_5X$ (X=heptane) species [43, 44, 69]. In addition to the cooling dynamics, there is also a fast initial decay in the kinetics when measured with small time steps of 33 fs. Shown in Figure 2.5 is the short time dynamics for $Mo(CO)_6$ in heptane probed at 1929 cm^{-1} (the peak of the $Mo(CO)_5$ A_1band), 1918 cm^{-1}, and 1908 cm^{-1}. The signals at different wavelengths are scaled to the same amplitude at the maximum absorbance change of the kinetics. The initial rise of the signal is well fitted by an instrument response limited rise. All the kinetics are well fitted by a fast exponential decay followed by a slower exponential rise or decay function. The fast decay component has a time constant shorter than 300 fs. They appear to be fitted best by 100 fs to 200 fs exponential decays. Fits with 150 fs exponential decay are shown in Figure 2.5. The amplitude of the fast component cannot be well determined because it is very sensitive to the time constant used for the fit. Within the noise of the data, the relative amplitude for the fast and slow component appear to be similar for the three different wavelengths.

The fast decay kinetics are also measured for different metal centers. Shown in Figure 2.6 are the kinetics measured at 1917 cm^{-1} for $M(CO)_6$ in heptane with M = Cr, W and Mo, represented by square, triangle and circles respectively. The signals from different metal carbonyls are scaled to have the same size at the peak. The kinetics for different metals are similar, consisting of a fast component and a slower component with

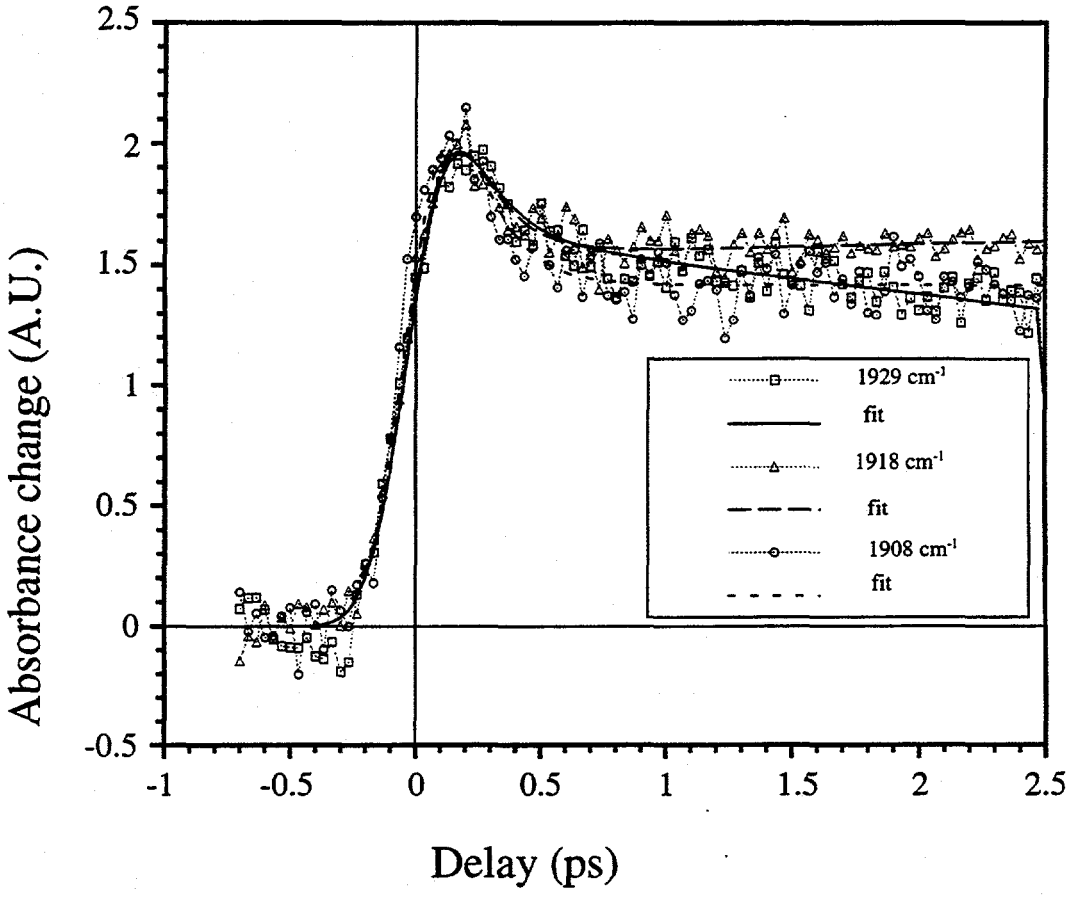

Figure 2.5 Early time dynamics for the formation and decay of $Mo(CO)_5$ in heptane probed at 1929, 1918, and 1908 cm^{-1}, represented by the squares, triangles, and circles. The biexponential fits, the dotted and solid lines, give time constants of 150 fs for the fast component and about 20 ps for the slower component.

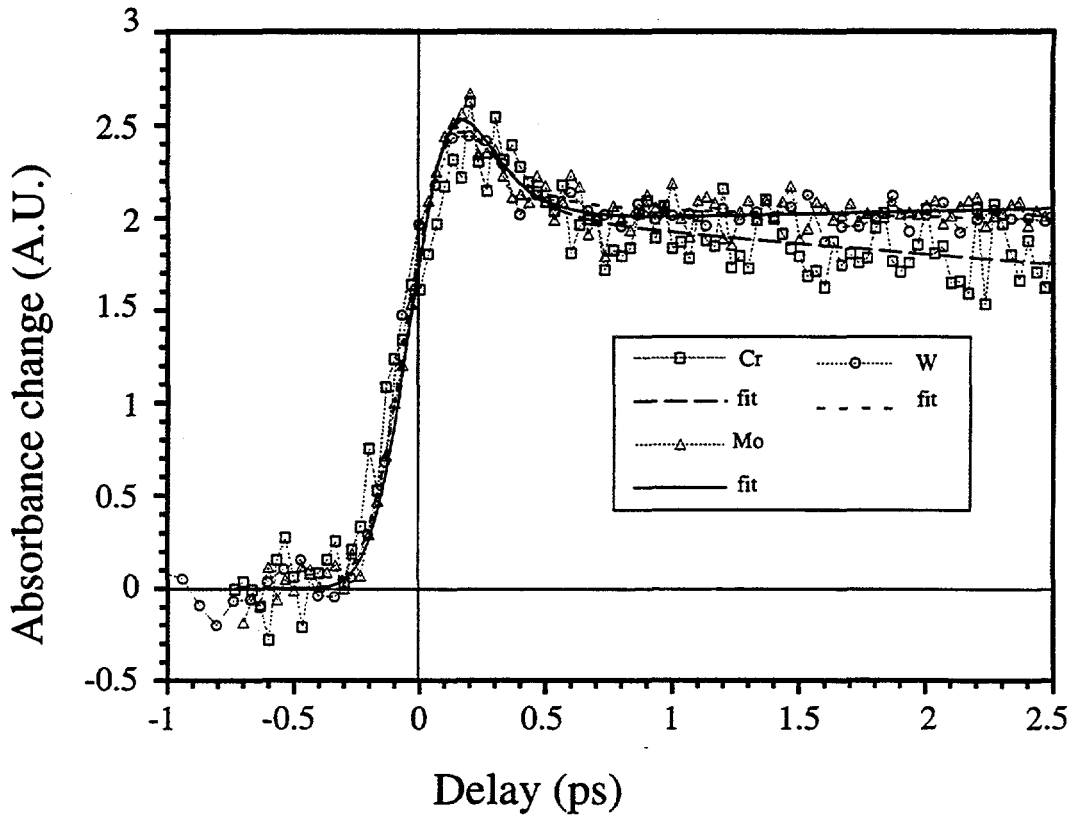

Figure 2.6 - Early time dynamics for the formation and decay of $M(CO)_6$ in heptane probed at 1917 cm^{-1}. M = Cr, W, and Mo are represented by the squares, triangles, and circles, respectively. The biexponential fits (dotted and solid lines), yield time constants of 150 fs for the fast compnent and about 20 ps for the slower component. The rises of the signals are instrument limited.

time constant of 10s of ps. The fast components are well fitted by exponential decays with time constants of approximately 150 fs, as shown in Figure 2.6. The relative amplitudes for the fast and slow components appear to be similar for different metal centers.

2.4 Discussion

2.4.1 Bleach Recovery

To understand the early time dynamics of the systems, we have probed the reformation of the ground state parent molecules and the formation and decay of the product. The photosubstitution quantum yields for $M(CO)_6$ in various alkane solvents are known to decrease as the chain length of the alkanes is increased. For $Cr(CO)_6$ this value decreases from 0.72 in *n*-pentane to 0.58 in *n*-dodecane. Since the alkane-solvated pentacarbonyl species produced in the photolysis are completely substituted by the entering ligands with a diffusion limited rate in these reactions, the quantum yields measure the yields of producing the pentacarbonyl species after any initial cage recombination is complete. Therefore, the non-unit quantum yields suggest that after UV photolysis some of the parent molecules are regenerated in the ground state through either fast geminate recombination of the photofragments or radiative or nonradiative relaxation from the excited state. A previous ultrafast IR spectroscopic study on these molecules did not observe any absorption bands (from ca. 1 ps to ns time scale) other than those of the parent and the pentacarbonyl species [43, 44, 69], suggesting that it is unlikely that there is any excited state population on that time scale. The parent molecule would then be reformed within 1 ps through fast cage recombination or nondissociative relaxation from the excited state,

giving rise to a partial bleach recovery of the parent molecule absorption bands.

A bleach recovery is indeed observed for all the three different metal carbonyls, as shown in Figure 2.1. The time scale for the bleach recovery cannot be taken as the time for reforming the ground state molecules, but rather it reflects the vibrational cooling of the molecules. The presence of vibrational cooling of the ground state molecule is evident when we probe at the longer wavelength side of the bleach as shown in Figure 2.3. It has been shown [41, 42, 95][43, 44, 69] that there are strong anharmonic couplings between the CO stretching and low frequency modes for many metal carbonyls. As a result of populating the low frequency modes, the CO stretching bands are broadened and red shifted. As shown in Figure 2.3, the bleach recovers initially and then increases again for the low frequency side of the CO stretching band. At the center and high frequency side the bleach recovers monotonically with a slower time constant. The initial recovery in the kinetics at the low frequency side is due to the absorption of the vibrationally hot parent molecules, which have a red-shifted CO stretching band, and the subsequent increase in bleach signal is caused by the vibrational cooling of those molecules. The recovery times measured at the center of the bleach are 112 ps, 70 ps and 70 ps for M = Cr, W and Mo respectively. These time constants reflect the cooling of both the low frequency modes that are anharmonically coupled to CO stretching mode and the CO stretch itself. Unfortunately the presence of vibrational population at $v=1$ and higher levels in the CO stretching mode cannot be unambiguously determined in this experiment since their absorption overlaps with the absorption of the pentacarbonyl species. The vibrational cooling rates of low frequency modes in these hexacarbonyls molecules have not been measured, but those for

the pentacarbonyl species have been studied [43, 44, 69]. It was found that the CO stretching bands of these pentacarbonyl species in hexane narrows in about 10 ps. This time constant is taken as the average cooling time of the low frequency modes, which is similar to other large polyatomic molecules [106-108]. The CO stretching time of $M(CO)_6$ in n-hexane has been measured to be about 140 ps. Our measured bleach recovery times fall between 10 ps and 140 ps suggesting that both low frequency modes and CO stretching mode are excited when the molecule is reformed in its electronic ground state.

From the quantum yields for substitution in *n*-heptane of 73%, 79% and 93% for $Cr(CO)_6$, $W(CO)_6$ and $Mo(CO)_6$, the percentage of parent molecules reformed are expected to be 27%, 21%, and 7% respectively. The actual percentage of bleach recovery, as shown in Figure 2.1, is measured to be 15%, 15%, and 6% for the three metal carbonyls in n-heptane. The relative amount of recovery agrees with the trend expected from the substitution quantum yields, but the absolute values are significantly lower than those expected. This suggests that the reformation of parent molecules is faster than we can measure at this wavelength. There should be a fast initial recovery of the bleach followed by the slower vibrational cooling shown in Figure 2.1 and 2.2. Unfortunately, as shown in Figure 2.3, the interference of the perturbed free induction decay signal makes it difficult to measure any fast dynamics in this spectral region. The bleach recovery for $Cr(CO)_6$ in *n*-dodecane is also measured. Compared with n-heptane solution, shown in Figure 2.2, the relative amount of bleach recovery agrees with the trend that there is a higher percentage of recovery in a longer chain alkane solvent. The measured 21% recovery for $Cr(CO)_6$ in n-dodecane is again smaller than the 42% expected from the quantum substitution yield

measurement.

2.4.2 Product Dynamics

Our measurements of the bleach recovery in these metal carbonyls suggests that there is a fast regeneration of the vibrationally hot ground state parent molecules. This recovery could be a fast relaxation from the electronic excited states and/or a fast cage recombination of CO and the pentacarbonyl intermediate. To understand the possible contribution of geminate recombination to the fast bleach recovery and therefore the non-unit quantum yield, we have studied the ultrafast dynamics of the pentacarbonyl species. To avoid the interference of the perturbed free induction decay signal, the measurements have to be made as far away from the parent molecule bleach as possible. At the peak, ca. 1927 cm^{-1}, and lower frequency side of the A_1 vibrational band of the three solvated $M(CO)_5$, the contribution from the perturbed free induction decay can be neglected and the product still has a significant absorption.

The signal at all wavelengths can be fit by an instrument response time limited rise followed by a fast decay of ca. 150 fs and a slower wavelength dependent decay or rise. Typical kinetics of the slow component are shown in Figure 2.4. The wavelength dependence and time constants for this component follow the vibrational cooling dynamics of the solvated pentacarbonyl species, which has previously been well studied by ultrafast visible [36-40] and IR [43, 44, 69] spectroscopy. At 1927 cm^{-1} (the peak of the A_1 band), the slow component grows with an exponential rise time constant of about 22 ps, while at 1917 cm^{-1} (to the red side of the peak), the signal decays with a time constant of about 26 ps, reflecting the spectral narrowing and blueshifting as a result of the cooling of

the low frequency modes that are coupled to the CO stretch.

The fast decays appear to be faster than 300 fs at all wavelengths, and are best fit by a time constant of approximately 150 fs. The detailed wavelength dependence for $Mo(CO)_6$ in heptane is shown in Figure 2.5. The relative amplitude of the fast and slower components seems to be the same for all the three wavelengths, covering the peak of the A_1 band and 10 cm^{-1} and 20 cm^{-1} away from this peak. Since the slower components are unambiguously assigned to the cooling of vibrationally hot pentacarbonyl species, the presence of the fast decay in the same spectral region with the same relative amplitude across the A_1 band suggests that this component also pertains to the nascent pentacarbonyl species. The fast decay is then attributed to the rapid geminate recombination of the pentacarbonyl species with the CO ligand that is still trapped in the solvent cage. The 150 fs time scale for the geminate recombination agrees with previous measurements in CH_2I_2 and metal carbonyl dimer, $Mn_2(CO)_{10}$, in which geminate recombination was observed to happen on the 300 fs time scale [87]. This ultrafast time scale for geminate recombination was also observed in a recent study on the dissociation of $I_2 \bullet Ar_n$ clusters [99-102], in which it was found that geminate recombination of the I atoms occurs 360 fs after the direct dissociation of I_2. Unfortunately, since the fast decay is faster than the time resolution, its amplitude cannot be accurately measured by the present experiment and therefore we cannot determine quantitatively the percentage of pentacarbonyls that recombine.

The kinetics measured at 1929 cm^{-1} for all three $M(CO)_6$ (M=Cr, W and Mo) molecules are compared in Figure 2.6. The best fits to the fast components give time constants of approximately 150 fs for all three metal carbonyls. Again, neither the

amplitude nor the time constant for the fast component can be accurately determined because of the lack of time resolution. If the quantum yield for CO dissociation is unity, we would expect to observe 27%, 21%, and 7% geminate recombination for Cr, W and Mo respectively based on the measured photosubstitution quantum yield [79, 80]. If we observe similar percentages of recombination for all three different metal carbonyls, the different photosubstitution quantum yields must then be caused by different yields for CO photodissociation from these molecules. At this point, the quality of the data does not allow a quantitative comparison between the time scale and percentage of geminate recombination for the three different metal carbonyls. Therefore the branching ratio between the dissociative and nondissociative pathway cannot be quantitatively determined.

The instrument response limited rise of the signal indicates that the pentacarbonyl species are produced much faster than 240 fs. Based on this result, the previously observed instrument response limited rise of the visible absorption signal in the 450 nm region may be assigned to the formation of the pentacarbonyl species [51, 52][87]. Furthermore the CO dissociation process is then complete within 100 fs [51, 52].

Unfortunately, the time resolution of about 250 fs in this experiment is not fast enough to provide an accurate measurement of the percentage of molecules that undergo geminate recombination. However, it is now possible to carry out femtosecond IR experiment with 40 fs time resolution [109]. Future experiments with time resolution on the order of 40 fs should allow a quantitative measurement of the percentage and time scale of geminate recombination. A comparison between the three different metal centers should shed light on how the electronic properties of the metal center affect the dissociation

dynamics of these metal carbonyls. A solvent dependence study should reveal what kind of solvent properties determine the time scale and amount of geminate recombination in the solution phase reaction.

2.5 Conclusion

UV photolysis leads to an efficient CO loss in $M(CO)_6$. Both the bleach recovery and product formation and decay have been studied by femtosecond IR spectroscopy with 240 fs time resolution. The percentage of the bleach recoveries are found to be smaller than the photosubstitution quantum yields indicating that reforming of the vibrationally hot ground state parent molecules occurs faster than our time resolution. The relative amount of bleach recovery observed for the three metal carbonyls and in different alkanes agrees with the trend expected from photosubstitution quantum yield measurement. The formation of the pentacarbonyl species is found to be instrument response limited. We observe a fast decay (< 300 fs) of the IR absorption of the pentacarbonyl species, which is assigned to the fast geminate recombination of these pentacarbonyls with CO after only one to two collisions with the surrounding solvent cage. Although the percentage of the pentacarbonyl species that undergoes this fast geminate recombination has not been quantitatively determined due to the lack of time resolution in this experiment, fast geminate recombination of the photoproduct certainly contributes to the non-unit photosubstitution quantum yield observed in these molecules. Future experiments with faster time resolution should quantitatively measure the amount of geminate recombination and its dependence on both the metal center and the solvent.

Chapter 3: Ultrafast Dynamics of $Cp^*Ir(CO)_2$ and $Cp^*Rh(CO)_2$ in Solution: The Origin of the Low Quantum Yields for C—H Bond Activation

The most exciting phrase to hear in science, the one that heralds new discoveries is not Eureka! (I found it!) but "that's funny..." -Isaac Asimov

***

3.1 Introduction

3.1.1 Organometallic Photochemistry

Organometallic chemistry has developed rapidly over the last several decades. This development is particularly notable in the area of solution photochemistry [110-119], which makes up a sizeable fraction of organometallic syntheses known. Interest in this area derives mainly from the fact that many of the reactions are very difficult or impossible to perform thermally while the analogous photochemical reactions only require relatively mild reaction conditions. From the perspective of an ultrafast spectroscopist, several classes of reactions are particularly interesting because they combine practical synthetic and catalytic importance [120-123] with a means of testing fundamental aspects of solution phase chemical reaction dynamics. Indeed, many of these reactions proceed on time scales comparable to or even faster than vibrational energy relaxation or redistribution. In such cases, the detailed molecular mechanisms underlying bond formation in the products can be strongly influenced by one or more of the energy dissipative mechanisms described above

in the hexacarbonyls.

One such class of reactions is Oxidative Addition [124-127] and includes the practically significant C—H [34, 128-133] bond activation reaction. The initial steps in this reaction are independently part of another fundamental reaction class called Photosubstitution [79, 110, 113, 134, 135]. Despite their extensive use, however, the individual mechanistic steps of these interesting and practically important photoinitiated reactions are not well understood. The extreme reactivity of most of the photochemically generated intermediates results in the species having lifetimes that are in the femtosecond and picosecond timescales. My research goal was to use the techniques of ultrafast IR and UV/Visible spectroscopy to observe and characterize these short-lived intermediates. Information about their structure, energetics, and lifetime could then be used to unambiguously determine the individual steps of several important reaction mechanisms.

3.1.2 Carbon-Hydrogen Bond Activation

Of all the classes of molecules available for use as starting materials in organic synthesis, the most abundant class is also the least accessible. Alkanes, which constitute a significant portion of the world's hydrocarbon resources are also among the least reactive compounds in organic chemistry. Their relatively inert nature is usually explained by their strong C—H bond energies which are typically 90-100 kcal/mole. As a result, there has been considerable effort aimed at developing a catalytic process to break or 'activate' the C—H bonds and convert the alkanes to other more reactive species such as alcohols and/or ketones.

In 1982, the first direct evidence for the photochemical activation of a solvent

alkane C—H bond with a transition metal complex was reported by Bergman et al. [136] and soon after by Graham [137]. Bergman used the pentamethylcyclopentadienyl (Cp*) Iridium complex $Cp^*Ir(H)_2(PMe_3)_3$ while Graham used a Cp* carbonyl complex $Cp^*Ir(CO)_2$. They found that when these complexes were dissolved in alkane solution and irradiated with UV light, the alkyl hydride was formed as the final product (Figure 3.1). These important discoveries of photochemical C—H activation generated considerable interest in the field and became the focus of a variety of experimental and theoretical studies. Besides NMR experiments [138][139], most spectroscopic studies have focused on the carbonyl complexes. This is because of the characteristically strong IR bands associated with CO ligands and the fact that the distinct absorptions of CO ligands are very sensitive to changes in both other ligands and solvent environments.

Much of the experimental evidence obtained by IR spectroscopy indirectly points toward a dissociative mechanism for the reaction [134]. This scheme begins with the loss of CO as the first step, resulting in the formation of a coordinatively unsaturated intermediate. In earlier studies of the photodissociation and subsequent solvation of transition metal hexacarbonyls (that do not involve C—H bond activation) it was shown that to a large extent, the solvation dynamics around an open site were controlled by the vibrational cooling of the pentacarbonyl precursor [38, 39, 70, 140]. This information concerning the initial steps of CO dissociation in metal carbonyls can then be compared to the results of C—H activating compounds to begin to Figure out why these molecules are so reactive.

In addition there is a central question concerning the metal-alkane complex and its

role in the C—H activation reaction. It is known to lower the barrier for C—H bond activation from 100 kcal/mol for unactivated bonds to approximately 5 kcal/mol for activated bonds. This question has been addressed by theoretical calculations which predict the formation of these complexes in C—H activating systems [130, 141-143]. Flash kinetic studies have also been carried out to observe the intermediates formed when $Cp^*Rh(CO)_2$ is excited in liquid noble gas solutions with added alkanes [144, 145]. As evidence for this dissociative mechanism, the unsaturated intermediate has been detected in the gas phase [146] and in low temperature matrices [147-150]. The solvated monocarbonyl intermediate has also been identified in the photolysis of $Cp^*Rh(CO)_2$ in liquid Xe and Kr solution [67, 134, 151]. Despite this progress, however, the individual steps of the mechanism have not yet been directly observed in room temperature alkane solution.

3.1.3 Low C—H activation quantum yield in $Cp^*M(CO)_2$

Two principal difficulties have together inhibited direct observation of the alkane complex intermediates and their subsequent reaction in room temperature solution. Firstly, the extreme reactivity of the photogenerated species leads to rapid reaction rates making the intermediates impossible to observe with conventional spectroscopic techniques. Secondly, the quantum efficiencies for forming the alkyl hydride product in the 'classic' C—H activating complexes such as $Cp^*Ir(CO)_2$ and $Cp^*Rh(CO)_2$ are on the order of 1% [152]. This value is too small to generate a concentration of intermediate species high enough to detect after each photolysis pulse. Experiments on $Cp^*Ir(CO)_2$ and $Cp^*Rh(CO)_2$ solutions by Heilweil et al. showed that the quantum yields were simply too

low to detect any photoproducts [45]. In this work, they observed a bleach and complete recovery of the C—O stretches within 40 ps. Since no new CO stretching bands were observed, it was not clear what lead to the bleach and rapid recovery of the parent CO stretching bands.

This chapter describes a picosecond UV/Vis study of these metal carbonyls which helps to clarify the origin of the bleach recovery and how it relates to the low quantum yield for the C—H activation reaction of $Cp^*M(CO)_2$ in alkanes. In light of the strong evidence for the CO dissociation pathway and the extreme reactivity of coordinatively unsaturated organometallic intermediates, we expect that the low quantum yield originates in the primary photophysical processes that take place *before* the M—CO bond is broken. The excited state dynamics then play a critical role in the subsequent photochemistry by determining the branching ratio between the dissociative and non-dissociative reaction pathways. The existence of lower lying excited states below the strong MLCT band is evident in the UV/Vis absorption spectrum of these compounds and has been demonstrated by wavelength dependent measurements of the C—H activation quantum yield. In an effort to investigate the dynamics of these excited states and how they affect the quantum yield for CO loss, we have performed transient visible absorption spectroscopy on room temperature solutions of $Cp^*Ir(CO)_2$ in cyclohexane and its congener $Cp^*Rh(CO)_2$ in *n*-pentane solution with 1 picosecond time resolution.

3.2 Experimental

The laser apparatus used to carry out the picosecond pump-probe experiments was

described in Chapter 1. Briefly, 1-ps, 10-μJ pulses at 295 nm were used to excite the sample (concentration ~ 1 mM) and transient absorption signals were measured by using 10 nm fwhm bandpass filters at selected probe wavelengths (440-740 nm) from a continuum generated in a water cell. In the Rh experiments, pump power was attenuated to avoid signals originating from the solvent. In the Ir experiments, however, the small signal size necessitated the use of the fairly strong pump powers. In order to eliminate the resulting solvent contribution to the observed signal for the Ir complex, a neat cyclohexane solvent scan was taken immediately preceding the sample scan. This scan was then subtracted from the overall signal [153]. Spectrometric grade cyclohexane and pentane were purchased from Fisher Scientific Co. The $Cp^*Rh(CO)_2$ complex was purchased from Strem Chemicals and was used as received while the Ir complex was prepared according to the literature [154].

3.3 Results and Discussion

After excitation into the M→CO CT bands of the Ir and Rh complexes at 295 nm, transient absorptions are observed at each wavelength probed from 440 to 740 nm for Ir (Figures 3.1-3.5) and 500 to 650 nm for Rh (Figures 3.6 and 3.7). A representative long timescale trace for Rh (Figure 3.8) shows that on the 100 ps timescale, the signal returns nearly to the baseline [153]. The data are summarized in Tables 1 and 2.

All of the transients consist of instrument limited (1.5 ps) rises followed by biexponential decays. The best fit to the data yield a fast component which decays in 2-3 ps and a slower component which decays in 30-40 ps. Within our signal-to-noise the time

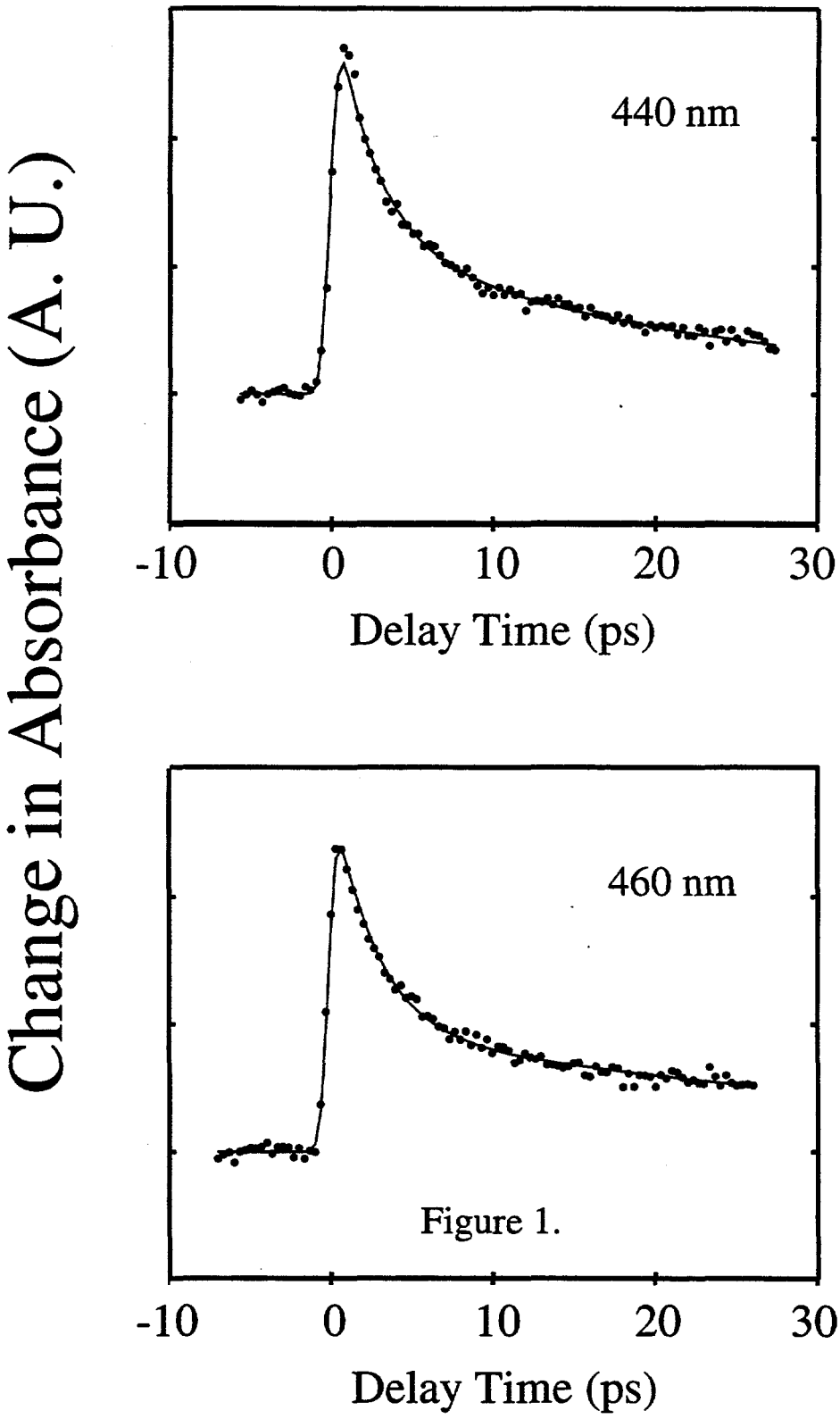

Figure 1.

Figure 3.1 - Transient Absorption of $Cp^*Ir(CO)_2$ in cyclohexane

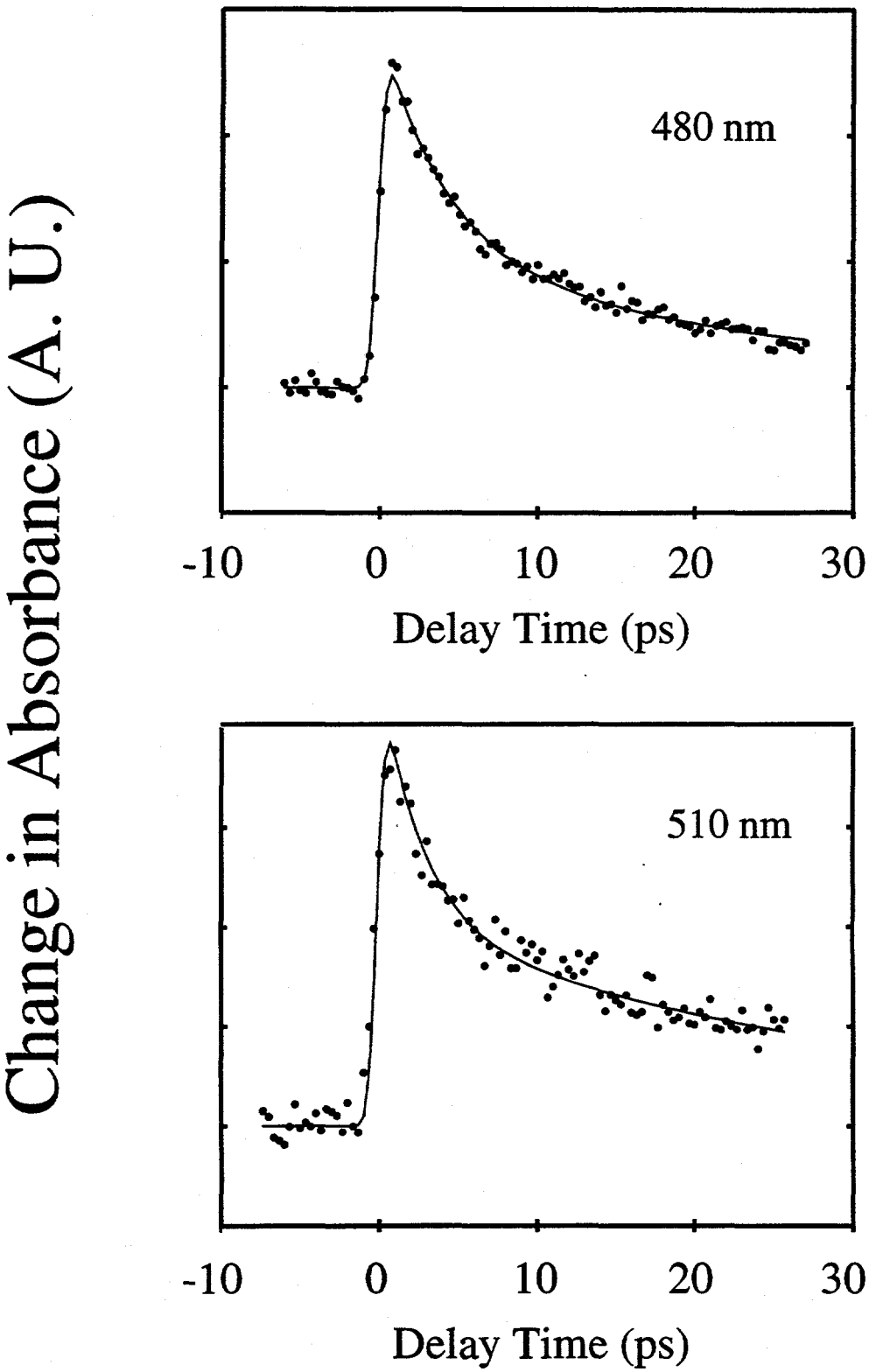

Figure 3.2 - Transient Absorption of $Cp^*Ir(CO)_2$ in cyclohexane

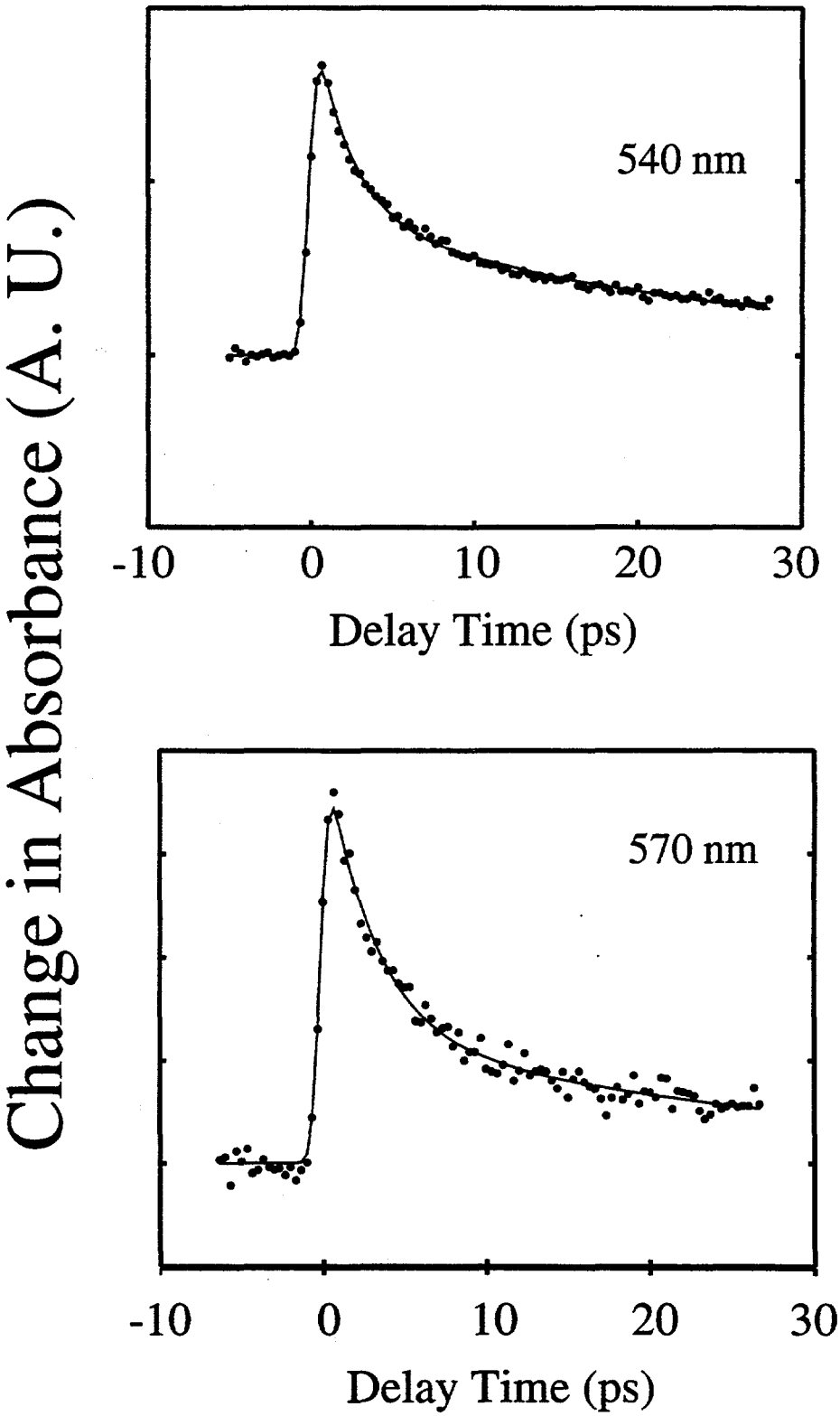

Figure 3.3 - Transient Absorption of $Cp^*Ir(CO)_2$ in cyclohexane

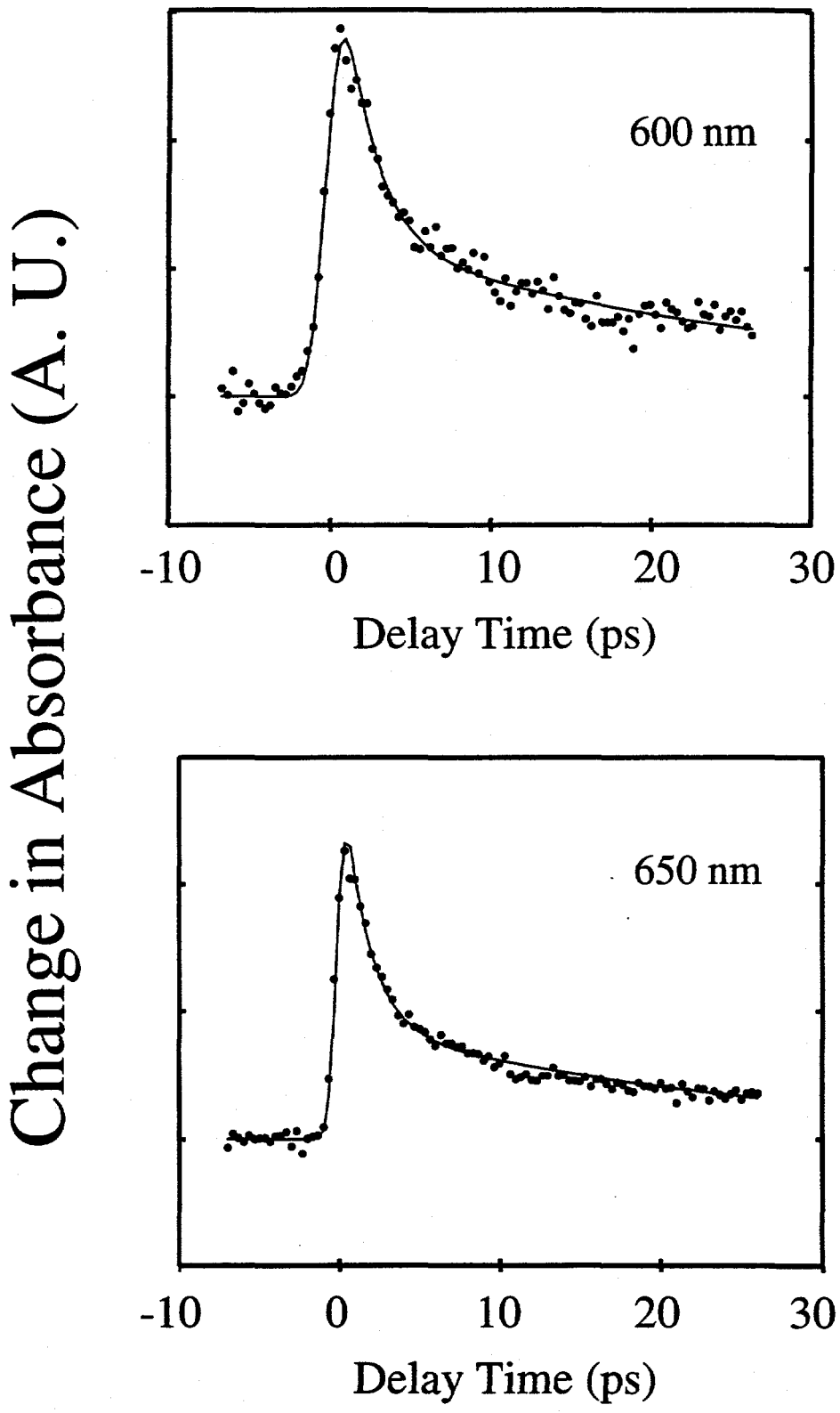

Figure 3.4 - Transient Absorption of $Cp^*Ir(CO)_2$ in cyclohexane

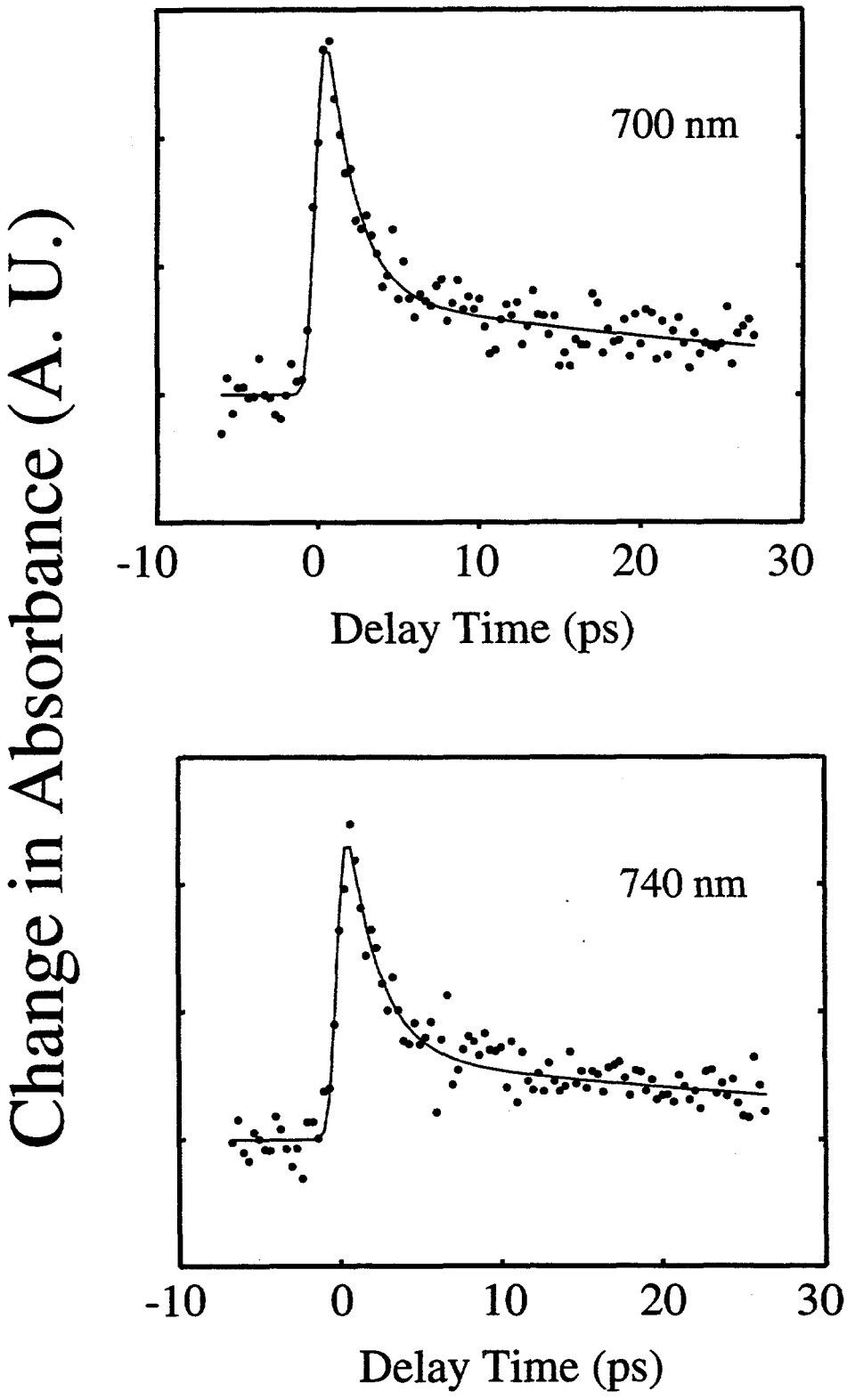

Figure 3.5 - Transient Absorption of $Cp^*Ir(CO)_2$ in cyclohexane

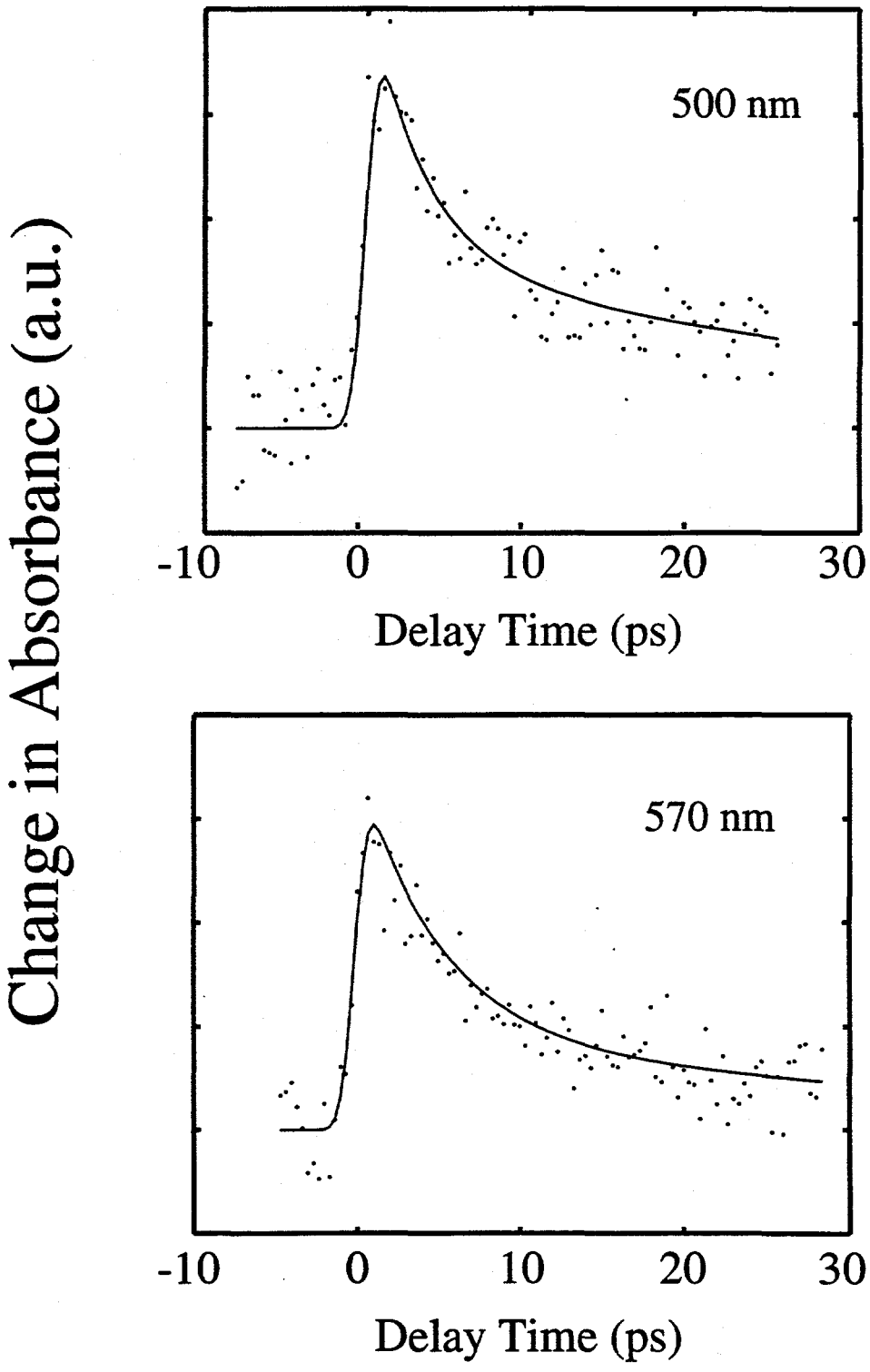

Figure 3.6 - Transient Absorption of $Cp^*Rh(CO)_2$ in pentane

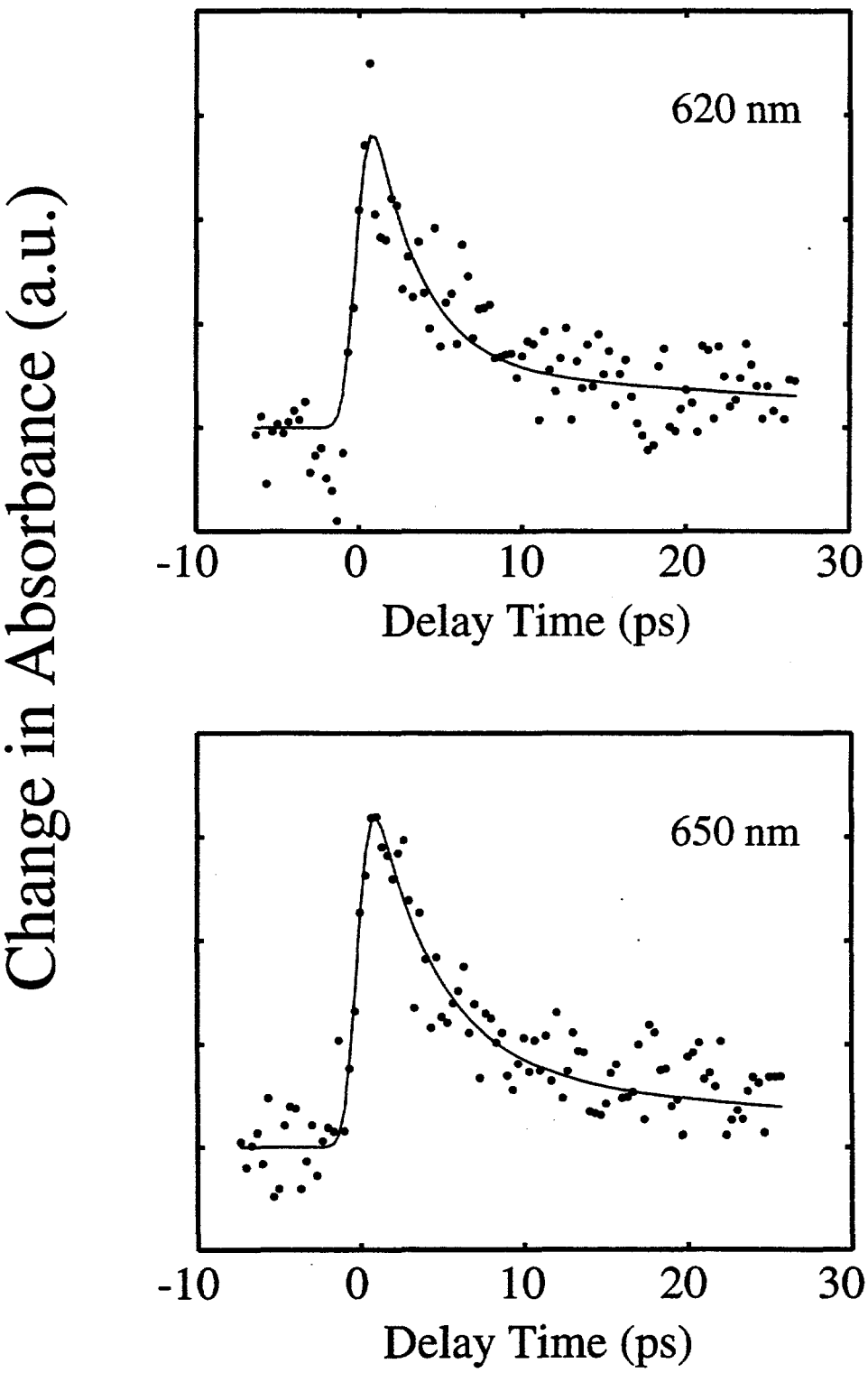

Figure 3.7 - Transient Absorption of $Cp^*Rh(CO)_2$ in pentane

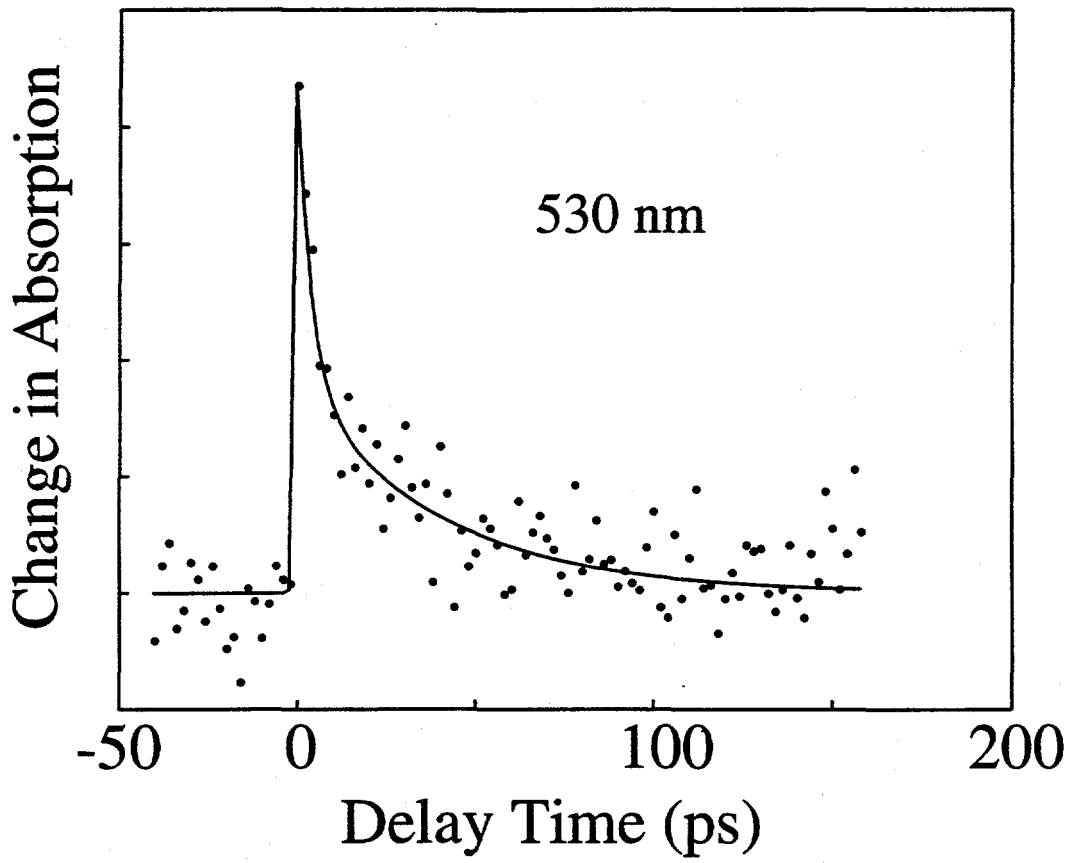

Figure 3.8 - Long time kinetics of $Cp^*Rh(CO)_2$ in pentane

λ (nm)	τ_i (ps)	C_1 (%)	τ_2 (ps)	C_2 (%)
440	2.6	61	24	39
460	2.6	66	35	34
480	4.0	61	25	39
510	2.7	54	33	46
540	2.3	59	25	41
570	3.0	68	30	32
600	2.0	70	30	30
650	1.5	71	30	29
700	1.8	78	40	22
740	2.0	77	40	23

Table 1. Summary of Iridium Data

λ (nm)	τ_1 (ps)	C_1 (%)	τ_2 (ps)	C_2 (%)
500	3.3	60	37	40
530	5.0	53	40	47
570	5.0	73	40	27
620	3.0	84	40	16
650	4.8	84	38	16
530 (long scan)	4.0	58	40	42

Table 2. Summary of Rhodium Data

constants are similar at all wavelengths probed while the amplitudes of the fast components appear to be larger at redder wavelengths. While the low signal-to-noise ratio of the Rh data does not allow a quantitative statement to be made concerning the recovery of the signal, it clearly returns to within a few percent of its original value by 100 ps. This recovery is consistent with both the earlier IR results [45] and the quantum yield measurements [155].

Neither the reactant $Cp^*Ir(CO)_2$ nor the product $Cp^*Ir(CO)(R)(H)$ absorb significantly in the 440-740 nm range we probed (Figure 3.9). Therefore, any transient absorptions detected at these wavelengths correspond to new intermediate species generated by photoexcitation. In addition, because we do not observe any wavelength dependence of the decay time constants, these transients cannot be due to the vibrational cooling of the hot parent molecule or photoproduct [38, 40]. Since we do not know how large the extinction coefficient is for the new species, we must consider the possibility that the transients are a result of the loss of CO to form a monocarbonyl intermediate despite the low quantum yield. The instrument limited risetimes are certainly consistent with the timescale for CO loss observed in other metal carbonyls. For example, CO dissociation in $M(CO)_6$ (M=Cr, Mo, W) has been observed to occur on the 300 fs time scale [52]. However, considering the timescales of the decays (see following paragraphs) and results from previous IR experiments [45][69], the behavior of the transients is inconsistent with that expected for a monocarbonyl. Such pathways are: (1) recombination with CO to reform the parent molecule and (2) reaction with the solvent.

We can rule out the possibility of CO recombination on the basis of the timescales

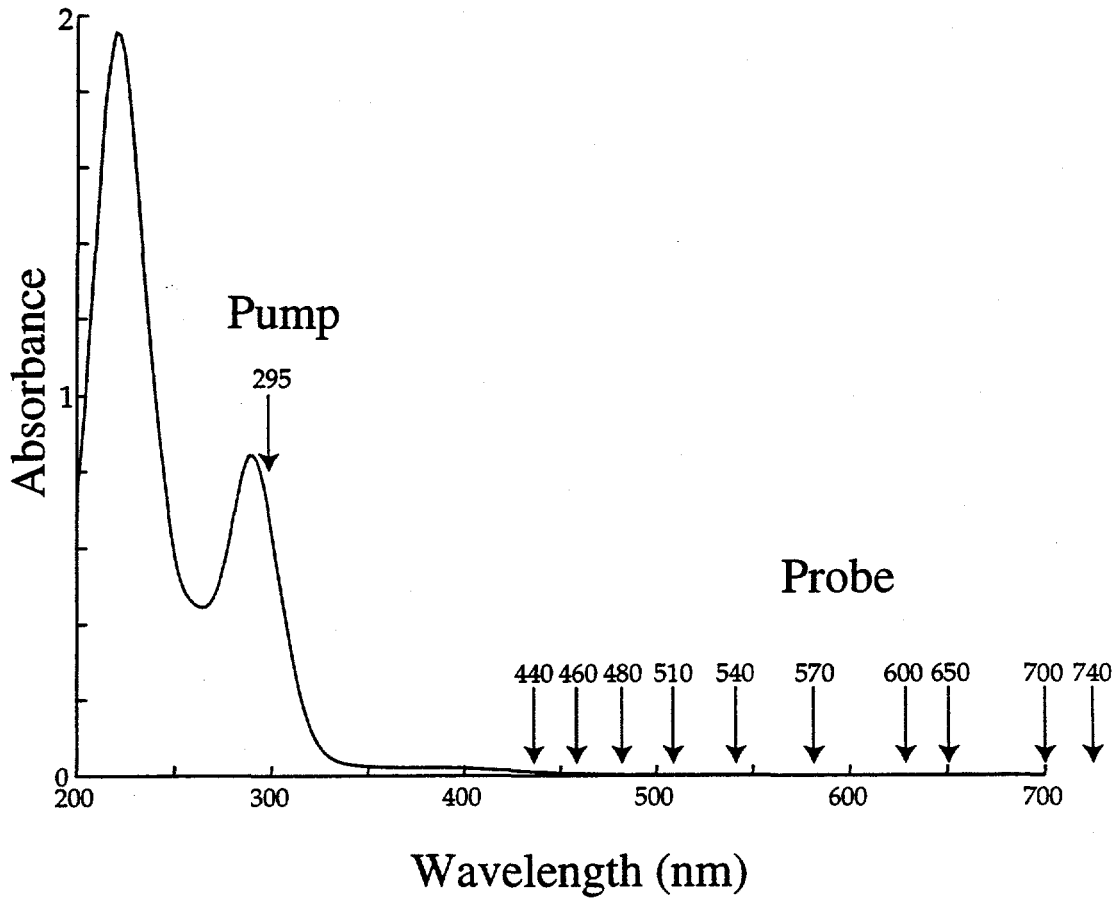

Figure 3.9 - Electronic absorption spectrum of $Cp^*Ir(CO)_2$ in cyclohexane

of the decays. One way recombination may occur is via a diffusion process, which at millimolar concentrations would take place in microseconds, orders of magnitude slower than we observe. The other possibility is geminate recombination. This could occur if the photolyzed CO is not able to escape the solvent cage before recombining with the monocarbonyl fragment to regenerate the parent species. From previous experiments probing this process, the timescale for geminate recombination is known to be on the order of 100 fs to 1 ps -- significantly faster than the decays we recorded [88]. Therefore, we conclude that the transients are not due to the recombination of CO with a monocarbonyl fragment.

In the recent femtosecond IR study of $Cp^*M(CO)_2$ (M=Ir, Rh) in n-hexane by Heilweil [45] , UV excitation at 289 nm was found to lead to a bleach of the parent molecule CO stretching bands. The bleach recovers with a 40 ps time constant, indicating the reformation of the parent molecules. No detectable amount of C—H activated product is observed. From this observation, we can conclude that the visible transients we see in the spectra of the Ir and Rh complexes are not due to the reaction of a monocarbonyl intermediate with the solvent.

In addition, the energy barrier for C—H bond activation has been determined from the experiments in liquid noble gases to be on the order of 6 kcal/mole [129, 144, 156]. Using a simple Arrhenius description, we can estimate how long it should take for the C—H activated product to form, corresponding to the time scale of the decay of a monocarbonyl. Using a pre-exponential factor of 1×10^{11} sec^{-1} and an energy barrier for metal insertion into the C—H bond of 6.0 kcal $mole^{-1}$, the C—H activated product should

form with a half-life on the order of 200 ns. This is several orders of magnitude longer than the time we measured, again implying that the transients are not reacting with the solvent to form the C—H activated product.

Ruling out the generation of a monocarbonyl species as the origin of the visible transients, we attribute our result to the first direct observation of a short-lived non-dissociative excited state due to UV excitation of $Cp^*Ir(CO)_2$ and $Cp^*Rh(CO)_2$. This finding is important because it provides an explanation for the low quantum yields for C—H activation by these complexes. Namely, after excitation by a UV photon, most molecules end up in one or more excited states that do not lead to CO loss. As a result of populating these states, the reactive coordinatively unsaturated species is never generated in most molecules. Instead, these molecules relax to the ground state within 40 ps. This scheme is shown in Figure 3.10. Furthermore, these observations support the results of the ultrafast IR study [45] which discussed the possibility of similar excited states to explain the bleach recovery in the parent CO stretches of $Cp^*Ir(CO)_2$ and $Cp^*Rh(CO)_2$ following UV excitation.

Since the transition at 295 nm contains mainly M—CO* charge transfer character [157], the non-dissociative excited state involved is most likely a lower-lying state that is strongly coupled to the M—CO* CT state. This is supported by the static absorption spectra of these molecules in alkane solutions, each of which show weak and broad absorption from 350 to 500 nm indicating that there are lower lying states below the strong metal to CO charge transfer band at 290 nm for Ir and 315 nm for Rh. Wavelength dependent quantum yield measurements of Si-H activation by $Cp^*Rh(CO)_2$ have found

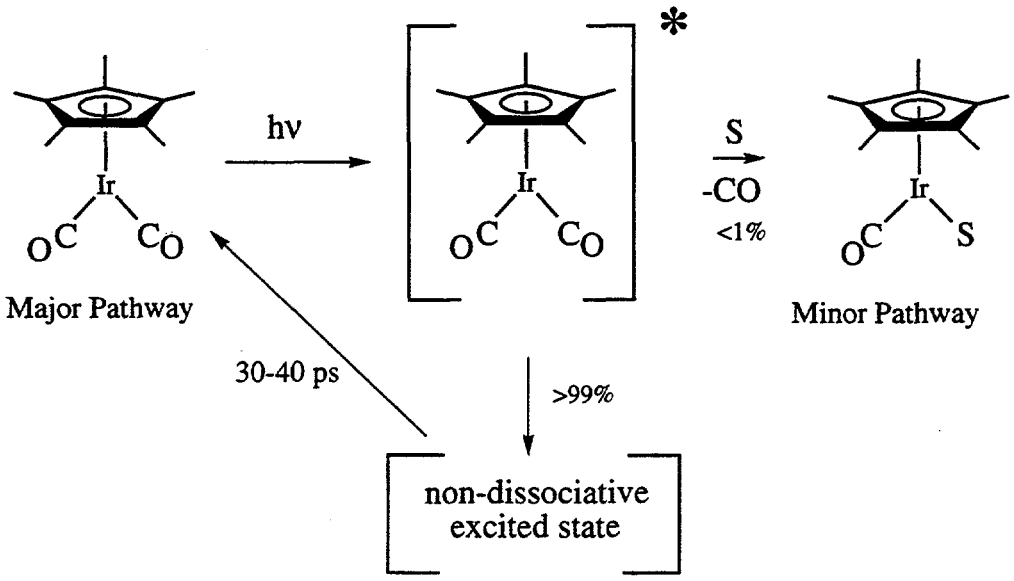

Figure 3.10 - Reaction scheme for $Cp^*M(CO)_2$ in alkanes.

that the quantum yield for this reaction decreases by an order of magnitude when the excitation wavelength is changed from 313 nm to 458 nm [135]. This reduced quantum yield indicates that the low lying state accessed by excitation at 458 nm has significantly less CO dissociation character. At this point, the exact nature of the excited state is still not known, although there have been some tentative assignments. Based on their wavelength dependent quantum yield measurement, Lees and coworkers suggest that excitation into these low lying states leads to a η^5 to η^3 ring slippage in the molecules, which can then undergo rapid reversible ring-slippage to relax back to the ground state [152][135]. While it is possible that the 40 ps transient we observe corresponds to this ring-slipped intermediate, our data only allow speculation concerning this issue. In addition, Pradella and coworkers have suggested that these excited states also have substantial M-Cp* anti-bonding character [158]. They based this assignment on the surprising results of a recent study of the photolysis of $Cp^*Rh(CO)_2$ in hexane solution in which they found that at $\lambda > 380$ nm the reaction pathway was consistent with the breaking of the Rh-Cp* bond.

It should also be noted that the fast component observed in our experiment was not identified in the IR study [45]. At early times the transient IR spectrum is broad and structureless due to the anharmonic coupling between the CO stretches and highly populated low frequency modes [69]. This broadening, in addition to an experimental artifact present at early times [69], may have obscured the fast transient in the IR spectrum. It is possible that this fast component is a result of the decay of the excited state to the ground state. This process would then produce a vibrationally excited ground state molecule in 2-3 ps. It is also possible that the short component is a result of the absorption

of an initially generated excited state that relaxes in 2-3 ps into a longer-lived excited state which decays in 30-40 ps. This model would be favored if there is a wavelength dependence of the relative amplitude of the fast and slow components. Although it appears that the relative amplitude of the short component is larger towards redder wavelengths, the signal to noise ratio of our data is not large enough to distinguish between these two possibilities. Future experiments probing the parent molecule absorption in the UV will provide an answer to this question.

3.4 Conclusion

Examination of the visible transient absorptions of $Cp^*Ir(CO)_2$ and $Cp^*Rh(CO)_2$ in room temperature solution has allowed us to directly observe the excited electronic state responsible for the low C—H activation quantum yield. These results elucidate the pathway taken by the majority of $Cp^*Ir(CO)_2$ and $Cp^*Rh(CO)_2$ molecules that absorb a UV photon: they decay back to ground state within 30-40 ps through non-dissociative short-lived excited states. Further insight into the excited state dynamics of these interesting organometallics will be gained after comparisons of the current results to those arising from both the highly efficient C—H activating $Tp^*Rh(CO)_2$ as well as the non C—H activating but highly dissociative $CpCo(CO)_2$ species.

Chapter 4: The Mechanism of a C—H Bond Activation Reaction in Room Temperature Alkane Solution

A man with new ideas is a crank until he succeeds. -Mark Twain

***

4.1 Introduction

Since the initial discovery that the strong carbon-hydrogen (C—H) bonds in alkanes undergo oxidative addition to certain transition metal complexes, the quest to understand and utilize this "C—H activation" reaction has been the focus of intense research effort (Figure 4.1) [33, 136, 137]. Both of these research goals should be furthered by developing a detailed understanding of the individual steps involved in metal-mediated C—H activation reactions. To monitor these elementary steps, spectroscopic techniques with microsecond time resolution are commonly used with the goal of identifying the reaction intermediates [35, 138, 149, 159, 160]. The extremely rapid reaction rate prevents these established methods from monitoring the earliest kinetics at room temperature. In order to use these conventional techniques, the experiments must be performed in the gas phase [146], in liquefied noble gases [129, 156], or in low temperature matrices [158, 161] to slow down the reaction.

Insight into the individual steps involved in metal-mediated C—H activation reactions have been obtained from spectroscopic techniques with microsecond time

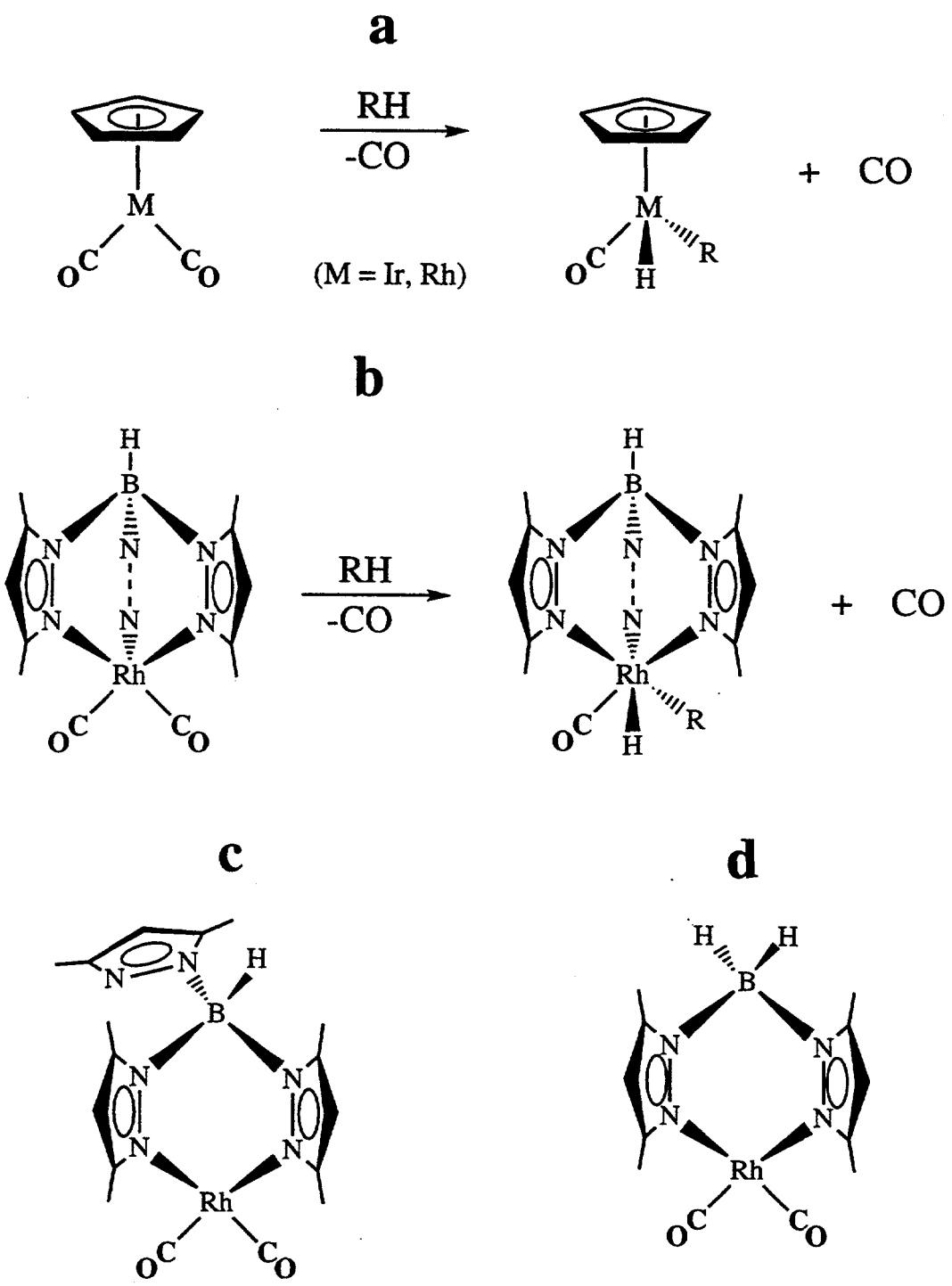

Figure 4.1 -C-H Activation reaction and structure of $Tp^*Rh(CO)_2$

resolution, with the goal of identifying the reaction intermediates. However, the extremely rapid reaction rate prevents these established methods from monitoring the earliest kinetics at room temperature, and requires that the experiments be performed in the gas phase, in liquefied noble gases, or in low-temperature matrices to slow down the reaction.

In the gas phase, photolysis of $CpRh(CO)_2$ ($Cp = C_5H_5$) yields the highly reactive CpRhCO, which reacts with alkanes at rates close to the gas-kinetic values (Fig. 1a) [146]. Low-temperature matrix work also showed the formation of CO-loss products [158, 161]. In liquid krypton solution, the solvated complex Cp*Rh(CO)•Kr ($Cp^* = C_5Me_5$, Me = methyl) is the first species observed. The alkane must then displace Kr before the final activation step can take place [129, 156]. These experiments established that the first step involves loss of a CO ligand to generate a coordinatively unsaturated intermediate. It is difficult, however, to generalize the results to room-temperature, neat alkane solution because of the extreme changes in reaction conditions. In contrast to earlier work, the goal of this work is to study the reaction under the most relevant conditions, room-temperature alkane solution. To accomplish this, and to overcome the reaction-rate measurement limitations inherent in microsecond spectroscopy, we used ultrafast spectroscopy with picosecond [37] and femtosecond [105, 162] time resolution. These techniques allow access to the inter- and intramolecular processes that take place on time scales faster than diffusion.

The next step in the study is clearly to monitor the actual chemistry which takes place from photolysis to the formation of the final product. Identification of the reaction intermediates is required to build a detailed picture of the overall bond-activation reaction.

Even with the time resolution available to us in the IR, the low quantum yields of ~1% for the C—H activation reaction of $Cp^*Ir(CO)_2$ and $Cp^*Rh(CO)_2$ make detection of the intermediate species impossible [45].

Fortunately, a rhodium compound that was originally reported to undergo "highly efficient" C-H activation in 1986 [163, 164] was recently reinvestigated and its quantum yields measured [155, 165]. This study by Lees on 3,5 tris-dimethyl-pyrazolylborato (Tp*) rhodiumdicarbonyl placed the quantum efficiency over 30%.

The CO vibrational stretching frequencies of $Tp^*Rh(CO)_2$ in pentane are 1981 cm^{-1} and 2054 cm^{-1}, which lie in a region of the spectrum that is readily accessible by our femtosecond spectrometer. Coupled with the 200 fs time resolution of our apparatus, the relatively high quantum yield of the $Tp^*Rh(CO)_2$ will enable us to address the important question of whether there are detectable intermediate complexes formed in room temperature solution. If so, what are their structures and the timescales for their formation and decay? By answering these questions, we will be able to unambiguously establish the C—H activation reaction mechanism in room temperature solution.

4.2 Experimental

These experiments were performed with our 30 Hz fs IR spectrometer with 200 fs time resolution (chapter 1.3). The sample was pumped by a UV pulse at 295 nm and the subsequent changes of the IR absorption in CO stretching mode region were probed as a function of both time and wavelength. $Tp^*Rh(CO)_2$ was synthesized according to a published procedure [166, 167] and fully characterized by conventional spectroscopic

methods. The sample solution, degassed and sealed under an N_2 atmosphere, was flowed through an airtight cell to ensure that each laser pulse probed a fresh volume of sample.

The nanosecond FTIR system used in this study has been previously reported in detail [30, 168]. It consists of a pulsed Nd:YAG laser to initiate the photochemistry and a modified Bruker IFS88 Step-Scan FTIR spectrometer for recording the transient absorptions. Samples in cyclohexane were excited at 355 nm and their spectra were collected from 1600 to 2300 cm^{-1}. In the configuration used in this work, the spectrometer has a time resolution of ~50 ns and frequency resolution of 4 cm^{-1}. Solutions of $Tp^*Rh(CO)_2$ in each solvent were filtered, degassed, and sealed in an airtight flow cell. The flow rate was set to insure that at a repetition rate of 10 Hz, each pulse encountered fresh sample. UV/Vis and IR spectra were collected throughout each run to monitor sample integrity. Solution concentrations were adjusted so that 80% of the excitation light was absorbed in the 1 mm path length of the IR cell. Similar procedures were followed for the $Bp^*Rh(CO)_2$ sample.

4.3 Results

In cyclohexane, $Tp^*Rh(CO)_2$ shows peaks at 1981 and 2054 cm^{-1} due to the antisymmetric and symmetric stretching modes of the two CO ligands. Upon irradiation, the static FTIR spectrum exhibits only a decrease in the intensity of the parent peaks and the corresponding formation of the final C—H activated product at 2032 cm^{-1}.

However, the ultrafast spectra reveal the interesting dynamics. Figure 4.2 shows the transient difference IR spectra of $Tp^*Rh(CO)_2$ in cyclohexane at -10, 10, 66, 200 and

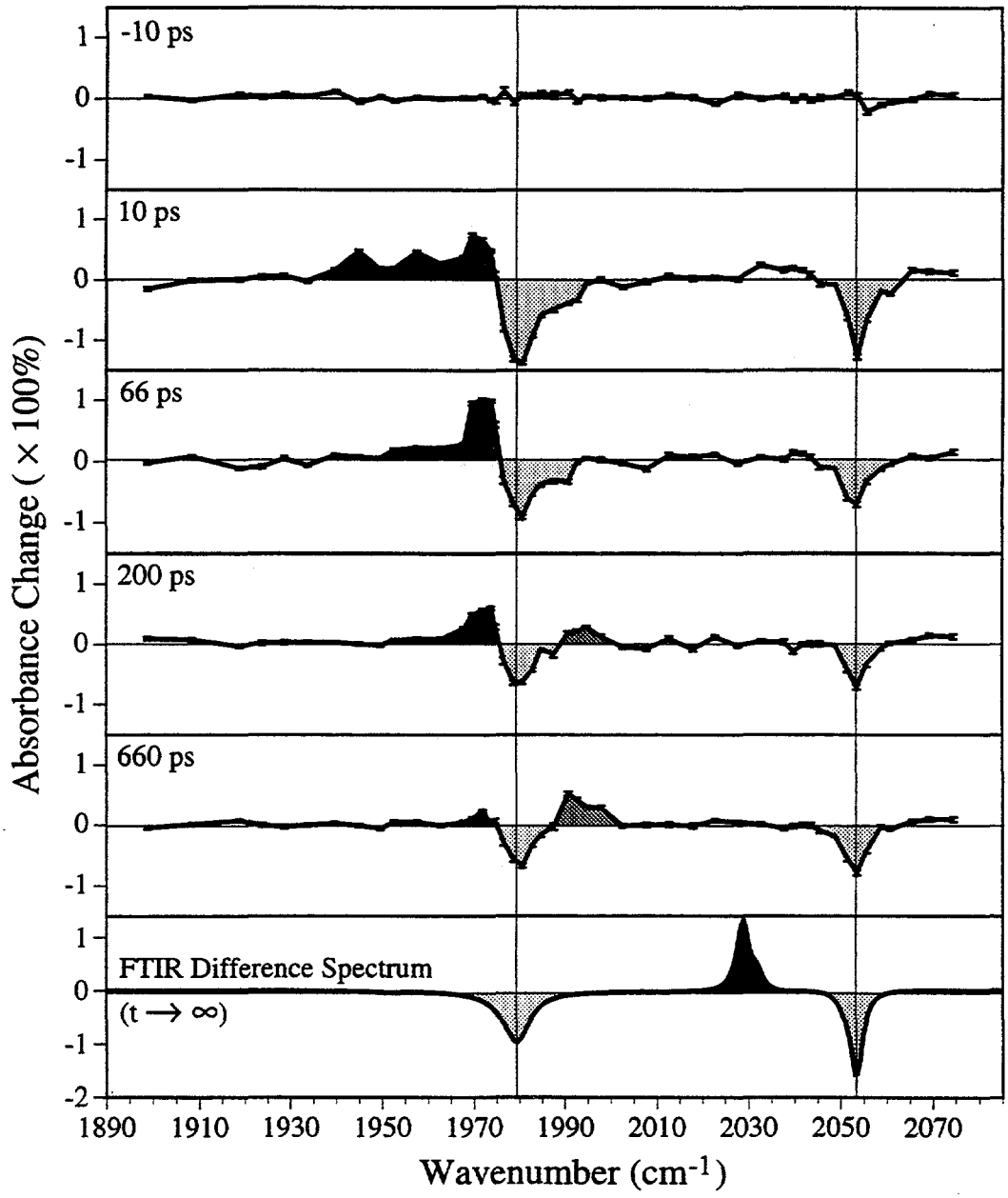

Figure 4.2 - Ultrafast IR spectrum of $Tp^*Rh(CO)_2$ in cyclohexane

660 ps. Similar spectral evolution was also observed in *n*-pentane solution (Figure 4.3). The last panel in Figure 4.2 is an FTIR difference spectrum of the sample after exposure to about 30 UV pulses at 308 nm from an excimer laser. The negative CO stretching bands at 1981 cm^{-1} and 2054 cm^{-1} indicate the depletion of the parent molecule while all positive absorption bands correspond to the creation of new species. Detailed kinetics of the spectral features in n-pentane were measured up to 1 ns as shown in Figures 4.4-4-7. A broad wavelength-independent background signal from CaF_2 windows has been subtracted from both the transient spectra and kinetics (Figure 4.4).

As shown in Figure 4.2, the bleaches at 1981 cm^{-1} and 2054 cm^{-1} partially recover within 66 ps. In addition, the detailed kinetics of the bleach at 2054 cm^{-1} are shown in Figure. 4.5. About 50% of the bleach recovers with a 70 ps time constant while the other half stays constant until ca. 1 ns, the longest delay time that can be achieved with our translation stage. This partial recovery is slightly smaller than the expected 70% recovery based on the reported 30% quantum yield [169]. This difference suggests that there is a fast reformation of the ground state parent molecule through the ultrafast geminate recombination of the CO and monocarbonyl species and/or radiative and radiationless decay from the excited state [105]. It is important to note, however, that the 70 ps recovery time is not necessarily an indication of the time scale of these processes. It can also reflect the vibrational relaxation of the rapidly formed hot ground state molecules.

The spectrum at 10 ps shows absorption bands at 1972, 1958 and 1945 cm^{-1}. These bands are assigned to the ν=0-1, 1-2 and 2-3 transitions, respectively, of the CO stretching mode of an intermediate. Photoproducts with vibrationally excited CO stretching

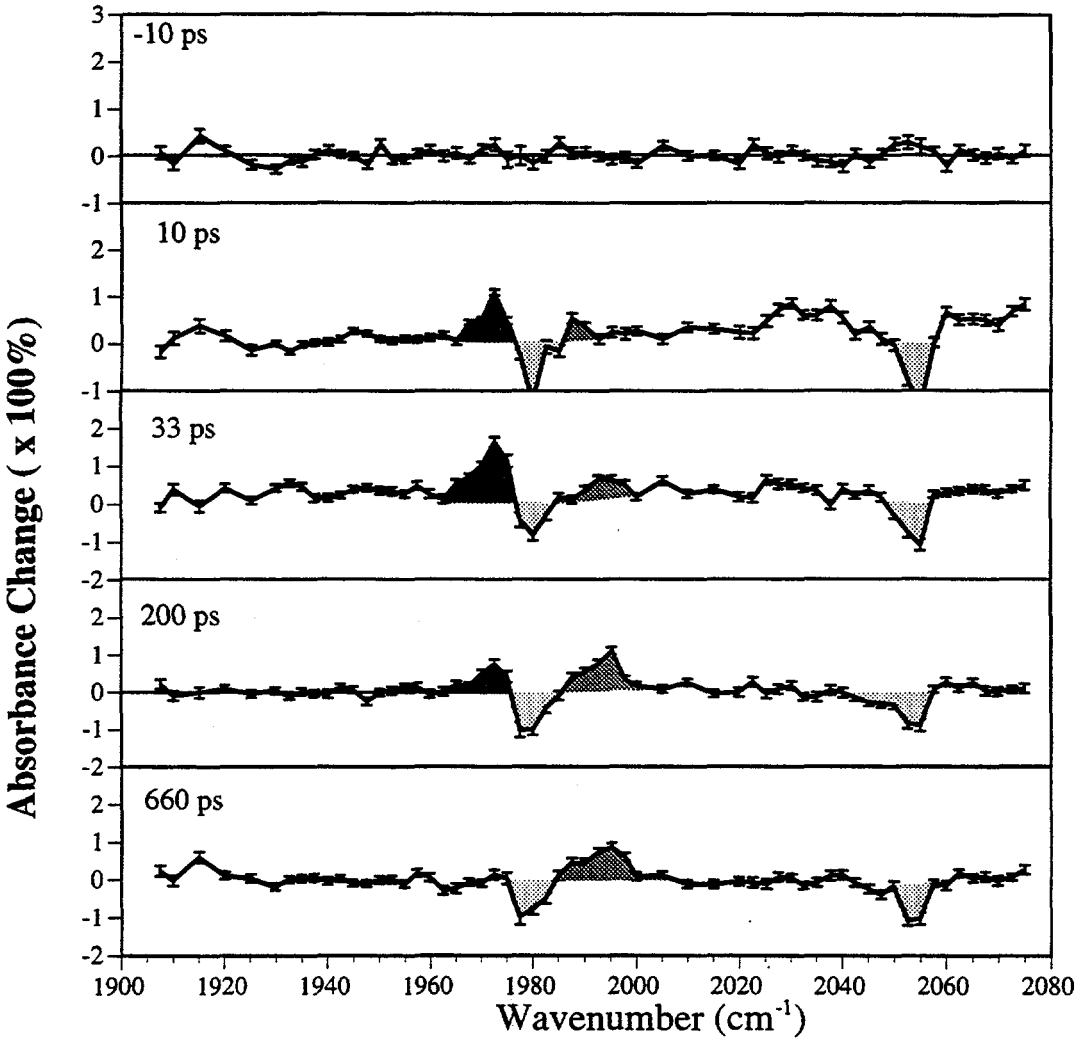

Figure 4.3 - Ultrafast IR spectrum of $Tp^*Rh(CO)_2$ in pentane

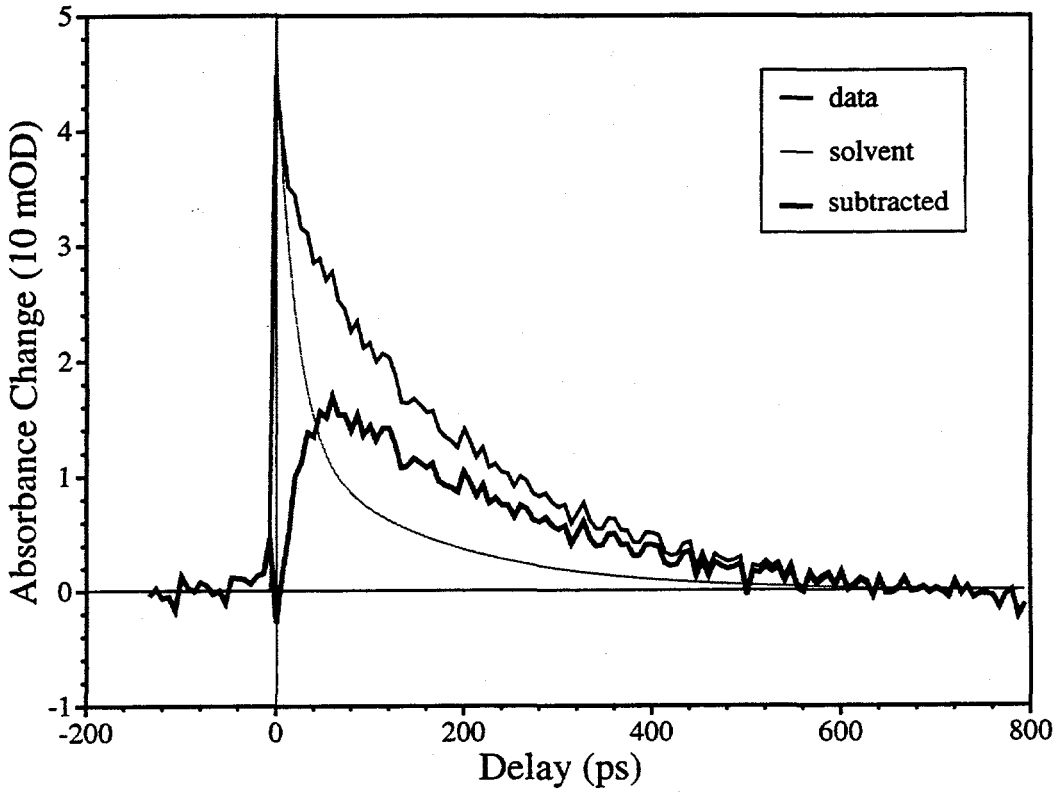

Figure 4.4 - Kinetics of $Tp^*Rh(CO)_2$ at 1973 cm^{-1} in cyclohexane.showing data subtraction.

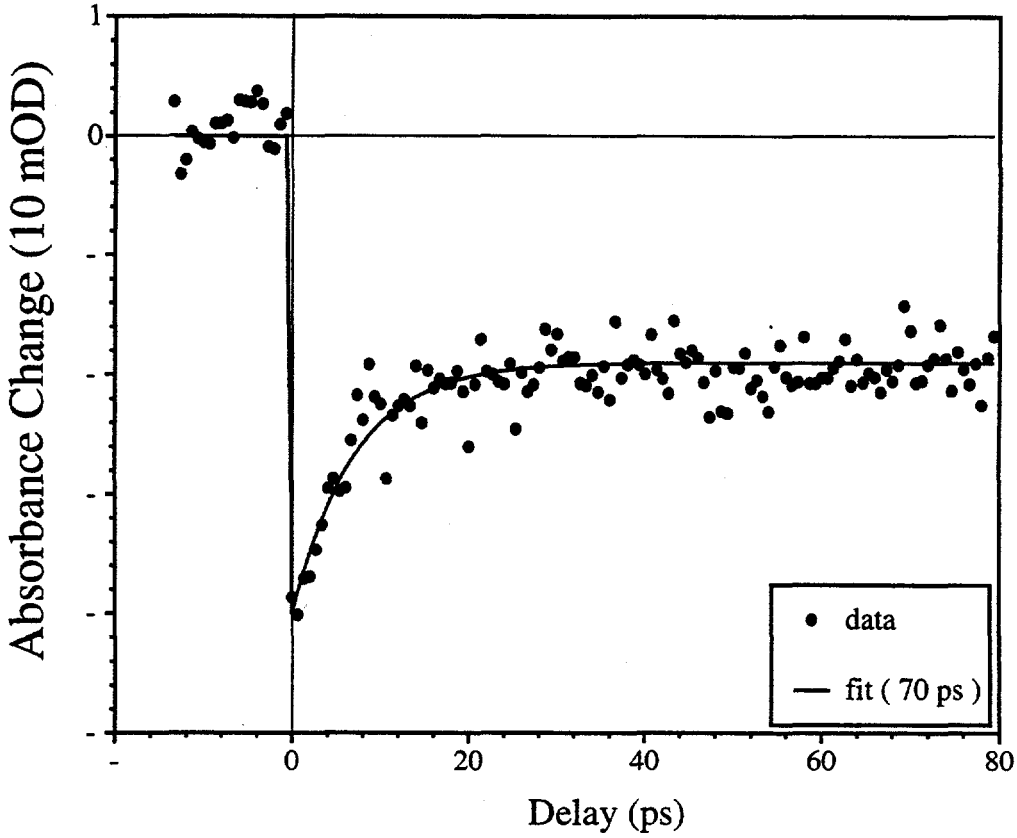

Figure 4.5 -Bleach recovery kinetics of $Tp^*Rh(CO)_2$ at 2054 cm^{-1} in pentane.

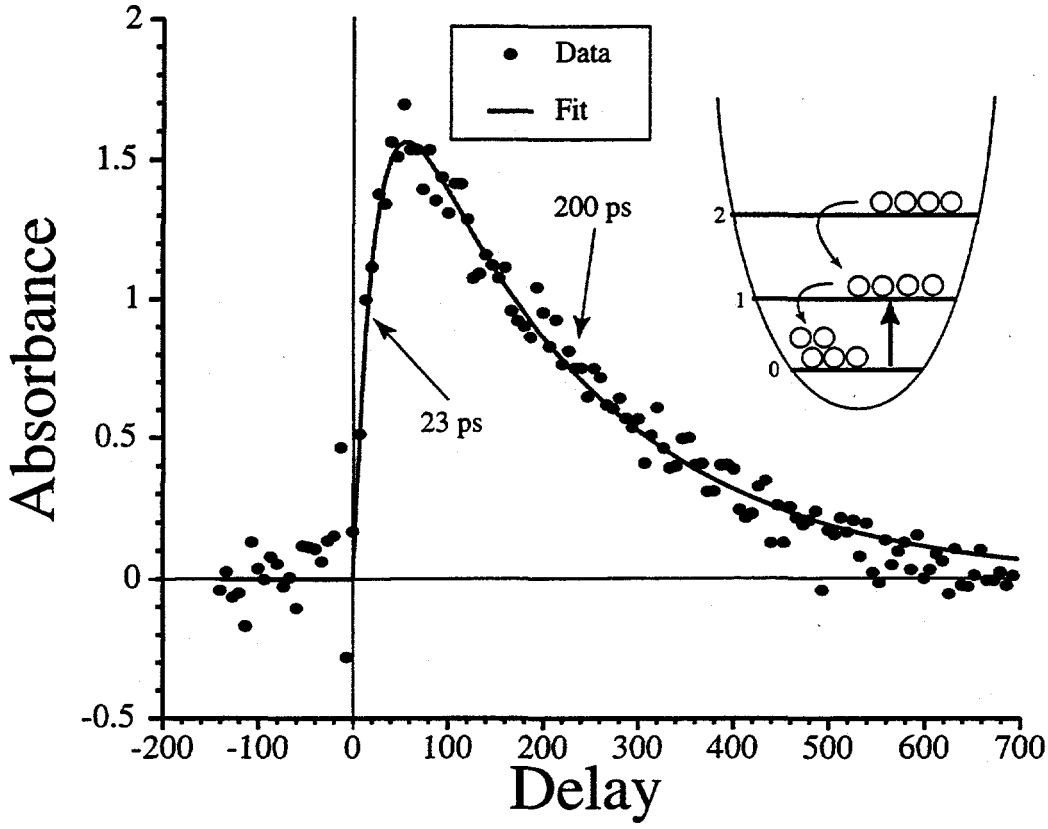

Figure 4.6 - Kinetics of $Tp^*Rh(CO)_2$ at 1973 cm^{-1} in pentane after subtraction.

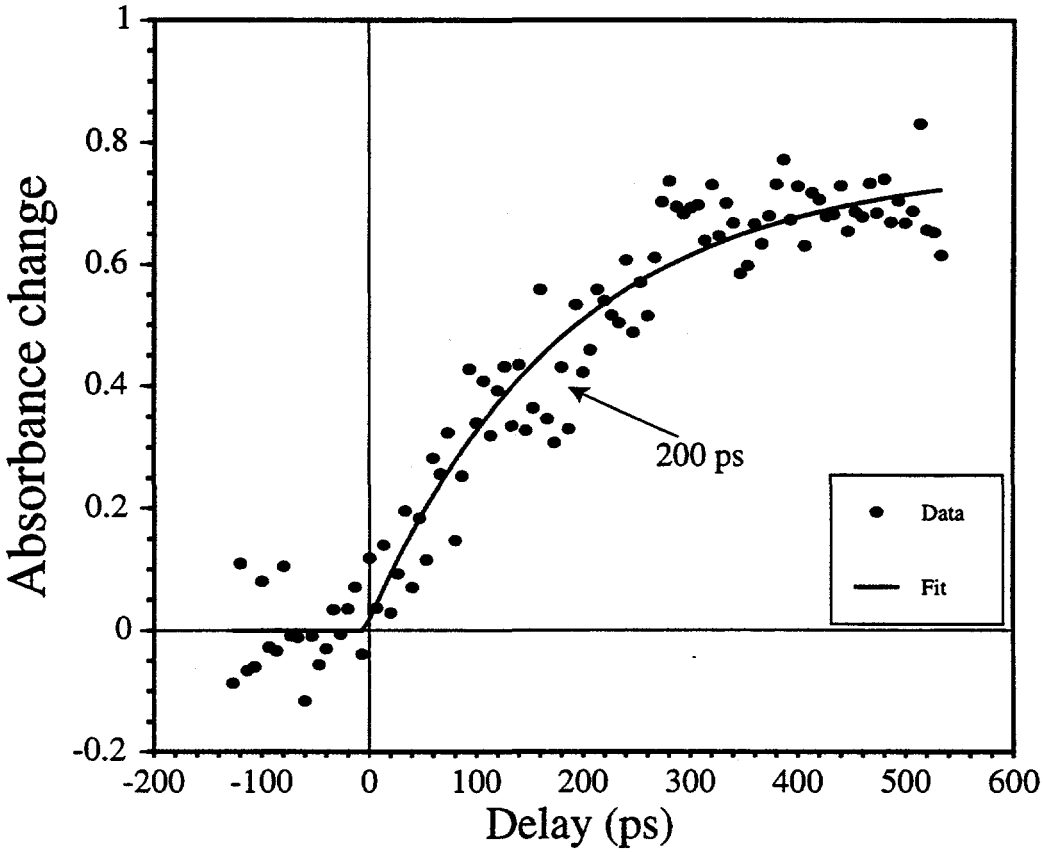

Figure 4.7 - Kinetics of $Tp^*Rh(CO)_2$ at 1990 cm^{-1}in pentane.

modes have been observed in the photolysis of other metal carbonyl such as $M(CO)_6$ (M=Cr, W, and Mo) [44, 105]. The observed anharmonic shift of about 13 cm^{-1} is also similar to those of other metal carbonyls [44, 140, 170]. The time scale for the vibrational cooling of this intermediate in n-pentane is found to be about 23 ps by monitoring the rise time of the signal at the v=0-1 transition frequency as shown in Figure 4.6. The spectrum at 66 ps shows that the vibrationally deactivated intermediate has only one absorption band at 1972 cm^{-1}, in the spectral region from 1900 to 2075 cm^{-1}. This species decays to form a new intermediate with a single absorption band at 1990 cm^{-1}.

We assign the first intermediate (denoted **A**) with CO absorption at 1972 cm^{-1} to Tp*Rh(CO)•RH (RH = alkane solvent), a complex between the monocarbonyl and the solvent [36]. The time scale for formation of the intermediate is consistent with those associated with solvent complex generation observed in previous studies of $CpCo(CO)_2$ [45] and $(acac)Rh(CO)_2$ (acac = acetyl acetonate) [170], and $M(CO)_6$ (M = Cr, Mo, and W) [38, 40, 68]. After the CO dissociated from the metal center, the solvent moved in to occupy the empty site on the metal, and formed a complex that vibrationally relaxed in 10 to 20 ps. The $Tp*Rh(CO)_2$ molecule shows similar reactivity and formed a new complex that vibrationally cools on a time scale of 23 ps. This monocarbonyl solvent complex then converts to the second intermediate, **B**, on a time scale of 200 ps (Figure 4.7).

The identity of **B** is more difficult to assign. There is some experimental and preliminary theoretical evidence to support the postulate that one of the pyrazolyl arms in the Tp*Rh(CO)•RH complex may detach from the metal center after photoexcitation [155, 165, 169, 171-173]. In the $Tp*Rh(CO)_2$ starting material, the three pyrazolyl arms are

coordinated to the Rh center to form an η^3 complex (Figure 1b) whereas the dechelated complex would be η^2 (Figure 1c). In room temperature solution, the $Tp^*Rh(CO)_2$ complex exists as a mixture of η^3 and η^2 isomers, with equilibrium constant $K_{eq} = 100$ favoring the η^3 species [155]. In addition, recent density functional theory calculations by Zaric and Hall [174] indicate that the closely related monocarbonyl complex TpRhCO (Tp = $HB—Pz_3$, Pz = pyrazolyl) may be stable in an η^2-bound configuration. Static low-temperature matrix studies [161] and ab initio calculations support the blue-shifted position of the CO stretch in η^2-Tp* complexes. Thus, the second intermediate observed in the ultrafast IR spectrum may be an η^2-Tp*RhCO•RH complex. Despite this support, there has been no experimental evidence for the involvement of an η^2 species in the early time dynamics of the C—H bond activation reaction at room temperature.

A model chemical system for probing the effect of dechelation on CO stretching frequencies and testing whether **B** is an η^2 solvent complex is $Bp^*Rh(CO)_2$ (Bp* = $H_2B—Pz_2^*$, Pz* = 3,5-dimethylpyrazolyl) (Fig. **1d**) [161]. This complex, with only two pyrazolyl rings attached to the boron atom, is a known stable η^2-species. Because it has only two Rh-N bonds instead of three, the CO stretches of this compound are blue-shifted 30 wavenumbers relative to the η^3-$Tp^*Rh(CO)_2$ complex. Photoinduced loss of CO from $Bp^*Rh(CO)_2$ should produce a monocarbonyl species whose coordination environment is similar to the proposed η^2-Tp*Rh(CO) intermediate. Briefly, the $Bp^*Rh(CO)_2$ compound was prepared according to the literature [175] and dissolved in dry cyclohexane (~ 1.4 mM). The solution was sealed under a nitrogen atmosphere and flowed through a 1-mm IR cell. After irradiation at 295 nm, the spectrum was collected from 1960 to 2090 cm^{-1} at

time delays of -10, 10, 66, 200, and 660 ps. The ultrafast IR spectra of Bp* in cyclohexane (Figure 4.8) show that at 10 ps, the bleaching of the parent peaks at 2010 and 2080 cm^{-1} coincides with the growth of a another peak at 1992 cm^{-1}. Thus, the spectrum of the η^2-Bp*RhCO matches that of the second intermediate in the $Tp^*Rh(CO)_2$ system. There is, however, no peak at 1972 cm^{-1} as there is in the $Tp^*Rh(CO)_2$ system, which suggests that the second intermediate in the reaction scheme is an η^2-Tp*RhCO•RH complex in which one of the Rh-N bonds is broken. With this proposed structure for the second intermediate, we have assigned all of the observable species in the ultrafast spectra and can focus on the bond-activation process.

In the $Tp^*Rh(CO)_2$ system, the newly assigned second intermediate was stable to ~1 ns, the longest time we could measure with our ultrafast system, so we could not observe the formation of the final C—H activated product. In order to understand the complete reaction and establish whether other intermediates are involved, we must observe the final bond activation step and link this with the ultrafast dynamics. Previous studies with microsecond time resolution showed that this step occurs in less than 1 μs [176], and so the time scale of the final bond-activating step is between 1 ns and 1 μs. In order to follow the rest of the chemistry, nanosecond IR experiments were performed to probe C—H activation of $Tp^*Rh(CO)_2$ in alkane solvents.

Representative nanosecond time-resolved spectra of $Tp^*Rh(CO)_2$ in cyclohexane (Figure 4.9) show a decrease in C—O absorption at 1981 and 2054 cm^{-1}, due to the fast depletion of the parent molecule, and a new absorption at 1990 cm^{-1} that grew in in less than 50 ns. The observation of a single peak indicates that we are observing a

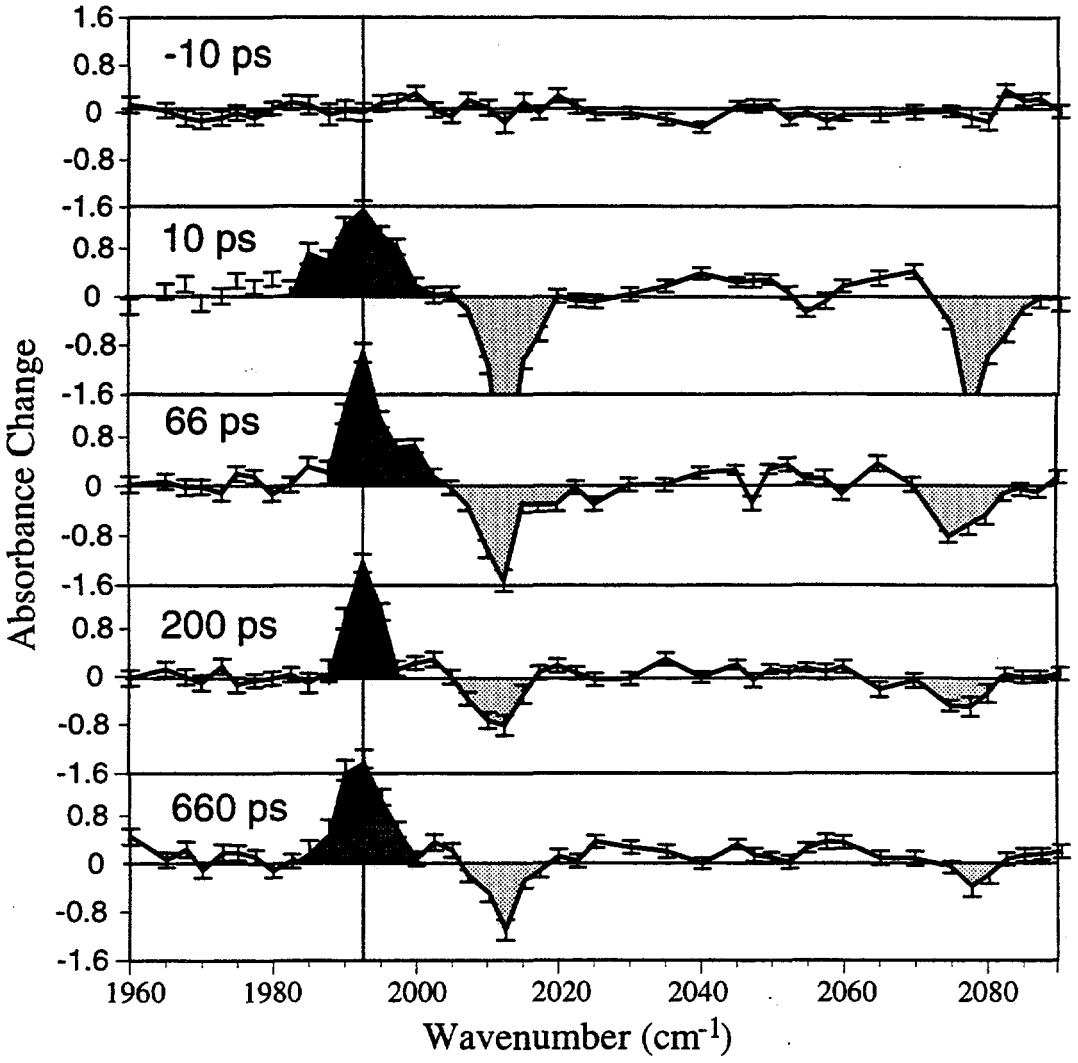

Figure 4.8 - Ultrafast Transient Absorption spectrum of $Bp^*Rh(CO)_2$ in cyclohexane.

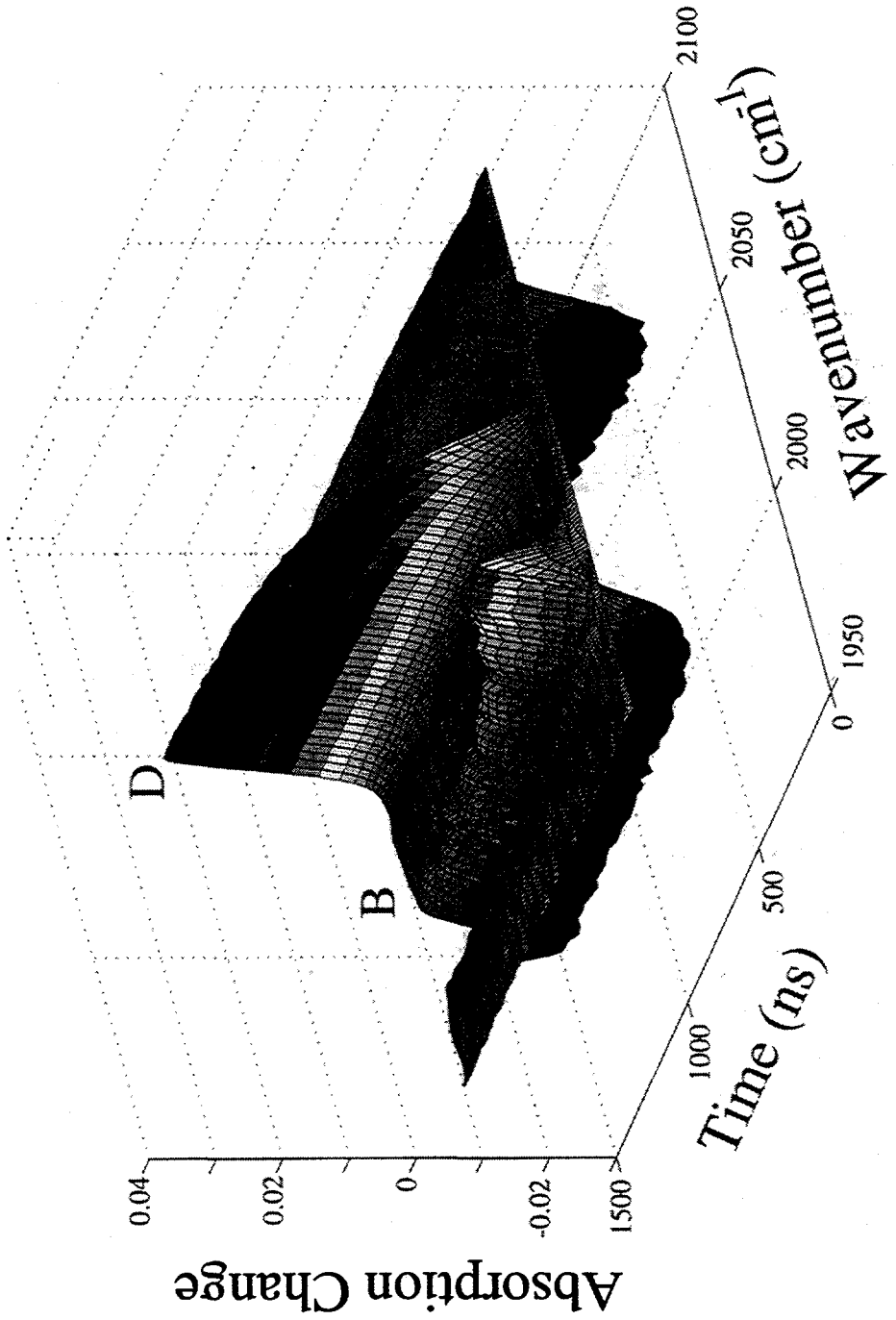

Figure 4.9 - Nanosecond Transient Absorption Spection of $Tp^*Rh(CO)_2$ cyclohexane

monocarbonyl species, and the frequency of the peak matches the longest lived η^2–Tp*Rh(CO)•RH transient observed in the ultrafast IR measurements on this same system (Figure 4.2). The signal at 1990 cm^{-1} decayed to below the baseline and could be fit to an exponential of ~280 ± 11 ns (curve **B** in Figure 4.10). The subsequent formation of the alkyl hydride product was observed at 2032 cm^{-1} (curve **D** in Figure 4.10). It grew in with a single exponential time constant of 230 ± 3 ns. The decay time of intermediate **B** is longer than the formation time of the final product **D** because of thermal effects associated with the parent bleach at 1981 cm^{-1}. Temperature changes in the sample due to absorption of the laser pulse caused a time dependent change in the refractive index of the sample [177]. Such effects appear as time dependent changes in absorbance near strong parent peaks and increase the observed lifetime of nanosecond transient intermediates. Because the transient at 1990 cm^{-1} was close to the parent bleach at 1981 cm^{-1}, it was strongly influenced by these effects whereas the final product at 2032 cm^{-1} was further away from the bleaches and was not affected.

4.4 Discussion

For the Bp*Rh$(CO)_2$ system, nuclear magnetic resonance (NMR) and IR studies showed that upon UV photolysis, there is no formation of C—H activated product, consistent with previous work [165, 171-173]. Time-resolved FTIR measurements showed only one peak at 1992 cm^{-1} due to the monocarbonyl solvent complex and no evidence for the formation of an alkyl hydride (Figure 4.11). The solvent complex was stable for longer than 1 μs, but static FTIR spectra show that it eventually recombined with

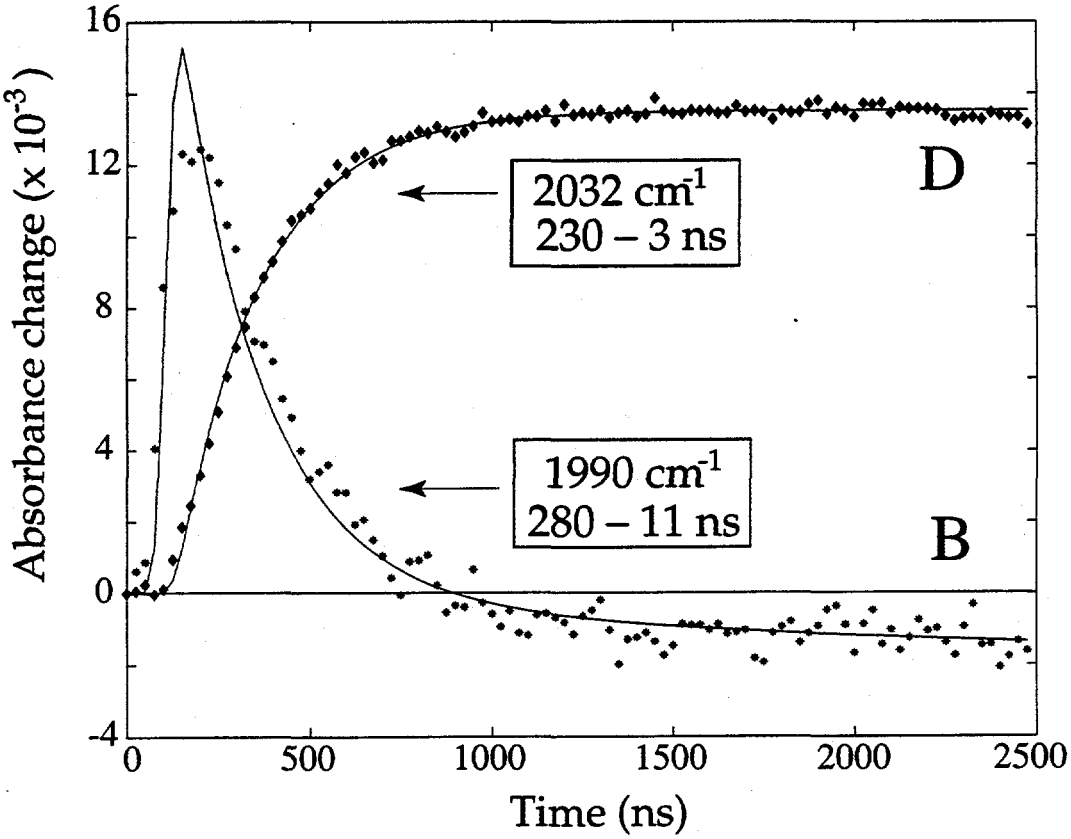

Figure 4.10 - Nanosecond Kinetics of Tp*Rh(CO)$_2$ in cyclohexane.

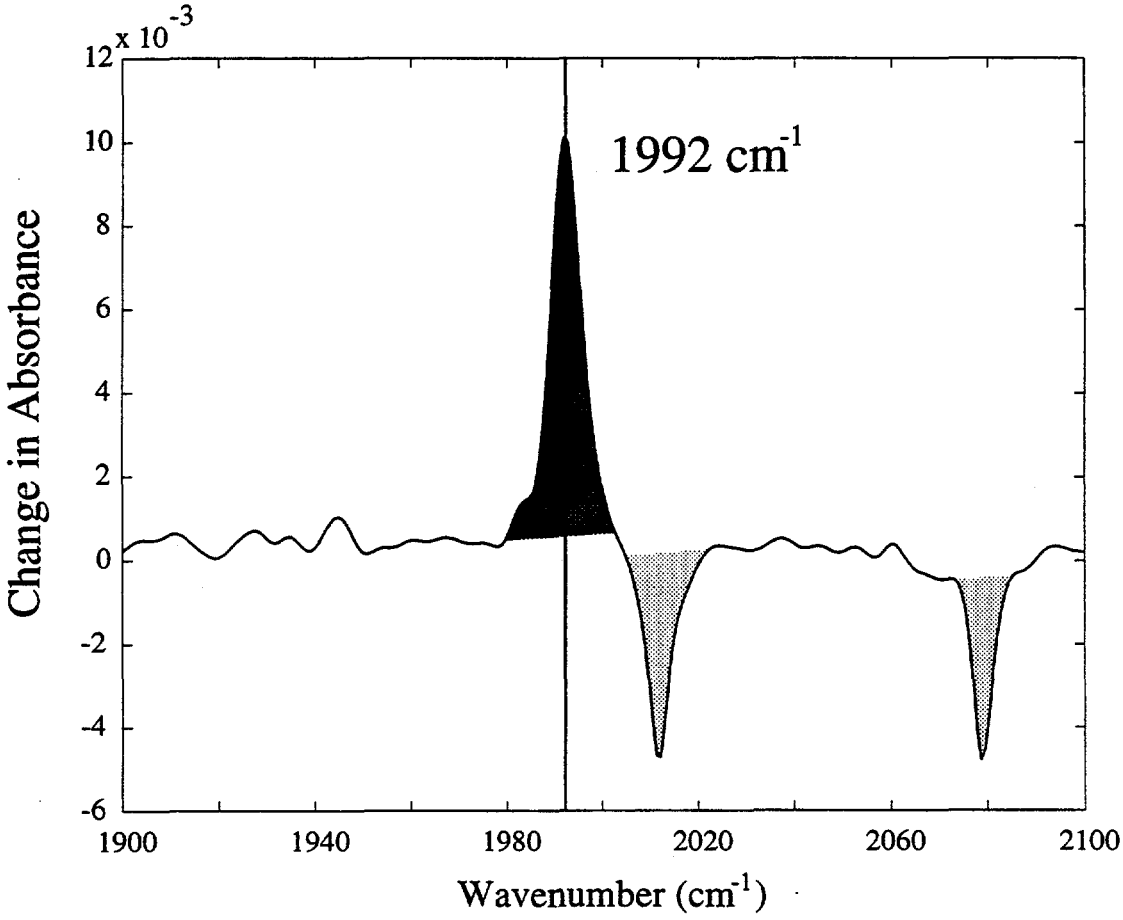

Figure 4.11 - Transient Absorption spectrum of $Bp^*Rh(CO)_2$ in cyclohexane 1 μs after excitation

CO or decomposes into unknown products. The inability of $Bp^*Rh(CO)_2$ to activate C—H bonds suggests that not only is dechelation necessary to provide reactivity at the metal center, but rechelation is required to stabilize the product that results from the reaction.

The nanosecond time scale of the reaction indicates that there is a significant thermal barrier involved in the formation of the C—H activated product. Rate constants k determined from the experiments presented here allow us to estimate values for the reaction barrier in room temperature solutions. For the cyclohexane reaction, a simple treatment with transition state theory and a rate constant of 4.3×10^6 s^{-1} (1/230 ns) at 295 K, gives the height of the free energy barrier, $\Delta G^{\ddagger}$, as ~8.3 kcal/mol. This estimate is comparable to the value of 7.2 kcal/mol calculated for the $Cp^*Rh(CO)_2$ system by extrapolating the results of 183 K liquid Kr-cyclohexane experiments to room temperature [144]. We can combine these data with our earlier ultrafast result to assemble a comprehensive reaction coordinate diagram (Figure. 4.12).

The rhodium dicarbonyl is initially in formal oxidation state (I). Upon UV irradiation, the compound loses one CO in less than 100 fs [51, 52] to form a vibrationally hot, coordinatively unsaturated (16-electron) complex, also in oxidation state (I). The reactive species generated is quickly solvated in a barrierless reaction and then vibrationally cools in 20 ps [43, 45, 140]. All subsequent processes that take place at the Rh center are either thermal, and do not require the absorption of additional photons, or depend on residual photon energy in the complex. The CO stretching absorption of the first detectable solvated intermediate **A** could be observed at 1972 cm^{-1}, red-shifted from the lowest frequency peak of the parent complex at 1981 cm^{-1}. Loss of one CO substantially reduces

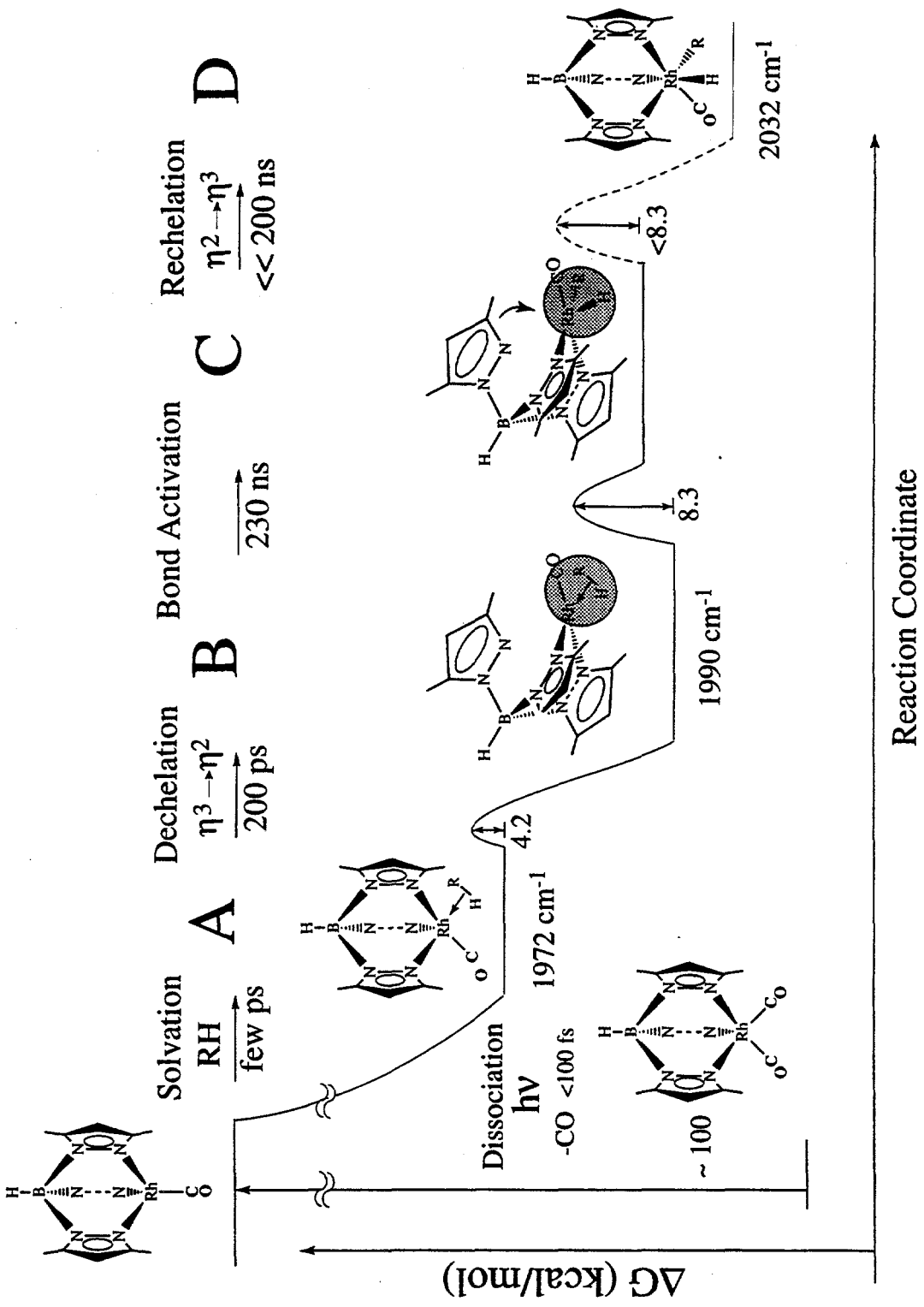

Figure 4.12 - Proposed mechanism for $Tp^*Rh(CO)_2$ C-H bond activation.

back-bonding from Rh and increases the electron density at the metal center. This change weakens the bonds between the Rh center and the σ-donating Tp* pyrazole ligands and eventually breaks of a Rh-N bond. The complex traverses a 4.2 kcal/mol barrier, [with k = 5.0 x 10^9 s^{-1} or 1/ 200 ps] and forms the η^2-Tp* monocarbonyl complex **B**. Removal of the electrons formerly donated to the metal by the now-detached arm of the Tp* ligand reduces the electron density at the metal again, shifting the CO absorption to higher frequency (1990 cm^{-1}). Detachment of the pyrazole ring in **B** increases the coordinative unsaturation of the solvate, making it more reactive toward C—H oxidative addition. The bond-breaking step occurs with a time constant of 230 ns, corresponding to a barrier of ~8.3 kcal/mol and forms the unstable η^2 C—H activated complex (**C**). This complex now has the metal center in formal oxidation state (III), which reduces its electron density, providing the driving force for rechelation of the dangling pyrazole ring to form the final product, Tp*Rh(CO)(R)(H) (complex **D**).

4.5 Conclusion

Monitoring the C—H bond activation reaction in the nanosecond regime with IR detection has made it possible to establish directly the time scale for C—H bond-activation in room-temperature solution. The final breaking of the C—H bond occurs during the last step of the reaction, 230 ns after photolysis in cyclohexane. Before this bond can be broken, the Tp*Rh$(CO)_2$ complex must dissipate its initial excess vibrational energy, and then break one of the Rh-N bonds. Immediately following the rate limiting C—H bond-activation step, the Rh-N bond reforms to stabilize the final product. These steps before

and after activation provide the structural and electronic environment around the metal center that allows the reaction to occur. Taking into account the ultrafast and nanosecond infrared experiments on $Tp^*Rh(CO)_2$ and the related $Bp^*Rh(CO)_2$, we have followed the C—H bond reaction in room temperature solution *over 10 orders of magnitude* in time to generate a complete picture of the overall mechanism.

References

1. A. Dienes, E. P. Ippen and C. V. Shank,*Applied Physics Letters* **19**, 258-60 (1971).

2. C. V. Shank, E. P. Ippen and A. Dienes,*IEEE Journal of Quantum Electronics* **QE**, 525 (1972).

3. E. P. Ippen, C. V. Shank and A. Dienes,*Applied Physics Letters* **21**, 348-50 (1972).

4. A. L. Harris, M. Berg and C. B. Harris,*Journal of Chemical Physics* **84**, 788 (1986).

5. M. Berg, A. L. Harris, J. K. Brown and C. B. Harris,*Optics Letters* **9**, 50-52 (1984).

6. J. C. King *Ultrafast Studies of Photodissociation in Solution: Dissociation, Recombination and Relaxation*; U. C. Berkeley, 1995.

7. D. C. Harris and M. D. Bertolucci *Symmetry and Spectroscopy: An Introduction to Vibrational and Electronic Spectroscopy*; Dover Publications, Inc.: New York, 1989.

8. V. Petrov and F. Noack,*Optics Letters* **21**, 1576-1578 (1996).

9. L. Shujie and T. Suzuki,*Optics Letters* **21**, 579-581 (1996).

10. A. J. Alcock and P. B. Corkum,*Canadian Journal of Physics* **57**, 1280-90 (1979).

11. C. Rolland and P. B. Corkum,*Journal of the Optical Society of America B* **3**, 1625-1629 (1986).

12. F. Seifert and V. Petrov,*Journal of Applied Physics* **vol.74**, 4798-800 (1993).

13. T. P. Dougherty and E. J. Heilweil,*Optics Letters* **19**, 129-131 (1994).

14. J. N. Moore, P. A. Hansen and R. M. Hochstrasser,*Chemical Physics Letters* **138**, 110-14 (1987).

15. A. E. Siegman *Lasers*; University Science Books: Mill Valley, 1986.

16. G. W. Flynn, L. O. Hocker, A. Javan, M. A. Kovacs and C. K. Rhodes,*IEEE Journal of Quantum Electronics* **2**, 378 (1966).

17. R. M. Osgood, Jr., E. R. Nichols, W. C. Eppers, Jr. and R. D. Petty,*Applied Physics Letters* **15**, 69-72 (1969).

18. R. M. Osgood, Jr. and E. R. Nichols,*Laser Focus* **5**, 37-40 (1969).

19. R. M. Osgood, Jr., W. C. Eppers, Jr. and E. R. Nichols,*IEEE Journal of Quantum Electronics* **QE**, 145-54 (1970).

20. R. M. Osgood, Jr., E. R. Nichols and W. C. Eppers, Jr.,*IEEE Journal of Quantum Electronics* **QE**, 173 (1970).

21. R. L. Fork, B. I. Greene and C. V. Shank,*Applied Physics Letters* **38**, 671-627 (1981).

22. N. Sarukura, Y. Ishida, H. Nakano and Y. Yamamoto,*Applied Physics Letters* **56**, 814-15 (1990).

23. S. Oda, Y. Segawa, N. Kodama, P. H. Kim and S. Namba,*Japanese Journal Of Applied Physics Part 2-Letters* **28**, L1977-L1978 (1989).

24. B. Dance,*Laser Focus World* **26**, 34-34 (1990).

25. P. F. Moulton,*Optics & Photonics News* **1**, 20-3 (1990).

26. P. Georges, T. Lepine, G. Roger and A. Brun,*Journal de Physique IV (Colloque)* **1**, 271-4 (1991).

27. N. Sarukura and Y. Ishida,*IEEE Journal of Quantum Electronics* **28**, 2134-41 (1992).

28. H. C. K. Built according to the design of M. M. Murnane, C. P. Hyang, M. T. Asaki, and D. Garvey,

29. H. Yang ; UC Berkeley, in preparation.

30. M. C. Asplund; UC Berkeley, in preparation.

31. H. Sun and H. Frei,*Journal Of Physical Chemistry B* **101**, 205-209 (1997).

32. G. L. Geoffroy and M. S. Wrighton *Organometallic Photochemistry*; Academic: New York, 1978.

33. B. A. Arndtsen, R. G. Bergman, T. A. Mobley and T. H. Peterson,*Accounts Of Chemical Research* **28**, 154-162 (1995).

34. R. G. Bergman,*Science* **223**, 902 (1984).

35. R. N. Perutz,*Chemical Society Reviews* **22**, 361-369 (1993).

36. T. Lian, S. E. Bromberg, H. Yang, G. Proulx, R. G. Bergman and C. B. Harris,*Journal Of the American Chemical Society* **118**, 3769-3770 (1996).

37. S. E. Bromberg, T. Q. Lian, R. G. Bergman and C. B. Harris,*Journal Of the American Chemical Society* **118**, 2069-2072 (1996).

38. J. C. King, J. Z. Zhang, B. J. Schwartz and C. B. Harris,*Journal Of Chemical Physics* **99**, 7595-7601 (1993).

39. J. Z. Zhang and C. B. Harris,*Journal Of Chemical Physics* **95**, 4024-4032 (1991).

40. M. Lee and C. B. Harris,*Journal Of the American Chemical Society* **111**, 8963-8965 (1989).

41. T. Lian, B. Locke, M. Iannone and R. M. Hochstrasser ; V ed.; Springer Proc. Phys:, 1991; Vol. 68.

42. P. A. Anfinrud, C. H. Han, T. Q. Lian and R. M. Hochstrasser,*Journal Of Physical Chemistry* **95**, 574-578 (1991).

43. M. W. George, T. P. Dougherty and E. J. Heilweil,*Journal Of Physical Chemistry* **100**, 201-206 (1996).

44. T. P. Dougherty and E. J. Heilweil,*Chemical Physics Letters* **227**, 19-25 (1994).

45. T. P. Dougherty, W. T. Grubbs and E. J. Heilweil,*Journal Of Physical Chemistry* **98**, 9396-9399 (1994).

46. E. Odriscoll and J. D. Simon,*Journal Of the American Chemical Society* **112**, 6580-6584 (1990).

47. X. L. Xie and J. D. Simon,*Journal Of the American Chemical Society* **112**, 1130-1136 (1990).

48. J. D. Simon and X. Xie,*Journal of Physical Chemistry* **93**, 291 (1989).

49. J. D. Simon and X. Xie,*Journal of Physical Chemistry* **91**, 5538 (1987).

50. J. D. Simon,*Journal of Physical Chemistry* **90**, 6751 (1986).

51. A. G. Joly and K. A. Nelson,*Journal of Physical Chemistry* **93**, 2876 (1989).

52. A. G. Joly and K. A. Nelson,*Chemical Physics* **152**, 69-82 (1991).

53. S. C. Yu, X. Xu, R. Lingle, Jr. and J. B. Hopkins,*Journal of the American Chemical Society* **112**, 3668 (1990).

54. J. D. Simon and K. S. Peters,*Chemical Physics Letters* **98**, 53 (1983).

55. L. J. Rothberg, N. J. Cooper, K. Peters and V. Vaida,*Journal of the American Chemical Society* **104**, 3536 (1982).

56. J. A. Welch, K. S. Peters and V. Vaida,*Journal of Physical Chemistry* **86**, 1941 (1982).

57. S. K. Kim, S. Pedersen and A. H. Zewail,*Chemical Physics Letters* **233**, 500-508 (1995).

58. A. Waldman, S. Ruhman, S. Shaik and G. N. Sastry,*Chemical Physics Letters* **230**, 110-116 (1994).

59. J. R. Sprague, S. M. Arrivo and K. G. Spears,*Journal Of Physical Chemistry* **95**, 10528-10531 (1991).

60. L. Wang, X. Zhu and K. G. Spears,*The Journal of Physical Chemistry* **93**, 2 (1989).

61. J. C. Owrutsky, D. Raftery and R. M. Hochstrasser,*Annual Review Of Physical Chemistry* **45**, 519-555 (1994).

62. J. A. Weich, V. Vaida and G. L. Geoffrey,*Journal of Physical Chemistry* **87**, 3635 (1983).

63. D. P. Gerrity, L. J. Rothberg and V. Vaida,*Journal of Physical Chemistry* **87**, 2222 (1983).

64. D. G. Leopold and V. Vaida,*Journal of the American Chemical Society* **105**, 6809 (1993).

65. S. Leutwyler and U. Even,*Chemical Physics Letters* **84**, 188 (1981).

66. J. M. Kelly, D. V. Bent, H. Herman, D. Schulte-Frohlinde and E. K. von Gustorf,*Journal of Organometallic Chemistry* **69**, 259 (1974).

67. R. N. Perutz and J. J. Turner,*Journal of the American Chemical Society* **97**, 4791 (1975).

68. X. B. Xu, R. Lingle, S. C. Yu, Y. J. Chang and J. B. Hopkins,*Journal Of Chemical Physics* **92**, 2106-2107 (1990).

69. T. P. Dougherty and E. J. Heilweil,*Journal Of Chemical Physics* **100**, 4006-4009 (1994).

70. S. M. Arrivo, T. P. Dougherty, W. T. Grubbs and E. J. Heilweil,*Chemical Physics Letters* **235**, 247-254 (1995).

71. E. J. Heilweil, R. R. Cavanagh and J. C. Stephenson,*Journal of Chemical Physics* **89**, 230 (1988).

72. E. J. Heilweil, R. R. Cavanagh and J. C. Stephenson,*Chemical Physics Letters* **134**, 181 (1987).

73. A. Tokmakoff, B. Sauter, A. S. Kwok and M. D. Fayer,*Chemical Physics Letters* **221**, 412-418 (1994).

74. A. Tokmakoff, B. Sauter and M. D. Fayer,*Journal Of Chemical Physics* **100**, 9035-9043 (1994).

75. M. Iannone, B. R. Cowen, R. Diller, S. Maiti and R. M. Hochstrasser,*Applied Optics* **30**, 5247-5249 (1991).

76. J. Nasielski and A. Colas,*Inorganic Chemistry* **17**, 237 (1978).

77. A. J. Rest and J. R. Sodeau,*Society of Faraday Transaction 2* **37**, 1691 (1977).

78. T. M. McHugh, R. Narayanaswamy, A. J. Rest and K. Salisbury,*Journal of the Chemical Society, Chemical Comunications* 209 (1979).

79. S. K. Nayak and T. J. Burkey,*Organometallics* **10**, 3745-3750 (1991).

80. S. Wieland and R. Vaneldik,*Journal Of Physical Chemistry* **94**, 5865-5870 (1990).

81. A. L. Harris, J. K. Brown and C. B. Harris,*Annual Review of Physical Chemistry* **39**, 341-366 (1988).

82. I. Benjamin, U. Banin and S. Ruhman,*Journal Of Chemical Physics* **98**, 8337-8340 (1993).

83. P. K. Walhout, J. C. Alfano, K. A. M. Thakur and P. F. Barbara,*Journal Of Physical Chemistry* **99**, 7568-7580 (1995).

84. J. C. Alfano, Y. Kimura, P. K. Walhout and P. F. Barbara,*Chemical Physics* **175**, 147-155 (1993).

85. D. A. V. Kliner, J. C. Alfano and P. F. Barbara,*Journal Of Chemical Physics* **98**, 5375-5389 (1993).

86. A. E. Johnson, N. E. Levinger and P. F. Barbara,*Journal Of Physical Chemistry* **96**, 7841-7844 (1992).

87. B. J. Schwartz, J. C. King and C. B. Harris ; B. J. Schwartz, J. C. King and C. B. Harris, Ed.; Kluwer Academic: Dordrecht, 1994, pp 235-248.

88. B. J. Schwartz, J. C. King, J. Z. Zhang and C. B. Harris,*Chemical Physics Letters* **203**, 503-508 (1993).

89. U. Banin, A. Waldman and S. Ruhman,*Journal Of Chemical Physics* **96**, 2416-2419 (1992).

90. U. Banin, R. Kosloff and S. Ruhman,*Israel Journal Of Chemistry* **33**, 141-156 (1993).

91. U. Banin and S. Ruhman,*Journal Of Chemical Physics* **99**, 9318-9321 (1993).

92. U. Banin and S. Ruhman,*Journal Of Chemical Physics* **98**, 4391-4403 (1993).

93. U. Banin, A. Bartana, S. Ruhman and R. Kosloff,*Journal Of Chemical Physics* **101**, 8461-8481 (1994).

94. U. Banin, R. Kosloff and S. Ruhman,*Chemical Physics* **183**, 289-307 (1994).

95. J. N. Moore, P. A. Hansen and R. M. Hochstrasser,*Journal of the American Chemical Society* **111**, 4563 (1989).

96. R. Zadoyan, Z. Li, P. Ashjian, C. C. Martens and V. A. Apkarian,*Chemical Physics Letters* **218**, 504-514 (1994).

97. C. Lienau, J. C. Williamson and A. H. Zewail,*Chemical Physics Letters* **213**, 289-296 (1993).

98. C. Lienau and A. H. Zewail,*Chemical Physics Letters* **222**, 224-232 (1994).

99. Q. L. Liu, J. K. Wang and A. H. Zewail,*Nature* **364**, 427-430 (1993).

100. Q. L. Liu, J. K. Wang and A. H. Zewail,*Journal Of Physical Chemistry* **99**, 11321-11332 (1995).

101. J. K. Wang, Q. L. Liu and A. H. Zewail,*Journal Of Physical Chemistry* **99**, 11309-11320 (1995).

102. E. D. Potter, Q. Liu and A. H. Zewail,*Chemical Physics Letters* **200**, 605-614 (1992).

103. J. M. Papanikolas, V. Vorsa, M. E. Nadal, P. J. Campagnola, J. R. Gord and W. C. Lineberger,*Journal Of Chemical Physics* **97**, 7002-7005 (1992).

104. J. M. Papanikolas, V. Vorsa, M. E. Nadal, P. J. Campagnola, H. K. Buchenau and W. C. Lineberger,*Journal Of Chemical Physics* **99**, 8733-8750 (1993).

105. T. Q. Lian, S. E. Bromberg, M. C. Asplund, H. Yang and C. B. Harris,*Journal Of Physical Chemistry* **100**, 11994-12001 (1996).

106. P. O. J. Scherer, A. Seilmeier and W. Kaiser,*Journal of Chemical Physics* **83**, 3948 (1985).

107. A. Seilmeier, P. O. J. Scherer and W. Kaiser,*Chemical Physics Letters* **105**, 1404 (1984).

108. F. Wondrazek, A. Seilmeier and W. Kaiser,*Chemical Physics Letters* **104**, 121 (1984).

109. K. Wynne, G. Haran, G. D. Reid, C. C. Moser, P. L. Dutton and R. M. Hochstrasser,*Journal Of Physical Chemistry* **100**, 5140-5148 (1996).

110. P. J. Giordano and M. S. Wrighton,*Inorganic Chemistry* **16**, 160 (1977).

111. R. H. Crabtree *The Organometallic Chemistry of the Transition Metals*; Wiley:, 1994.

112. D. M. Roundhill *Photochemistry and Photophysics of Metal Complexes*; Plenum Press: New York, 1994.

113. F. Basolo,*Coordination Chemistry Reviews* **125**, 13 (1993).

114. P. Costa, S. Sostero and O. Traverso,*Coordination Chemistry Reviews.* **125**, 53 (1993).

115. A. W. Adamson,*Coordination Chemistry Reviews* **125**, 1 (1993).

116. V. Carassiti,*Coordination Chemistry Reviews* **125**, 351 (1993).

117. N. Serpone and M. A. Jamieson,*Coordination Chemisry Reviews* **93**, 87 (1989).

118. C. M. Lukehart *Fundamental Transition Metal Organometallic Chemistry*; Brooks/Cole Publishing Company: Monterey, 1985.

119. A. J. Pearson *Metallo-organic Chemistry*; John Wiley & Sons: New York, 1985.

120. M. M. Taqui Khan and A. E. Martell *Homogeneous Catalysis by Metal Complexe, V. I and II*; Academic Pres: New York, 1974.

121. B. M. Trost,*Angewante Chemie, International Edition English* **34**, 259 (1995).

122. A. F. Noels, M. Graziani and A. J. Hubert *Metal Promoted Selectivity in Organic Synthesis*; Kluwer Academic Publishers:, 1991.

123. R. S. Dickson *Homogeneous Catalysis with Compounds of Rhodium and Iridium*; D. Reidel Publishing Co: Boston, 1985.

124. G. J. Kubas, G. Kiss and C. D. Hoff,*Organometallics* **10**, 2870 (1991).

125. U. Shubert ; U. Shubert, Ed.; Academic Press: New York, 1990; Vol. 30.

126. Y. Akio *Organotransition metal Chemistry: Fundamental Concepts and Applications*; John Wiley & Sons: New York, 1986.

127. J. U. Mondal and D. M. Blake,*Coordination Chemistry Reviews* **47**, 205 (1982).

128. B. A. Arndtsen and R. G. Bergman,*Science* **270**, 1970-1973 (1995).

129. A. A. Bengali, B. A. Arndtsen, P. M. Burger, R. H. Schultz, B. H. Weiller, K. R. Kyle, C. B. Moore and R. G. Bergman,*Pure and Applied Chemistry* **67**, 281-288 (1995).

130. M. R. A. Blomberg, P. E. M. Siegbahn, U. Nagashima and J. Wennerberg,*Journal Of the American Chemical Society* **113**, 424-433 (1991).

131. R. Degani ; R. Degani, Ed., Jan. 18 1982.

132. R. G. Bergman,*Journal of Organometallic Chemistry* **400**, 273 (1990).

133. R. H. Crabtree,*Chemical Reviews* **85**, 245 (1985).

134. B. H. Weiller, E. P. Wasserman, C. B. Moore and R. G. Bergman,*Journal Of the American Chemical Society* **115**, 4326-4330 (1993).

135. D. P. Drolet and A. J. Lees,*Journal Of the American Chemical Society* **114**, 4186-4194 (1992).

136. A. H. Janowicz and R. G. Bergman,*Journal of the American Chemical Society* **104**, 352 (1982).

137. J. K. Hoyano and W. A. G. Graham,*Journal of the American Chemical Society* **104**, 3723 (1982).

138. R. N. Perutz,*Pure and Applied Chemistry* **62**, 1103-1106 (1990).

139. R. Choukroun and G. D. Raoulty,*Journal of Organometallic Chemistry* **392**, 189 (1990).

140. W. T. Grubbs, T. P. Dougherty and E. J. Heilweil,*Chemical Physics Letters* **227**, 480-484 (1994).

141. J. Song and M. B. Hall,*Organometallics* **12**, 2006 (1993).

142. P. E. M. Siegbahn,*Journal Of the American Chemical Society* **118**, 1487-1496 (1996).

143. M. R. A. Blomberg, P. E. M. Siegbahn and M. Svensson,*New Journal Of Chemistry* **15**, 727-733 (1991).

144. R. H. Schultz, A. A. Bengali, M. J. Tauber, B. H. Weiller, E. P. Wasserman, K. R. Kyle, C. B. Moore and R. G. Bergman,*Journal Of the American Chemical Society* **116**, 7369-7377 (1994).

145. M. B. Sponsler, B. H. Weiller, P. O. Stoutland and R. G. Bergman,*Journal Of the American Chemical Society* **111**, 6841-6843 (1989).

146. E. P. Wasserman, C. B. Moore and R. G. Bergman,*Science* **255**, 315-318 (1992).

147. P. B. Graham, M. D. Rausch, K. Taschler and W. Phillipsborn,*Organometallics* **10**, 3049 (1991).

148. P. E. Bloyce, A. J. Rest and I. Whitwell,*Journal of the Chemical Society, Dalton Transactions* 813-821 (1990).

149. R. N. Perutz, S. T. Belt, A. McCamley and M. K. Whittlesey,*Pure and Applied Chemistry* **62**, 1539-1545 (1990).

150. A. J. Rest, I. Whitwell, W. A. G. Graham, A. Hoyano and D. McMaster,*Journal of the Chemical Society, Dalton Transactions* (1987).

151. B. H. Weiller, E. P. Wasserman, R. G. Bergman, C. B. Moore and G. C. Pimentel,*Journal Of the American Chemical Society* **111**, 8288-8290 (1989).

152. D. Marx and A. J. Lees,*Inorganic Chemistry* **27**, (1988).

153. With the same pump power, the neat solvent scans have a bigger signal than the iridium complex at long times. This is because more UV photons are available to excite the solvent molecule in the neat scans than in the $Cp^*Ir(CO)_2$ solution due to the absorbance of the complex itself. The solvent scan is thus scaled to obtain the same value at long time based on the result from the IR experiment that almost all the excited $Cp^*Ir(CO)_2$ returns to the ground state in 40 ps. This scaling procedure is justified since both the solvent signal alone and the total signal were measured to be linearly dependent on

pump power. Although the solvent signal is thought to result from two-photon ionization of solvent molecules, the presence of a two-photon process does not necessarily guarantee a quadratic power dependence of the solvent signal due to the non-Gaussian beam shape. This was shown by earlier absorption studies in xenon using the same experimental setup.

154. R. G. Ball, W. A. G. Graham, D. M. Heinekey, J. K. Hoyano, A. D. McMaster, B. M. Mattson and S. T. Michel,*Inorganic Chemistry* **29**, 2023-2025 (1990).

155. A. A. Purwoko and A. J. Lees,*Inorganic Chemistry* **34**, 424-425 (1995).

156. A. A. Bengali, R. H. Schultz, C. B. Moore and R. G. Bergman,*Journal Of the American Chemical Society* **116**, 9585-9589 (1994).

157. F. Pradella, D. Rehorek, M. Scoponi, S. Sostero and O. Traverso,*Journal Of Organometallic Chemistry* **458**, C16-C16 (1993).

158. F. Pradella, D. Rehorek, M. Scoponi, S. Sostero and O. Traverso,*Journal Of Organometallic Chemistry* **453**, 283-288 (1993).

159. R. N. Perutz,*Chemistry & Industry* 462-466 (1991).

160. R. N. Perutz, J. N. Hill and A. McCamley,*Coordination Chemistry Reviews* **111**, 111-116 (1991).

161. P. E. Bloyce, J. Mascetti and A. J. Rest,*Journal Of Organometallic Chemistry* **444**, 223-233 (1993).

162. S. E. Bromberg, H. Yang, M. C. Asplund, T. Lian, B. K. McNamara, K. T. Kotz, J. S. Yeston, M. J. Wilkens, H. Frei, R. G. Bergman and C. B. Harris,*Science* (1997).

163. C. K. Ghosh and A. G. G. W,*Journal of the American Chemical Society* **109**, 4726 (1987).

164. C. K. Ghosh and A. G. G. W,*Journal of the American Chemical Society* **111**, 375 (1989).

165. A. J. Lees and A. A. Purwoko,*Coordination Chemistry Reviews* **132**, 155-160 (1994).

166. S. May, P. Reinsalu and J. Powell,*Inorganic Chemistry* **19**, 1582 (1980).

167. Trofimenko,*Journal of the American Chemical Society* **89**, 6288 (1967).

168. J. J. Turner, M. W. George, F. P. A. Johnson and J. R. Westwell,*Coordination Chemistry Reviews* **125**, 101-114 (1993).

169. A. A. Purwoko, D. P. Drolet and A. J. Lees,*Journal Of Organometallic Chemistry* **504**, 107-113 (1995).

170. J. D. Beckerle, M. P. Casassa, R. R. Cavanagh, E. J. Heilweil and J. C. Stephenson,*Chemical Physics* **160**, 487-497 (1992).

171. A. A. Purwoko and A. J. Lees,*Inorganic Chemistry* **35**, 675-682 (1996).

172. A. A. Purwoko, D. P. Drolet and A. J. Lees,*Journal Of Organometallic Chemistry* **513**, 289-289 (1996).

173. A. A. Purwoko, S. D. Tibensky and A. J. Lees,*Inorganic Chemistry* **35**, 7049-7055 (1996).

174. S. Zarick and M. B. Hall, Personal Communication.

175. F. Bonati, G. Mingetti and G. Banditelli,*Journal of Organometallic Chemistry* **87**, 365 (1975).

176. S. T. Belt, F. W. Grevels, W. E. Klotzbucher, A. McCamley and R. N. Perutz,*Journal Of the American Chemical Society* **111**, 8373-8382 (1989).

177. T. Yuzawa, C. Kato, M. W. George and H. Hamaguchi,*Applied Spectroscopy* **48**, 684 (1994).